Maejo Int. J. Sci. Technol. **2009**, *3*(03), 352-365

Maejo International

Journal of Science and Technology

ISSN 1905-7873

Available online at www.mijst.mju.ac.th

Full Paper

Estimation of power dissipation of a 4H-SiC Schottky barrier diode with a linearly graded doping profile in the drift region

Rajneesh Talwar [1,*] and Ashoke K. Chatterjee [2]

[1] Department of Electronics and Communication Engineering , RIMT-Institute of Engineering and Technology, Mandi Gobindgarh, Punjab, India-147301

[2] Department of Electronics and Communication Engineering, Thapar University, Patiala, Punjab, India-147004

[*] Corresponding author, e-mail: talwarrajneesh@gmail.com

Received: 23 February 2009 / Accepted: 30 August 2009 / Published: 7 September 2009

Abstract : The aim of this paper is to establish the importance of a linearly graded profile in the drift region of a 4H-SiC Schottky barrier diode (SBD). The power dissipation of the device is found to be considerably lower at any given current density as compared to its value obtained for a uniformly doped drift region. The corresponding values of breakdown voltages obtained are similar to those obtained with uniformly doped wafers of 4H-SiC.

Keywords : Schottky barrier diode, 4H-SiC, power dissipation, breakdown voltage

Introduction

Compared to silicon, silicon carbide (SiC) has certain physical properties that put it on a higher platform for use in solid-state power devices. A low intrinsic carrier concentration of the order of 10^{-7} per cc, a 10x higher breakdown electrical field, typically about 3 MV/cm, and a 3-fold higher thermal conductivity coupled with a large saturated drift velocity of $2*10^{7}$ cm/s [1] are some of the salient features of SiC. These devices are extremely attractive in applications requiring blocking voltages ranging from 300 V to 3 kV [2]. High-voltage SiC devices are thinner and can be heavily doped if

Maejo Int. J. Sci. Technol. **2009**, *3*(03), 352-365

needed. At equivalent breakdown voltages, they offer specific on-resistance (R_{on-sp}) which may be up to two orders of magnitude lower compared to silicon devices [3].

The forward voltage drop of SiC devices is well below 2.5 V for a 600V Schottky barrier diode (SBD) even at a current density of 4000 A/cm^2 and R_{on-sp} of these devices, due to the thinner drift region, is 200 times less than that of the silicon counterparts [4].

The comparison of 6H-SiC with 4H-SiC would reflect a major advantage which the latter offers with respect to the electron mobility, which is twice or 10 times that of the former in the direction perpendicular to or along the 6H-SiC c-axis respectively [5]. Obviously 4H-SiC SBD's have lower R_{on-sp} at high voltages (greater than 200 V) compared to SBD's made from other semiconductors such as Si, GaAs and even 6H-SiC [4-5].

Experimentally obtained R_{on-sp} for 4H-SiC diodes is as low as 1.5 mΩ-cm^2 at forward current density of 732 A/cm^2 at 2 V, with a breakdown voltage of 1400 V , a 10-μm-thick epitaxial drift layer doped with 7.5x10^{15} atoms/cc and argon-edge termination [6]. More recent achievements of R_{on-sp} for 4H-SiC SBD's are 2 mΩ-cm^2 and 1.4 mΩ-cm^2 at breakdown voltages of 1000 V and 800 V respectively [7-8].

R_{on-sp} of a SBD is the sum of the n-type epitaxial drift layer and the n+ substrate resistance given by [9] :

$$R_{on-sp} = \frac{W}{eN_D\mu_n} \qquad (1)$$

where W is the thickness of the drift region , N_D is the epitaxial layer doping density and μ_n is the electron mobility. The magnitude of N_D is set so that the drift layer punch-through occurs at the same voltage at which avalanche breakdown takes place. For a constant drift layer thickness W, it is possible to reduce R_{on-sp} of the SBD by either increasing the value of μ_n in equation (1) using models similar to the ones prepared for 4H- and 6H-SiC [10] or by changing the doping profile in the drift region of the device. Doping-dependent mobility as well as high- and low-field mobility models well suited for simulation and device design have been proposed by Roschke and Schwierz [11]. However, high-field mobility values in 4H-SiC are generally low and somewhat difficult to increase. To date the most reliable experimental data for velocity-field profile of 4H-SiC have been reported by Khan and Cooper [12]. Accordingly, the reduction of R_{on-sp} may be done by increasing the magnitude of the drift layer doping, i.e. N_D or N_A.

A novel way for reduction of R_{on-sp} is suggested in this paper which uses a linearly graded profile in the drift region with a low doping level near the metal–semiconductor contact at the top of a 4H-SiC SBD and a higher doping level near the substrate. Such a drift layer would give a moderately high mobility as estimated from the effective doping level of the drift region obtained by integrating the linear function within its limits. The high doping level near the substrate would provide a low-series parasitic resistance of the drift layer. The overall effect would result in a reduction of R_{on-sp} and power dissipation of the device. The results of power dissipation reduction at an on-state current density of 1000 amperes/cm^2 for the uniformly doped drift region of SBD's are compared with linearly graded drift region of SBD's with comparable levels of carrier concentration. It is estimated that there is a drop of 74.4% to 7.74% in power dissipation with linearly graded drift region of the devices.

Maejo Int. J. Sci. Technol. **2009**, *3*(03), 352-365

Theory

The common device structure of a 4H-SiC SBD is shown in Figure 1 and it's equivalent circuit is also drawn in Figure 2. The SBD shown in Figure 1 consists of a block of n-type 4H-SiC crystal with a given height 'h'. The metal contact at the top has a cross-sectional area 'A' and there is a base contact which may be formed using a metal or an alloy. Boron implant is made for edge termination on either side of the Schottky contact. An overlap exists between the top metallic contact of width 'd' and the contact length 'a'. The current flow from the top contact is considered trapezoidal in shape spreading through the drift region by an angle 'α′' with the vertical at the corner edge of the boron implant beneath the contact. A standard value of $\alpha'=26^{O}$ is taken for this model [13], which allows a small spread of current from the top contact to uniformly flow into the n^{+}-substrate below. The equivalent circuit shown in Figure 2 of the SBD has $R_{on\text{-}sp}$ which is the sum of the series $R_{on\text{-}sp}$ of the drift region (R_D) and the parasitic series resistance (R_s) with uniform current flow. Beneath this region is the n^{+}-type heavily doped substrate region whose resistance may be considered to be zero.

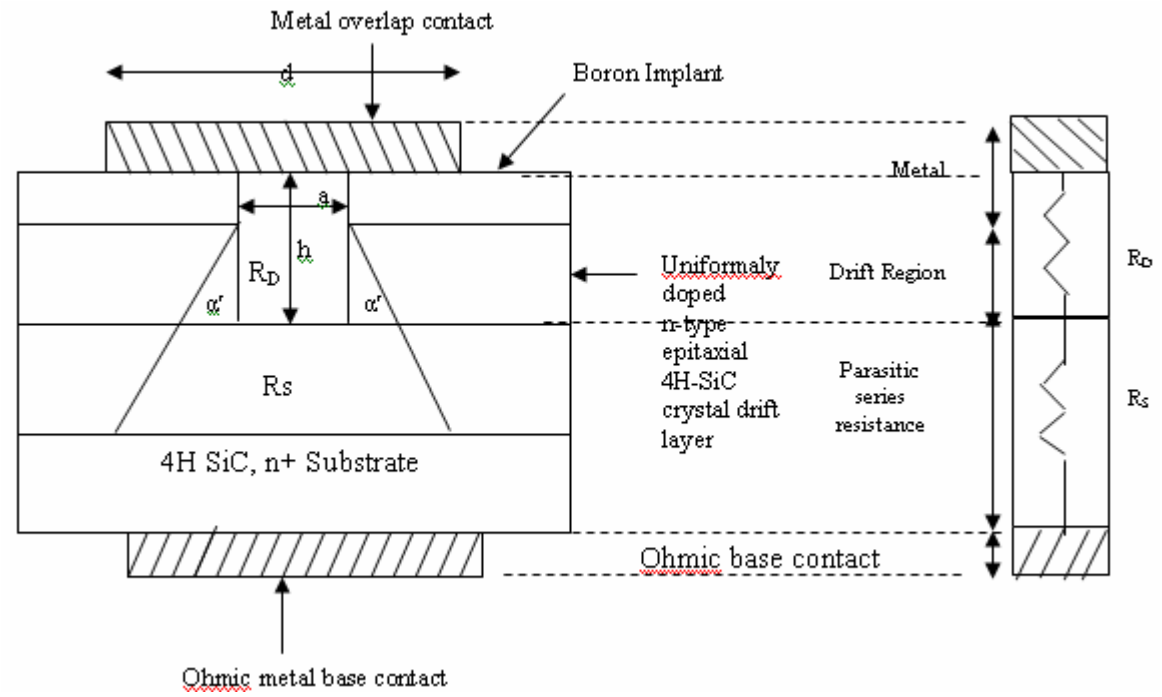

Figure 1. The structure and regions of a 4H-SiC SBD

Figure 2. Equivalent circuit of SBD shown in Figure 1

The equation to evaluate $R_{on\text{-}sp}$ of the device can be given by [13] :

$$R_{on-sp} = \rho_D \frac{d}{\tan\alpha'} \ln[1+\frac{2h}{a}\tan\alpha']$$

$$R_{on-sp} = \rho_D \frac{a}{\tan\alpha'} \ln[1+\frac{2h}{a}\tan\alpha'] \qquad (2)$$

Maejo Int. J. Sci. Technol. **2009**, *3*(03), 352-365

where d = a for minimum overlap of contact metal considered and

$$\rho_D = \frac{1}{\mu_N e N_D} \qquad (3)$$

where N_D is the donor density in the n-type epitaxial layer.

In the model proposed here for the 4H-SiC SBD, the epitaxial layer is not uniformly doped but is linearly graded with a gradient α. Near the contact, the device has the lowest doping level (N_o), which increases with the gradient to any desired doping level (N) at the substrate. This is shown in Figure 3. The equivalent circuit of the device is similar to Figure 2, with R_D replaced by R_D' and the new $R_{s'}$ (< R_s) being used. $R_{s'}$ has a lower value than R_s as the doping level is nearer to the substrate than the contact at the top of the device. The doping level N_D of the epitaxial layer has to be replaced by the effective doping level N_{eff} of the linearly graded drift layer.

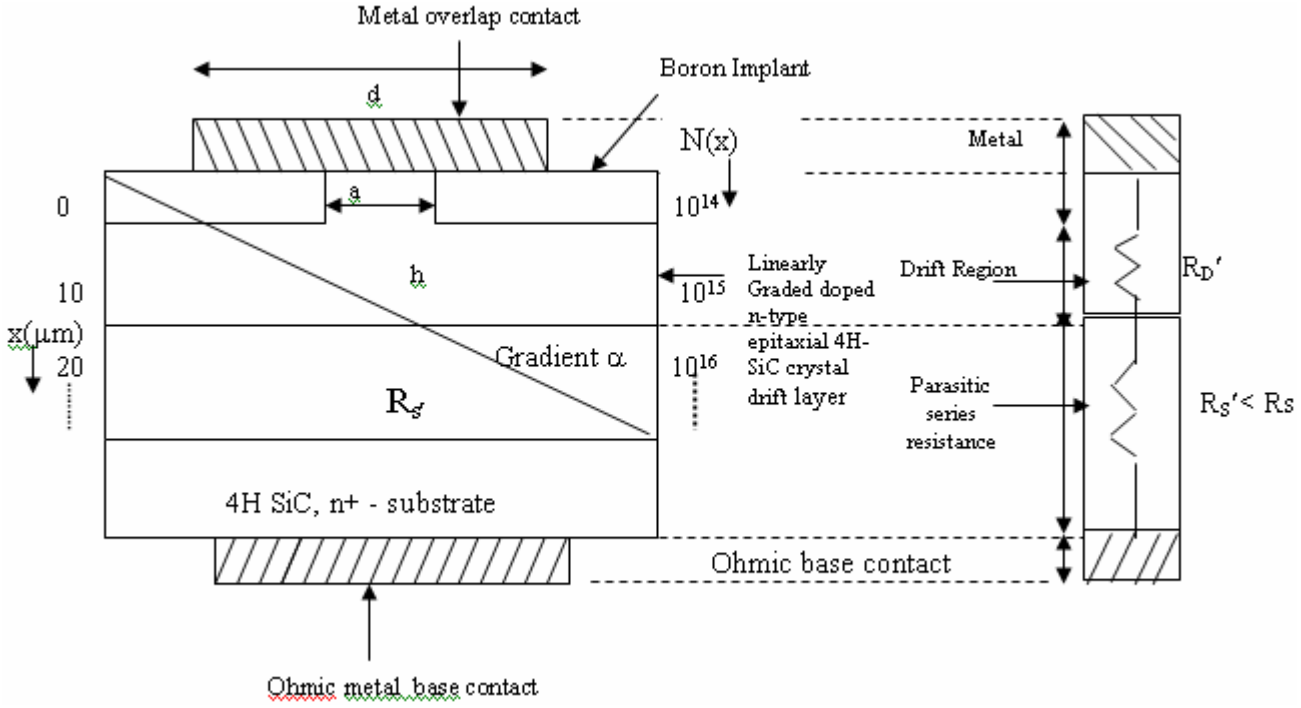

Figure3. The 4H-SiC SBD with linearly graded drift region doping profile with gradient α

Figure 4. The equivalent circuit of the SBD shown in Figure 3

Formulation of N_{eff}

Consider the cross section of the epitaxial layer of Figure 3 as shown in Figure 5. The resistance dR of a thin element of thickness dx at a distance x from the top of this device can be expressed as

$$dR = \frac{1}{\mu_n' e N(x)} \frac{dx}{A} \qquad (4)$$

Maejo Int. J. Sci. Technol. **2009**, *3*(03), 352-365

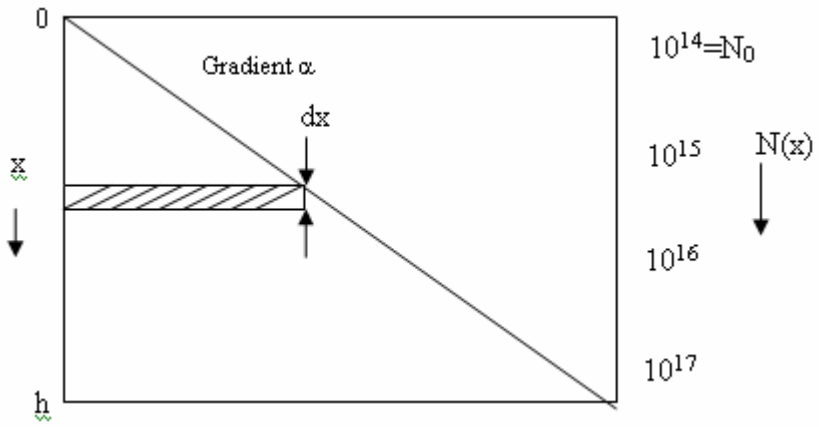

Figure 5. Cross section of drift region of a 4H-SiC SBD with linearly graded profile and gradient α

where A is the cross-sectional area in the direction perpendicular to the figure. The total resistance R of this layer can be evaluated by writing $N(x) = N_0 + \alpha x$ and integrating within limits of x from 0 to h, where h is the height of the device. This gives

$$R = \int_0^h \frac{1}{\mu_n' eA} \frac{dx}{(N_0 + \alpha x)} \tag{5}$$

Writing $Z = N_0 + \alpha x$, then $dZ = \alpha dx$, which gives

$$R = \frac{1}{\mu_n' eA} \int_{N_0}^{N_0+\alpha h} \frac{dZ}{\alpha Z} = \frac{1}{\mu_n' eA\alpha} \ln\left[\frac{N_0 + \alpha h}{N_0}\right] = \frac{1}{\mu_n' eA\alpha} \ln\left[1 + \frac{\alpha h}{N_0}\right] \tag{6}$$

If the effective concentration of this layer is N_{eff}, then R may also be written as

$$R = \frac{1}{\mu_n' e N_{eff}} \frac{h}{A} \tag{7}$$

Comparing equations (6) and (7), N_{eff} may be written as

$$N_{eff} = \frac{\alpha h}{\ln(1 + \frac{\alpha h}{N_0})} \tag{8}$$

The magnitude of $R_{on\text{-}sp}$ of the linearly graded drift layer, i.e $R'_{on\text{-}sp}$, can be obtained from equation (2) with ρ_D replaced by ρ_D' :

$$R'_{on-sp} = \rho_D' \frac{a}{\tan\alpha'} \ln[1 + \frac{2h}{a} \tan\alpha'] \tag{9}$$

where $\rho_D' = \frac{1}{\mu_n' e N_{eff}}$ (10)

with μ_n' being the value of mobility corresponding to doping level N_{eff} of the drift region.

Maejo Int. J. Sci. Technol. **2009**, *3*(03), 352-365

Device height 'h'

The height 'h' of the device has been set using a specific value of reverse bias voltage as the punch-through breakdown voltage. This is also set close to the avalanche breakdown voltage of the device using the condition $\alpha_p W = 1$, the condition for avalanche breakdown, and has been set equal to W, the depletion width at punch-through. The α_p is the hole impact ionisation coefficient, wherein it is assumed that hole in n-type wide depletion region in the drift layer started the ionisation process [14].

Calculation of power dissipation (P_D)

The equation for power dissipation P_D can be written as [9]:

$$P_D = \frac{1}{2}\left(J_{on}{}^2 AR_{on-sp} + J_L A V_B\right) \quad (11)$$

where J_{on} is the on-state current density, A is the device cross-sectional area for current flow, V_B is the reverse blocking voltage and J_L is the leakage current density. For a 50% duty cycle, the magnitude of J_L in SiC devices is too small compared to that in silicon devices and hence the second term in equation (11) can be neglected giving :

$$P_D = \frac{1}{2}(J_{on}{}^2 AR_{on-sp}) \quad (12)$$

Evaluation of the on-state current density (J_{on})

The current-voltage equation of the Schottky diode using thermionic emission theory has been given by Bethe [15] :

$$J_F = J_S[\exp(eV_D/\eta kT) - 1] \quad (13)$$

where J_F is the on-state forward current density and V_D is the voltage drop across the Schottky diode and J_s is the reverse leakage current density given by

$$J_s = A^* T^2 \exp(-e\,\varphi_B/\eta kT) \quad (14)$$

where A^* is the Richardson constant in amperes $cm^{-2}K^2$, φ_B is the barrier height in volt and T is the device temperature in ^oK.

The basic current–voltage equation for such a diode has been derived by Bhatnagar et al. [16]. The diode forward voltage drop (including drift layer) V_F can be expressed as

$$V_F = V_D + J_F R_{on\text{-}sp} \quad (15)$$

Combining equations (13) through (15) and writing J_{on} for J_F, the voltage V_F may be expressed as

$$V_F = \frac{\eta kT}{e}\ln\left(\frac{J_{on}}{A^*T^2}\right) + \varphi_B + J_F R_{on-sp} \quad (16)$$

Values of J_{on} for different values of V_F in the on state of the diode can be obtained by iteration with a simple technique and C++ program [17]. Under forward bias and in the on state, the magnitude of V_D and V_F is small, and thus the effect of barrier height lowering, $\Delta\phi$, has not been included in equations (14) and (16) above.

Maejo Int. J. Sci. Technol. **2009**, *3*(03), 352-365

The calculation of power dissipation has been performed, knowing N_D, N_{eff}, $R_{on\text{-}sp}$, $R'_{on\text{-}sp}$ and the magnitude of J_{on} and V_F, for both uniformly doped and linearly graded drift layers of the 4H-SiC SBD's.

Calculation of breakdown voltages

The punch-through breakdown voltage (V_{PBV}) is determined at a high reverse bias voltage (V_R) for a uniformly doped semiconductor of 4H-SiC SBD and the depletion region width (W) at this voltage is set equal to the device height (h). The avalanche breakdown voltage is obtained using the condition $\alpha_p W = 1$, to give the magnitude of α_p. The critical field (E_c) corresponding to this value of α_p is obtained from [18]. The magnitude of the avalanche breakdown voltage (V_{AvBV}) is then obtained using the equations:

$$V_{AvBV} = \frac{1}{2} E_c W \text{ , for uniformly doped drift region of SBD, and} \quad (17)$$

$$V_{AvBV} = \frac{2}{3} E_c W' \text{ , for linearly graded drift region of SBD} \quad (18)$$

The depletion region width in the two cases is calculated using the formula:

$$W = \sqrt{\frac{2\varepsilon_S (V_{bi} + V_R)}{eN_D}} = \sqrt{\frac{2\varepsilon_S V_R}{eN_D}} \text{ , for uniformly doped drift region of SBD,} \quad (19)$$

where V_{bi} is the built-in potential and $V_{bi} << V_R$, the applied reverse voltage which is equal to the avalanche breakdown voltage, and

$$W' = \sqrt[3]{\frac{12\varepsilon_S (V_g + V_R)}{e\alpha}} = \sqrt[3]{\frac{12\varepsilon_s V_R}{e\alpha}} \text{ , for linearly graded drift region of SBD,} \quad (20)$$

where V_g is the gradient voltage and $V_g << V_R$, the applied reverse voltage which is equal to the avalanche breakdown voltage. In the two equations, ε_s denotes the permittivity of 4H-SiC and α in equation (20) is the concentration gradient which is 10^{14} near the top of the device, and increases linearly to 10^{15}, 10^{16} ------, near the substrate over the device height (h).

The calculation of E_c for avalanche breakdown in a linearly graded profile is made using equation [20]:

$$E_C = \frac{e\alpha W'^2}{8\varepsilon_S} \quad (21)$$

where W' is the depletion region width at breakdown.

Calculations and related graphs

The device height 'h' is set equal to the maximum depletion region width 'W' corresponding to a breakdown voltage of 5 kV for the uniformly doped epitaxial layer with the lowest doping level of 10^{14} per cc using equation (19). This gives a value of 231μm for the device height 'h' taking $\varepsilon_s = 9.7$ for 4H-SiC. The doping-dependent mobility value is obtained from Roschke and Schwierz [11]. The

Maejo Int. J. Sci. Technol. **2009**, *3*(03), 352-365

magnitude of $R_{on\text{-}sp}$ is calculated using equation (2) with angle $\alpha' = 26^o$ and Schottky contact of length 'a' equal to 100 μm. The contact width is equal to 78.5 μm. The device cross-sectional area 'A' is then 78.5 x 10^{-6} cm^2. Specific values of the on-state current density (J_{on}) ranging from 100 to 1000 amps/ cm^2 are used and the corresponding values of power dissipation (P_D) are calculated using equation (12). This is repeated for doping levels of 10^{15}, 10^{16} and 10^{17} per cc. The results are shown in Table 1(A).

Table 1(A). Calculation of power dissipation (P_D) of 4H-SiC SBD with uniformly doped drift region

Current density (amps /cm^2)	N_d = 1x 10^{14} atoms/cc	N_d = 1x 10^{15} atoms /cc	N_d = 1x 10^{16} atoms/cc	N_d = 1x 10^{17} atoms/cc
	μ_n= 960 cm^2 per Vs	μ_n= 950 cm^2 per Vs	μ_n= 900 cm^2 per Vs	μ_n= 600 cm^2 per Vs
	$R_{on\text{-}sp}$ =1.577 Ω-cm^2	$R_{on\text{-}sp}$ =159.38x10^{-3} Ω-cm^2	$R_{on\text{-}sp}$ =16.82x10^{-3} Ω-cm^2	$R_{on\text{-}sp}$ =2.52 x 10^{-3} Ω-cm^2
J_{on}	P_D(1) Watts	P_D(2) Watts	P_D(3) Watts	P_D(4) Watts
100	0.6195	62.55x10^{-3}	6.601 x 10^{-3}	989.1 x 10^{-6}
200	2.478	0.2502	26.40 x 10^{-3}	3.956 x 10^{-3}
400	9.912	1.0008	0.1056	15.82 x 10^{-3}
600	22.302	2.2518	0.2376	35.607 x 10^{-3}
800	39.649	4.0032	0.4225	63.30 x 10^{-3}
1000	61.95	6.255	0.660	98.91 x 10^{-3}

In the case of linearly graded profiles, the device height 'h' is kept the same as in the case of the uniformly doped epitaxial layers (i.e 231 μm). The concentration gradients selected arbitrarily are 10^{14}-10^{15}, 10^{14}-10^{16}, 10^{14}-10^{17} and 10^{14}-10^{18} over the device height of 231μm. This gives the concentration gradient 'α' in each case. The effective carrier concentration 'N_{eff}' for linearly graded epitaxial layer is calculated using equation (8). The value of the average doping dependent carrier mobility (μ_n') for any specific concentration gradient is obtained from Roschkc and Schwierz [11]. $R'_{on\text{-}sp}$ is then calculated using equation (9), treating the medium doping level as equal to N_{eff}. The depletion region width 'W' for a reverse bias voltage of 5 kV is calculated using equation (20). The power dissipation for a given concentration gradient at the same current density levels in the case of the uniformly doped epitaxial layer device above is calculated using equation (12) with the same value of the device cross-sectional area 'A' and the corresponding values of $R'_{on\text{-}sp}$. The results are shown in Table 1(B).

The plots of power dissipation versus current density for uniformly doped and linearly graded epitaxial layers of 4H-SiC SBD are obtained from the data given in Tables 1(A) and 1(B) and are shown in Figure 6 .

Maejo Int. J. Sci. Technol. **2009**, *3*(03), 352-365

Table 1(B). Calculation of power dissipation (P_D) of 4H-SiC SBD with linearly graded drift region

Current density (amps /cm^2)	N_{eff} = 3.905 x 10 ^{14} atoms/cc	N_{eff} = 2.148 x10^{15} atoms/cc	N_{eff} = 1.446 x10^{16} atoms/cc	N_{eff} = 1.085 x10^{17} atoms/cc
	μ_n'= 960 cm^2 per Vs	μ_n'= 950 cm^2 per Vs	μ_n'= 900 cm^2 per Vs	μ_n'= 600 cm^2 per Vs
	R_{on-sp} =0.04038 Ω-cm^2	R_{on-sp} =0.07418 Ω-cm^2	R_{on-sp} = 11.63 x10^{-3} Ω-cm^2	R_{on-sp} =2.325 x10^{-3} Ω-cm^2
J_{on}	P_D(1) Watts	P_D(2) Watts	P_D(3) Watts	P_D(4) Watts
100	0.15849	29.115e-3	4.565e-3	912.56e-6
200	0.63396	0.1164	18.260e-3	3.650e-3
400	2.5358	0.4658	73.042e-3	14.60e-3
600	5.7056	1.048	164.34e-3	32.85e-3
800	10.143	1.863	0.29217	58.40e-3
1000	15.849	2.9115	0.4565	91.25e-3

It is seen that linearly graded profiles give theoretically a much lower power dissipation (P_D) than do the uniformly doped profiles in 4H-SiC SBD's. The percentage fall in power dissipation between two adjacent graphs of linearly doped and uniformly doped profiles in Figure 6 ranges from 7.74% to 74.4% for J_{on} of 1000 amps/cm^2. This is shown in Figure 7.

The punch-through breakdown voltage (V_{PBV}) is set at 5 kV for the case of uniformly doped epitaxial layer with a doping level of 10^{14} per cc and a depletion region width 'W' of 231μm. The condition for avalanche breakdown represented by $\alpha_p W = 1$ gives the value of α_p. The magnitude of the electrical field for avalanche breakdown (E_c) is obtained from Ayalew [18] from the plot of α_p versus E for 4H-SiC. The value of V_{AvBV}, the avalanche breakdown voltage, is then obtained from equation (17). This is repeated for doping levels of 10^{15}, 10^{16} and 10^{17} per cc, as shown in Table 2(A).

The punch-through breakdown voltage for the linearly graded epitaxial layer is obtained from the depletion region width 'W'' at 5 kV for a given concentration gradient 'α' of 3.88 x 10^{16}cm^{-4}. The value of the critical field (E_c) for linearly graded profile is calculated using equation (21) and the value of W′ obtained at 5 kV is treated as the depletion width for avalanche breakdown. The magnitude of V_{AvBV} is then calculated using equation (18).This is repeated for other values of α and the results are shown in Table 2(B).

Maejo Int. J. Sci. Technol. **2009**, *3*(03), 352-365

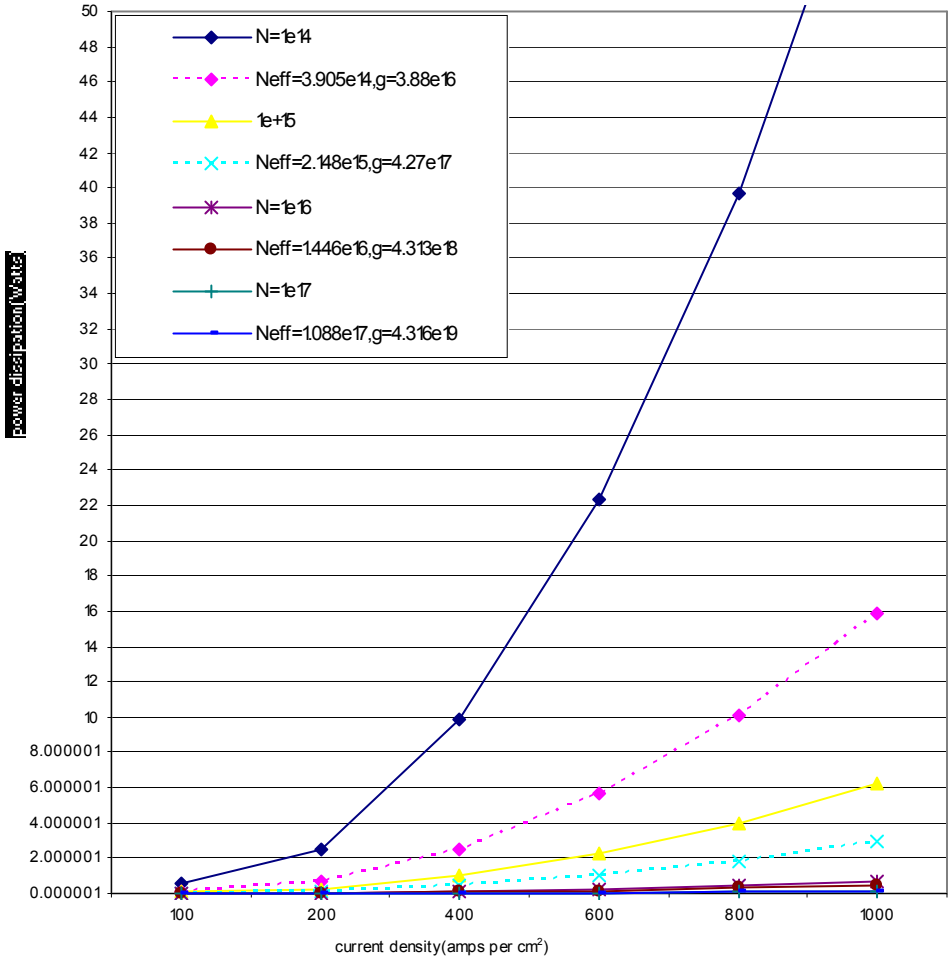

Figure 6. Plots of power dissipation versus on-state current density for uniformly doped and linearly graded drift region in 4H-SiC SBD

Maejo Int. J. Sci. Technol. **2009**, *3*(03), 352-365

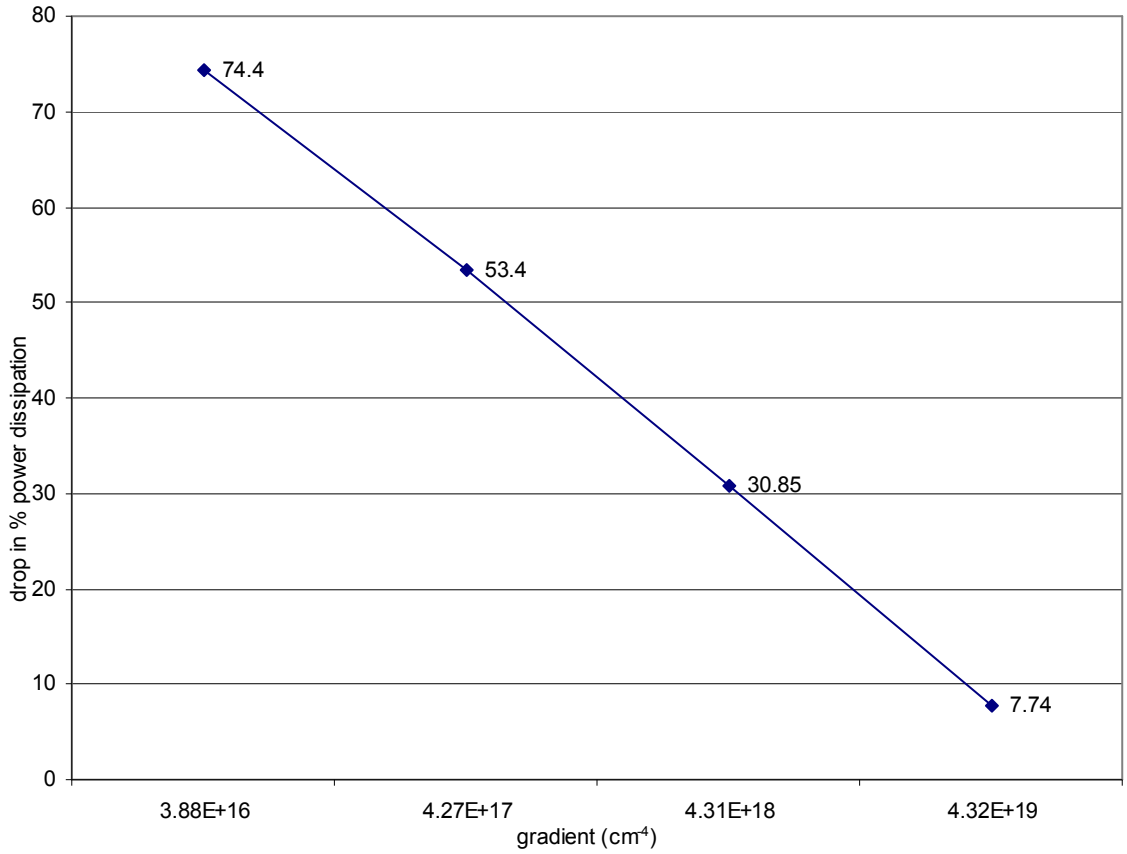

Figure 7. Percentage drop in power dissipation versus concentration gradient in 4H-SiC SBD compared to SBD with uniformly doped drift region

Table 2(A). Breakdown voltages of 4H-SiC SBD for uniformly doped epitaxial layer (Device height = h = W = 231 μm)

Doping level (N_D per cc)	W (μm)	α_p (cm^{-1})	E_c (V per cm) x 10^6	V_{AvBV} (kV)	V_{PBV} (kV)
10^{14}	227	44.05	1.33	14.94	5
10^{15}	71.78	139.31	1.66	5.95	5
10^{16}	22.7	440.05	1.82	2.06	5
10^{17}	7.17	1394.7	2.12	0.7575	5

Maejo Int. J. Sci. Technol. **2009**, *3*(03), 352-365

Table 2(B). Breakdown voltages of 4H-SiC SBD for linearly graded epitaxial layer (Device height = h = W = 231 μm)

Gradient α (cm^{-4})	W′ (μm)	$E_C = \left(\frac{e\alpha W'^2}{8\varepsilon_S}\right)$	V_{AvBV} (kV)	V_{PBV} (kV)
3.88×10^{16}	201.07	3.72×10^5	4.986	5
4.27×10^{17}	90.3	8.25×10^5	4.966	5
4.31×10^{18}	41.8	2.86×10^6	4.966	5
4.31×10^{19}	19.4	3.84×10^6	4.966	5
4.4×10^{19}	22.7	5.26×10^6	7.960	8

Discussion and Conclusions

The curves shown in Figure 6 show that the linearly graded epitaxial drift region of 4H-SiC SBD′s have consistently lower power dissipation than the uniformly doped epitaxial layer devices. A tally of such an effect can be verified by comparing the power dissipation of the devices when evaluated at a current density of 1000 amps/cm^2. The comparison between the curve for the uniformly doped epitaxial layer device with a doping level of 10^{14} per cc and that for the linearly graded profile with a gradient of 3.88×10^{16} cm^{-4} at N_{eff} of 3.905×10^{14} shows that there is a 74.4% drop in power dissipation. When the drop in power dissipation is evaluated at other current density levels, it is found that the drop in per cent power dissipation remains at the same level. This is, however, not so for other sets of curves, where this type of tally shows a constant decline in per cent power dissipation for a given N_{eff} compared to nearly similar levels of doping in the uniformly doped profiles. In other words, compared to the uniformly doped epitaxial layers, the linearly graded profiles show a significantly lower power dissipation. Figure 7 shows this in a different perspective where the percentage fall in power dissipation is found to increase with a decrease in concentration gradient from 74.4% at a gradient of 3.88×10^{16} cm^{-4} to 7.74% at a gradient of 4.316×10^{19} cm^{-4}

Calculation of breakdown voltages shown in Table 2(A) shows that for uniformly doped epitaxial layer devices doped to a level of 10^{15} per cc, the punch-through and avalanche breakdown voltages are almost equal to 5 kV. Linearly graded epitaxial layer devices show a similar avalanche breakdown at 7.96 kV for a gradient of 4.4×10^{19} cm^{-4} for which the punch-through breakdown voltage is 8 kV. This device can therefore have a breakdown voltage of 7.96 kV which is almost equal to the punch-through breakdown voltage of 8 kV.

An analysis of the results shown in Tables 2(A) and 2(B) shows that the critical field 'E_c' increases with doping level in the case of uniformly doped epitaxial layer devices while it does with gradient α in the case of linearly graded epitaxial layer devices. However, the magnitude of E_c in the former case is somewhat higher than that in the latter case. The depletion region width in devices with uniformly doped profiles is normally larger than that with linearly graded ones.

In conclusion it may be said that the 4H-SiC SBD's with linearly graded epitaxial layers have considerably lower power dissipation but need not necessarily provide a higher avalanche breakdown

voltage. Lastly, the device height 'h' of 231µm used in this work may be difficult to grow in 4H-SiC using epitaxial technology. However, wafers with better crystalline perfection may be selected for making these devices.

References

1. T. P. Chow, "SiC and GaN high-voltage power switching devices", in: Silicon Carbide and Related Materials 1999, Materials Science Forum (Ed. C. H. Carter, Jr, R. P. Devaty and G. S. Rohrer), Vols. 338-342, Trans. Tech. Publications Ltd., Switzerland, **2000**, pp. 1155-1160.
2. R. Rupp, M. Treu, A. Mauder, E. Griebl, W. Werner, W. Bartsch and D. Stephani, "Performance and reliability issues of SiC-Schottky diodes", in: Silicon Carbide and Related Materials 1999, Materials Science Forum (Ed. C. H. Carter, Jr, R. P. Devaty, and G. S. Rohrer) Vols. 338-342, Trans. Tech. Publications Ltd., Switzerland, **1999**, 1167-1170.
3. M. S. Mazzola and S. E. Saddow, "High voltage SiC power device field terminations", 2nd International All Electric Combat Vehicle Conference, 8-12 June, **1997**, Dearborn, MI, USA , pp. 1-6.
4. J. B. Dufrene, G. Carter, J. B.Casady, I. Sankin, D. C. Sheridan, W. Draper and M. Mazzola, "High voltage silicon carbide diode development", 16th Annual IEEE Conference on Applied Power Electronics, 4-8 March, **2001**, Anaheim, CA, USA, pp.1253-1257.
5. W. J. Schaffer, G. H. Negley, K. G. Irvine and J. W. Palmour, "Conductivity anisotropy in epitaxial 6H and 4H SiC in diamond, SiC and nitride wide band gap semiconductors", *Mater. Res. Soc. Proc.*, **1994,** *339*, 595-600.
6. D. Alok, B. J. Baliga and P. K. Mclarty, "A simple edge termination for silicon carbide devices with nearly ideal breakdown voltage", *IEEE Trans. Electron Devices*, **1993**, *15*, 394-395.
7. R. Raghunathan, D. Alok and B. J. Baliga, "High voltage 4H-SiC Schottky barrier diodes", *IEEE Trans. Electron Devices*, **1995**, *16*, 226-227.
8. A. Itoh, T. Kimoto and H. Matsunami, "High performance high-voltage 4H-SiC Schottky barrier diodes", *IEEE Electron Device Lett.*, **1995**, *16*, 280-282.
9. M. Bhatnagar and B. J. Baliga, "Comparison of 6H-SiC, 3C-SiC and Si for power devices", *IEEE Trans. Electron Devices*, **1993**, *40*, 645-655.
10. W. J. Schaffer, G. H. Negley, K. G. Irvine and J. W. Palmour, "Conductivity anisotropy in epitaxial 6H and 4H-SiC", *Mater. Res. Soc. Symp. Proc.*, **1994**, *339*, 595-600.
11. M. Roschke and F. Schwierz, "Electron mobility models for 4H, 6H and 3C SiC", *IEEE Trans. Electron Devices*, **2001**, *48*, 1442-1447.
12. I. A Khan and J. A. Cooper, Jr., "Measurement of high-field electron transport in silicon carbide", *IEEE Trans. Electron Devices*, **2000**, *47*, 269-273.
13. B. J. Baliga, "Modern Power Devices", Wiley, New York, **1997**, Ch. 4.
14. S. M. Sze, "Physics of Semiconductor Devices", 3rd Edn., John Wiley and Sons, New York, **1999**, p100.

Maejo Int. J. Sci. Technol. **2009**, *3*(03), 352-365

15. H. A. Bethe, "Theory of the boundary layer of crystal rectifiers", MIT Radiation Laboratory Report No. 43-12, **1942,** obtainable from Publications Board, Department of Commerce, Washington D.C.
16. M. Bhatnagar, P. K. McLarty and B. J. Baliga, "Silicon carbide high voltage (400V) Schottky barrier diodes", *IEEE Electron Device Lett.,* **1992**,*13*, 501-503.
17. R. Talwar and A. K.Chatterjee, "A method to calculate the voltage-current characteristics of 4H SiC Schottky barrier diode", *Maejo Int. J. Sci. Technol.***, 2009**, *3*, 287-294.
18. Dissertation Tesfaye Ayalew**,** http://www.iue.tuwien.ac.at/phd/ayalew/node74.html
19. S. M. Sze , "Physics of Semiconductor Devices", 3rd Edn., John Wiley and Sons, New York, **1999**, p. 81.

Maejo Int. J. Sci. Technol. **2009**, *3*(03), 366-370

Maejo International

Journal of Science and Technology

ISSN 1905-7873

Available online at www.mijst.mju.ac.th

Short Communication

Microwave-induced acetylation of 2-methyl-5-hydroxy-1,4-naphthoquinone (plumbagin)

Jirawan Banditpuritat [1], Waya S. Phutdhawong [2] and Weerachai Phutdhawong [3, 4, *]

[1] Department of Chemistry, Maejo University, Sansai, Chiang Mai 50290, Thailand
[2] Department of Chemistry, Faculty of Science, Silpakorn University, Nakhon Pathom 73000, Thailand
[3] Department of Chemistry, Faculty of Liberal Arts and Science, Kasetsart University, Kampeang Saen Campus, Nakhon Pathom 73140, Thailand
[4] The Research Promotion and Technology Transfer Centre, Faculty of Liberal Arts and Science, Kasetsart University, Kampeang Saen Campus, Nakhon Pathom 73140, Thailand
* Corresponding author, e-mail: faaswcp@ku.ac.th

Received: 4 May 2009 / Accepted: 23 September 2009 / Published: 24 September 2009

Abstract: A rapid route for acetylation of 2-methyl-5-hydroxy-1,4-naphthoquinone (plumbagin) using acetic anhydride and iodine under irradiation in a modified commercial domestic microwave is reported. The acetate was obtained in high yield after a short reaction time compared to conventional method and ultrasonic method.

Key words: microwave reaction, plumbagin, acetylation, plumbagin acetate

Introduction

Quinones, notably anthraquinones and naphthoquinones, occur widely in natural products and are of considerable interest due to their varied biological properties, e.g. as an antimalarial [1-2], anticancer [3-6] and antimicrobial [2,7]. Moreover, they are also useful as dyes and pigments [8].

Maejo Int. J. Sci. Technol. **2009**, *3*(03), 366-370

Plumbagin (2-Methyl-5-hydroxy-1,4-naphthoquinone) is well distributed among the *Plumbago* spp. This compound has been described in the literature and is known to possess various pharmaceutical activities [7, 9-11].

The protection of the phenols as their acetates is a commonly-used transformation in organic synthesis as the acetate group is easily installed and removed [12]. Acetylation of the hydroxyl group of plumbagin is usually required for its synthetic utility. It has been shown that iodine is an effective catalyst in the activation of acetic anhydride for promoting the acetylation reaction [13]. Recently, acetylation of deactivated and hindered phenols using microwave irradiation coupled with the use of iodine as catalyst was reported by Deak et al. [14]. The resulting substantial reduction of reaction time and appreciably increased yields obtained by these researchers prompted us to investigate the acetylation of plumbagin by a similar method using our modified domestic microwave oven, in comparison with conventional and ultrasonic-bath methods.

Materials and Methods

Chemicals

Plumbagin was procured from natural source by a method adapted from that of Chairungsi et al. [15]. Briefly, fresh roots of *Plumbago rosea* Linn. were washed, cut, and repeatedly macerated in 50% aqueous ethanol at room temperature for 24 h to obtain a combined aqueous alcoholic extract, the major part of which was then distilled. The yellow distillate obtained was partitioned with dichloromethane:water (4:1). The organic layer was separated and dried over Na_2SO_4. After evaporation of the solvent it gave 0.4 % yield of pure plumbagin. The identity of the compound was confirmed by m.p., TLC, IR and GC-MS. All other chemicals and solvents used were of AR grade.

Acetylation of plumbagin

For microwave-induced acetylation, a mixture of plumbagin (0.5 g), iodine (0.0067 g) and acetic anhydride (5 mL) was heated in our modified domestic microwave oven [16-17] at 62-65 °C (450 W) for 4 min. For conventional acetylation, a mixture of plumbagin (0.5 g), acetic anhydride (5 mL) and iodine (0.0067 g) or pyridine (5 mL) was stirred at room temperature overnight. For ultrasonic bath acetylation, a mixture of plumbagin (0.5 g), acetic anhydride (5 mL) and iodine (0.0067 g) or pyridine (5 mL) was sonicated in an ultrasonic bath (Decon, FS300B) at 27-28^o C for 4 min [18]. Each acetylated mixture was then worked up by addition of dichloromethane. The resulting mixture was successively washed with water, saturated $NaHCO_3$ and water. The organic extract was dried over Na_2SO_4 and the solvent removed by evaporation under reduced pressure. The crude product was purified by crystallisation in hexane and characterised by m.p. determination and spectroscopic methods (IR, NMR, GC-MS).

Maejo Int. J. Sci. Technol. **2009**, *3*(03), 366-370

Results and Discussion

The acetylation of plumbagin (Figure 1) was carried out by three methods in order to compare the respective yields and reaction times. The results are shown in Table 1. Acetylation using the adapted microwave oven at 450 W and a temperature of 62-65^{o} C for 4 min gave a high yield (98%) of the acetate, while acetylation using conventional method with acetic anhydride-iodine or acetic anhydride-pyridine mixture gave moderate yields (70% and 66% respectively). Acetylation by ultrasonic bath method for 4 min with acetic anhydride-iodine or acetic anhydride-pyridine mixture gave the acetate in 38% and 83% yields respectively. Increasing the sonication time to 8 and 12 min decreased the yield to 35% and 30% respectively for iodine-catalysed reaction, and to 67% and 50% respectively for pyridine-catalysed reaction. Thus, the acetylation of plumbagin, an important natural product used as starting material for the synthesis of many plumbagin-based compounds, employing a microwave irradiation in the presence of iodine as catalyst seems to be a more efficient and enviromentally friendly method compared to the conventional or ultrasonic acetylation.

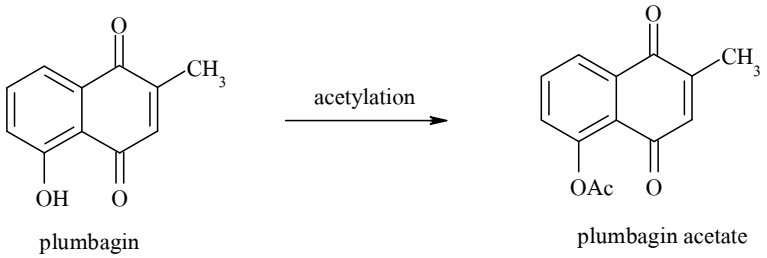

Figure 1. Acetylation of plumbagin

Table 1. Comparison of different methods of acetylation of plumbagin

Method	Reaction time	Reaction temperature (°C)	% Yield of plumbagin acetate (catalyst: I_2)	% Yield of plumbagin acetate (catalyst: pyridine)
Microwave	4 min	62-65	98	-
Conventional	24 h	room	70	66
Ultrasonic bath	4 min	27-28	38	83
	8 min		35	67
	12 min		30	50

Maejo Int. J. Sci. Technol. **2009**, *3*(03), 366-370

Acknowledgement

The authors are grateful to the Thailand Research Fundation (TRF) for financial support.

References

1. K. Likhitwitayawuid, R. Kaewamatawong, N. Ruangrungri and J. Krungkrai, "Antimalarial naphthoquinones from *Nepenthes thorelii* ", *Planta Medica*, **1998**, *64*, 237-241.
2. K. O. Eyong, G. N. Folefoc, V. Kuete, V. P. Beng, K. Krohn, H. Hussain, A. E. Nkengfack, M. Saeftel, S. R. Sarite and A. Hoerauf, "New bouldiaquinone A: A naphthoquinone-anthraquinone ether coupled pigment, as a potential antimicrobial and antimalarial agent from *Newbouldia laevis*", *Phytochemistry*, **2006**, *67*, 605-609.
3. F. Noboru, Y. Yamashita, Y. Arima, M. Nagashima and H. Nakano, "Induction of topoisomeraseII-mediated DNA cleavage by the plant naphthoquinones plumbagin and shikonin", *Antimicrob. Agents Chemother.*, **1992**, *36*, 2589-2594.
4. N. Kongkathip, B. Kongkathip, P. Siripong, C. Sangma, S. Luangkamin, M. Niyomdecha, S. pattanapa, S. Piyaviriyagul and P. Kongsaeree, "Potent antitumor activity of synthetic 1,2-naphthoquinones and 1,4-naphthoquinones", *Bioorg. Med. Chem.*, **2003**, *11*, 3179-3191.
5. D. J. Kapadia, V. Balsubramanian, H. Tokuda, T. Konoshima, M. Takasaki, J. Koyama, K. Tagahaya and H. Nishino, "Anti-tumor promoting effects of naphthoquinone derivatives on short term Epstein-Barr early antigen activation assay and in mouse skin carcinogenesis.", *Cancer Lett.*, **1997**, *113*, 47-53.
6. J. A. Valderrama, O. Espinoza, M. F. González, R. A. Tapia, J. A. Rodriguez, C. Theoduloz and G. Schmedia-Hirschmann, "Studies on quinones. Part 40: Synthesis and cytotoxicity evaluation of anthraquinone epoxides and isomerization products.", *Tetrahedron*, **2006**, *62*, 2631-2638.
7. S. Ribeiro de Paiva, M. Raquel Figueiredo and T. Verônica Aragão, "Antimicrobial activity in vitro of plumbagin isolated from *Plumbago species*.", *Mem. Inst. Oswaldo Cruz, Rio de Janeiro,* **2003**, *98*, 959-961.
8. W. Steglich, B. Fugmann and S. Lang-Fugmann (ed.), "ROMPP Encyclopedia: Natural Products", Georg Thieme Verlag, Stuttgart, **2000**.
9. P. Panichayupakaranant and S. Tewtrakul, "Plumbagin production by root cultures of *Plumbago rosea*." *Electron. J. Biotechnol.*, **2002**, *5*, 1-5.
10. C. Obua, O. Odyek, W. W. Anokbonggo, S. K. Apio, P. Waako and J. W. Ogwal-Okeng, "Antimalarial activity of some plants used in traditional medicine in Uganda", *East Central Afr. J. Pharm. Sci.*, **2002**, *5*, 33-37.
11. S. Kavimani, R. Ilango, M. Madheswaran, B. Jayakar, M. Gupta and U. K. Majumdar, "Antitumour activity of plumbagin against dalton's ascitic lymphoma", *Indian J. Pharm. Sci.*, **1996**, *58*, 194-196.

Maejo Int. J. Sci. Technol. **2009**, *3*(03), 366-370

12. T. W. Greenes and P. G. M. Wuts, "Protective Groups in Organic Synthesis", John Wiley and Sons, Inc., New York, **1991**.
13. K. P. R. Kartha and R. A. Firld, "Iodine: a versatile reagent in carbohydrate chemistry IV. Per O-acetylation, regioselective acylation and acetolysis.", *Tetrahedron*, **1997**, *53*, 11753-11766.
14. N. Deak, A.-M. Mariotte and A. Boumendjel, "Microwave mediated solvent-free acetylation of deactivated and hindered phenols.", *Green Chemistry*, **2001**, *3*, 263-264.
15. N. Chairungsi, K. Jumpatong, P. Suebsakwong, W. Sengpracha, W. Phutdhawong and D. Buddhasukh, "Electrocoagulation of quinone pigments.", *Molecules*, **2006**, *11*, 514-522.
16. W. Phutdhawong and D. Buddhasukh, "Facile microwave-assisted synthesis of 9,10-dihydro-9,10-ethanoanthracene-11-carboxylic acid methyl ester.", *Molecules*, **2005**, *10*, 1409-1412.
17. W. Phutdhawong, D. Buddhasukh, S. G. Pyne, A. Rujiwatra and C. Pakawatchai, "Microwave-assisted facile synthesis and crystal structure of cis-9,10,11,15-tetrahydro-9,10[3',4']-furanoanthracene-12,14-dione.", *Syn. Comm.*, **2006**, *36*, 881-883.
18. L . Ji-Tai , M. Xian-Tao and Z. Xin-Li, "One-pot synthesis of benzylacetamide from oxime under ultrasound irradiation", *Ultrason. Sonochem.*, **2009**, *16*, 590-592.

Maejo Int. J. Sci. Technol. **2009**, *3*(03), 371-378

Maejo International

Journal of Science and Technology

ISSN 1905-7873

Available online at www.mijst.mju.ac.th

Full Paper

Nutritive value and nutrient digestibility of ensiled mango by-products

Sompong Sruamsiri * and Pirote Silman

Faculty of Animal Science and Technology, Maejo University, Sansai, Chiang Mai, 50290, Thailand

* Corresponding author, e-mail: sompong@mju.ac.th

Received: 8 April 2009 / Accepted: 5 October 2009 / Published: 6 October 2009

Abstract: Mango canning by-products (seed and peel) together with ensiled mango peel were subjected to analysis of dry matter (DM), ash, crude protein (CP), crude fibre (CF), ether extract (EE), nitrogen-free extract (NFE), gross energy (GE), neutral detergent fibre (NDF) and acid detergent fibre (ADF). In vitro digestibility of DM (IVDMD), ADF (IVADFD) and NDF (IVNDFD) was determined after digesting the by-products in buffered rumen fluid for 24 or 48 h in an incubator. CP content in peel, seed and peel silage is 4.68, 4.19 and 5.27% respectively. As expected, mango seed has a higher fibre content than mango peel and peel silage as indicated by NDF (53.01 vs 25.87 and 27.56% respectively) and ADF (31.02 vs 19.14 and 17.68% respectively). However, mango seed also has greater GE than mango peel and peel silage (4,070 vs 3,827 and 3,984 kcal/g DM respectively), probably due partly to its high fat content.

Four head of male native cattle were used to determine nutrient digestibility of ensiled mango by-products by randomly allowing them to receive ensiled mango peel with rice straw (EMPR) and different levels of Leucaena leaves. Treatments consisted of: 1) ensiled mango peel + rice straw (90:10); 2) ensiled mango peel + rice straw + Leucaena leaves (85:10:5); 3) ensiled mango peel + rice straw + Leucaena leaves (80:10:10); and 4) ensiled mango peel + rice straw + Leucaena leaves (75:10:15). Addition of Leucaena leaves to silage increased apparent digestibility of DM (53.84, 55.43, 59.04 and 58.69% for the four formulations above respectively), probably because of increasing amounts of CP from Leucaena leaves, resulting in greater digestibility of NDF (39.11, 44.47, 47.12 and 43.32% for the four formulations above respectively). Total digestible nutrients (TDN) and digestible energy (DE) showed the same trends as apparent digestibility of DM.

Key words: mango by-products, mango peel, mango seed, apparent digestibility, energy value

Maejo Int. J. Sci. Technol. **2009**, *3*(03), 371-378

Introduction

Mango is considered as one of the most delicious fruits in Thailand. Its harvesting time is between January and May, which is in the dry season when green forage is in shortage. Mango is an excellent source of vitamin A and C, as well as a good source of potassium, beta-carotene and fibre. Normally, it is produced for human consumption as raw or ripe mango products. During the processing of ripe mango, its peel and seed are generated as waste, which is approximately 40-50 % of the total fruit weight. Mango peel is a good source of dietary fibre and its chemical composition may be comparable to that of citrus fibre. The peel has a high value of antioxidant activity and glucose retardation index while its aroma and flavour is pleasant [1]. The peel is thus palatable to cattle but very few farmers use it for animal feed because of the high moisture and acidity content.

During the processing of ripe mango, the waste (peel and seed) is a problem for canning factories. Its disposal may appreciably increase environmental pollution due to its rapid decay, thus becoming a good source of house fly multiplication. However, Omole et al. [2], Govinda Naik et al. [3] and Naveen et al. [4] reported that fruit waste and by-products may be used as alternative feed in livestock rations either as dry product or as silage. Therefore, the ensiling of mango by-products especially mango peel may be an economical way to reduce the problem of waste disposal from mango production as well as increase their utilisation as animal feed.

To produce good silage from mango peel, it would be desirable to mix it with dry materials such as rice straw to adjust moisture and with Leucaena leaves to increase protein content for proper fermentation of the ensiled products. This study was conducted to determine the nutritive value of mango by-products and evaluate the digestible nutrients of ensiled mango by-products with rice straw and Leucaena leaves (Figure 1). The feed could possibly be used to set up a feeding strategy for Thai native beef cattle fed with low quality roughage.

Materials and Methods

Composition

Ripe mango (*Mangifera indica*) by-products were obtained from a cannery plant in Sarapee district, Chiang Mai province. The by-products were dried on the truck overnight before ensiling and sampling for analysis. Peel and seed were hand- separated and the separated products were mixed thoroughly. Random samples of peel and seed were taken for analysis of dry matter (DM), ash, crude protein (CP), crude fibre (CF), ether extract (EE), nitrogen free extract (NFE) and gross energy (GE) according to the methods described in AOAC [5]. Organic matter (OM) was calculated from DM (OM =DM – ash). The analysis of neutral detergent fibre (NDF) and acid detergent fibre (ADF) was carried out according to the methods of Goering and Van Soest [6].

Maejo Int. J. Sci. Technol. **2009**, *3*(03), 371-378

mango peel

mango seed

EMPR+0%LL
(peel : rice straw =90:10)

EMPR+5%LL
(peel : rice straw : LL=85:10:5)

EMPR+10%LL
(peel : rice straw: LL=80:10:10)

EMPR+15%LL
(peel : rice straw: LL=75:10:15)

Figure 1. By-products from mango and ensiled mango by-products

In vitro digestibility

In vitro digestibility of DM (IVDMD), NDF (IVNDFD) and ADF (IVADFD) of mango peel, mango seed and mango peel silage was determined using ANCOM^{II} Daisy Incubators (ANKOM Technology, Macedon, NY). Samples were ground (1mm) and incubated in buffered rumen fluid for 24 h and 48 h. Rumen fluid was obtained from 2 fistulated native bulls before ad libitum feeding with guinea grass. The experimental design was Completely Randomised Design.

Maejo Int. J. Sci. Technol. **2009**, *3*(03), 371-378

Apparent digestibility

Four head of male native beef cattle at four years of age with average body weight of 236 ± 13.3 kg were randomly allocated to one of the four dietary treatments according to Latin Square Design. The treatments consisted of (1) 90:10 ensiled mango peel + rice straw (EMPR, 90:10), (2) 85:10:5 ensiled mango peel + rice straw + Leucaena leaves (EMPR+5%LL=85:10:5), (3) 80:10:10 ensiled mango peel + rice straw + Leucaena leaves (EMPR+10%LL= 80:10:10), and (4) 75:10:15 ensiled mango peel + rice straw + Leucaena leaves (EMPR+15%LL= 75:10:15). The diets were fed to the animal twice daily at 2.0 % of the body weight (DM basis). Water and mineral blocks were freely available throughout the experimental periods. Total collection method was assigned for the determination of apparent total tract digestibility of nutrients. The experiment was conducted at Maejo University during July - October 2008.

The experiment consisted of four periods with each digestibility period lasting 19 days and preliminary period taking place in the first 14 days while collection period was in the last 5 days. Feed intake was recorded daily throughout the entire experiment. Dietary DM intake was calculated on DM basis. Feed, feces and leftover feed were individually collected and used for the calculation of nutrient digestibility. Total digestible nutrients (TDN) were calculated using the equation: TDN = digestible CP + digestible CF + digestible NFE + digestible EE × 2.25 [7]. Gross energy of feed and feces was determined using an adiabatic bomb calorimetre (IKA calorimetre system C 5000). Digestible energy was then calculated. The data were analysed according to 4x4 Latin Square Design [8]. The significant differences between treatments were analysed based on Duncan's new multiple range test [9].

Results and Discussion

Composition

The composition of ripe mango by-products are shown in Table 1. The dry matter content of mango peel was lower than that of mango seed. At present the price (0.20 Baht per kg) of mango by-products may be economical as a source of roughage, even though their CP content is low. Crude protein content of mango peel in this experiment (4.68%) was lower than the value reported by Ojokoh (8.64%) [10], but higher than that reported by Naveen et al. (3.9%) [4] and Buwjoom and Maneewan.(3.18%) [11]. This might be due to differences in varieties, cultivation and method of by-product collection. However, mango peel in this experiment was higher in CP and NFE (4.68 and 76.13% of DM) but lower in CF and ADF (10.10 and 19.14 % of DM), when compared to mango seed. Mango seed was higher in GE and CF, mainly because the kernel is usually a good source of starch, fat and protein. This agreed with Elegbede et al [12] who reported that mango kernel was high in fat and starch (12.8 and 32.8% respectively).

Maejo Int. J. Sci. Technol. **2009**, *3*(03), 371-378

Table 1. Composition of ripe mango by-products

By-product	DM (%)	% of DM						GE (kcal/g DM)
		CP	CF	EE	NFE	NDF	ADF	
Mango peel	20.10	4.68	10.10	1.21	76.13	25.87	19.14	3,827
Mango seed	23.88	4.19	30.84	2.72	47.79	53.01	31.20	4,070
Ensiled mango peel	18.27	5.27	9.02	1.63	75.87	27.56	17.68	3,984

Ensiled mango peel was highest in CP but lower in CF and ADF. This might be due to the fact that during fermentation process carbohydrates including cellulose, pectin, lignocellulose, starch and sugar are broken down by microorganisms to produce microbial biomass, and therefore the fibre content decreased but CP content increased. Results from this experiment agreed with those of Ojokoh [10], who reported that fermentation of mango peel increased protein content of the fermented product while there was a decrease in fibre content.

In vitro digestibility

Compared with mango seed, mango peel and mango peel silage were higher in IVDMD, IVNDFD and IVADFD at 24 h and 48 h (Tables 2-3). However, the in vitro digestibility of DM, ADF and NDF in mango seed suggests that it might be acceptable for feeding ruminants if it was ground, as performed for this laboratory analysis. The high NDF (53.01%, Table 1) of the hard outer shell is compensated by the highly digestible, high energy content inside the shell. Feeding trials are needed to determine if ground mango seed is acceptable as ruminant feed. Also, methods for separation of the seed shell from the kernel should be investigated.

Table 2. In vitro DM and fibre digestibility (%) of mango by-products at 24 h

Item	IVDMD**	IVNDFD**	IVADFD*
Mango peel	$69.28^{A} \pm 2.3$	$40.63^{B} \pm 1.8$	$37.88^{a} \pm 2.2$
Mango seed	$55.77^{B} \pm 1.9$	$36.24^{C} \pm 1.6$	$30.14^{b} \pm 1.7$
Mango peel silage	$74.11^{A} \pm 2.1$	$48.33^{A} \pm 2.1$	$40.17^{a} \pm 2.1$

* Means with different superscripts significantly differ (P<0.05).
** Means with different superscripts highly differ (P<0.01).

Table 3. In vitro DM and fibre digestibility (%) of mango by-products at 48 h

Item	IVDMD**	IVNDFD**	IVADFD*
Mango peel	$75.95^{B} \pm 3.2$	$48.51^{A} \pm 1.8$	$41.29^{a} \pm 1.6$
Mango seed	$45.12^{C} \pm 2.1$	$40.27^{B} \pm 1.3$	$34.06^{b} \pm 1.1$
Mango peel silage	$79.89^{A} \pm 1.4$	$52.71^{A} \pm 1.6$	$43.54^{a} \pm 1.4$

* Means with different superscripts significantly differ (P<0.05).
** Means with different superscripts highly differ (P<0.01).

Maejo Int. J. Sci. Technol. **2009**, *3*(03), 371-378

Apparent digestibility

From Table 4, it can be seen that increasing Leucaena leaves in the silage tended to increase DM, CP, EE, CF and GE but NFE tended to decrease with increasing Leucaena leaves in the silage. The positive effect of Leucaena leaves was due to the nutritive value of this legume, which is high in protein, DM and GE [13,14]. Furthermore, the physical characteristics of ensiled mango peel and rice straw with or without Leucaena leaves were good although their DM was slightly lower than the optimal range for good ensiling products. This should be due to the high moisture content in the peel as well as to its sugar being converted to lactic acid by lactic acid bacteria. The physical characteristics of rice straw were better after the ensiling process. Its structure was softer with a light yellow colour and lactic acid odour from the fermentation process.

Table 4. Composition of ensiled mango peel + rice straw with or without Leucaena leaves

Item	DM (%)	% of DM						GE (kcal/g DM)
		CP	CF	EE	NFE	NDF	ADF	
EMPR(90:10:0)	18.76	4.91	29.25	1.96	55.49	46.22	31.28	3,632
EMPR+LL(85:10:5)	19.24	5.97	32.19	2.49	49.62	52.64	33.54	3,733
EMPR+LL(80:10:10)	20.42	6.88	33.16	2.68	48.74	52.88	35.43	3,818
EMPR+LL(75:10:15)	21.65	8.47	34.22	2.91	45.26	53.23	36.36	3,869

Table 5 shows that the values for the apparent digestibility of the nutrients (DM, OM, CP, CF, EE, NFE and ADF) in EMPR with different amounts of Leucaena leaves were higher than those in EMPR alone. The apparent digestibility figures for CP, CF and NFE were highly different ($P<0.01$) while those for EE, NDF and ADF were significantly different ($P<0.05$). No significant difference was found on the apparent digestibility of DM and OM ($P>0.05$). Supplementation of Leucaena leaves in the silage thus increased the apparent digestibility, which agrees with results of Geerts et al. [15], who found that nutrient digestibility of the diet increased with increasing crude protein content but decreased with increasing fibre content.

Table 5. Apparent digestibility of ensiled mango peel + rice straw with or without Leucaena leaves

Nutrient \ Apparent digestibility, %	EMPR	EMPR + 5%LL	EMPR +10%LL	EMPR +15%LL
DM	53.84 ± 4.6	55.43 ± 2.3	59.04 ± 3.5	58.69 ± 2.8
OM	56.81 ± 3.3	58.56 ± 2.1	61.30 ± 3.1	60.18 ± 3.4
CP**	39.44^{C} ± 2.0	45.18^{B} ± 4.4	56.55^{A} ± 5.1	54.32^{A} ± 2.2
CF**	41.64^{C} ± 3.6	46.86^{B} ± 3.2	50.41^{A} ± 4.3	50.06^{A} ± 2.9
EE*	46.51^{b} ± 2.2	52.10^{a} ± 0.9	53.21^{a} ± 4.5	53.36^{a} ± 4.6
NFE**	47.25^{C} ± 3.5	58.15^{A} ± 3.6	59.30^{A} ± 1.8	54.67^{B} ± 5.1
NDF*	39.11^{b} ± 3.5	44.47^{a} ± 1.8	47.12^{a} ± 4.4	43.32^{a} ± 4.0
ADF*	29.82^{c} ± 4.3	37.37^{a} ± 2.0	36.61^{a} ± 5.3	34.04^{b} ± 5.3

* Means with different superscripts significantly differ ($P<0.05$).
** Means with different superscripts highly differ ($P<0.01$).

Maejo Int. J. Sci. Technol. **2009**, *3*(03), 371-378

Calculation of total digestible nutrients (TDN) from digestibility of nutrients shows that EMPR with different percentages of Leucaena leaves had higher average values of TDN than that of EMPR alone (Table 6) and thus the former can be used as roughage source for ruminants especially in the dry season. The variation of DE of the silages followed the same pattern as that of TDN.

Table 6. Total digestible nutrients (TDN) and digestible energy (DE) of ensiled mango peel + rice straw (EMPR) with or without Leucaena leaves

Item	TDN (% DM)	DE (Mcal / kg DM)
EMPR	45.63 $\pm$ 4.0	1.91 $\pm$ 0.5
EMPR + 5%LL	53.45 $\pm$ 3.2	2.08 $\pm$ 0.4
EMPR + 10%LL	56.53 $\pm$ 2.7	2.33 $\pm$ 0.6
EMPR + 15%LL	54.67 $\pm$ 3.6	2.16 $\pm$ 0.4

Conclusions

Mango by-products (peel and seed) from canning plants are found to be low in CP and DM content, while mango peel silage is higher in CP but lower in CF and ADF than fresh mango peel. The digestibility of nutrients (DM, OM, CP, CF, NFE, NDF and ADF) of ensiled mango peel with rice straw increases with increasing admixture of Leucaena leaves. Calculation of TDN from digestibility of nutrients shows that ensiled mango peel with different levels of Leucaena leaves has a higher average value of TDN than silage without Leucaena leaves.

In vitro digestibility shows that all forms of mango peel by-products can be used as cattle feed. Further study in cattle is needed to determine if ground mango seed is also acceptable as feed as in vitro results suggest.

Acknowledgement

This study was supported by a grant from the "Establishment of a Feeding Standard of Beef Cattle and Feedstuff Database for the Indochinese Peninsula Research Fund" of Japan International Research Centre for Agricultural Sciences.

References

1. J. A. Larrauri, I. Goni, N. Martin-Carron, P. Ruperez and F. Saura-Calixto, "Measurement of health-promoting properties in fruit dietary fibres: antioxidant capacity, fermentability and glucose retardation index", *J. Sci. Food Agric.*, **1999**, *71*, 515-519.

2. A. J. Omole, I. O. Ayodeji and M. A. Raji, "The potential of peels of mango, plantain, cocoyam and pawpaw as diets for growing snails (*Archachatina marginata*)", Livest. Res. Rural Dev., **2004,** *16*(12), paper 102.
3. B. G. Naik, Z. P. Rao, J. R. Prasad, P. V. V. S. Reddy and P. S. Reddy, "Performance of broilers influenced by incorporating mango (Mangifera indica) fruit pulp waste (MFPW) in their ration", *Indian J. Anim. Nutri.*, **2002**, *19*, 301-303.
4. Z. Naveen, J. R. Prasad and Z. P. Rao, "Chemical composition and in vitro dry matter digestibility of some fruit wastes", *Tamilnadu J. Vet. Anim. Sci.,* **2006**, *2*, 229-233.
5. AOAC, "Official Method of Analysis", 16th Edn., Association of Official Analysis Chemists, Gaithergurg, Maryland, **1998**.
6. H. K. Goering and P. J. Van Soest, "Forage fiber analysis (apparatus, reagents, procedure, and some applications)", Agriculture Handbook, No.370, USDA-ARS, Washington, DC., **1970**.
7. W. G. Pond, D. C. Church and K. R. Pond, "Basic Animal Nutrition and Feeding", 4th Edn., John Wiley and Sons, New York, **1995**.
8. R. G. D. Steel and J. H. Torrie, "Principles and Procedures of Statistics", 2nd Edn., McGraw-Hill, New York, **1980**.
9. SAS, "Statistical Analysis System User Guide: Version 6", 4th Edn., SAS Institute, Carry NC, **1994**.
10. A. O. Ojokoh, "Effect of fermentation on the chemical composition of mango (*Mangifera indica R*) peels", *Afri. J. Biotech.,* **2007**, *6*, 1979-1981.
11. T. Burjoom and B. Maneewan, "The survey on source and qualities of agricultural waste/by-products in Sansai, Doi Saket, Mae Rim, Mae Taeng districts, Chiang Mai province for its prospective use as raw material in animal feed composition", 9th Maejo University Annual Conference, **2008**, Chiang Mai, Thailand.
12. J. A., Elegbede, I. I. Achoba and H. Richard, "Nutrient composition of mango (*Mangifera indica*) seed kernel from Nigeria", *J. Food Biochem.*, **1996,** *19*, 391-398.
13. H. M. Shelton and J. L. Brewbaker, "*Leucaena leucocephala*—the most widely used forage tree legume", in "Forage Tree Legumes in Tropical Agriculture" (Ed. R. C. Gutteridge and H. M. Shelton), CAB International, Wallingford, **1994**, pp. 15-29.
14. G. Jaurena and G. Pichard, "Contribution of storage and structural polysaccharide to the fermentation process and nutritive value of *Leucaena leucocephala* ensiled alone or mixed with cereal grain", *Anim. Feed Sci. Technol.,* **2001**, *92*, 159-173.
15. N. E. Geerts, D. L. De Brabander, J. M. Vanancker, J. L. De Boever and S. M Botterman, "Milk urea concentration as affected by complete diet feeding and protein balance in the rumen of dairy cattle", *Livest. Prod. Sci.,* **2004**, *85*, 263-273.

Maejo Int. J. Sci. Technol. **2009**, *3*(03), 379-387

Maejo International

Journal of Science and Technology

ISSN 1905-7873

Available online at www.mijst.mju.ac.th

Full Paper

Production of *Spirulina platensis* using dry chicken manure supplemented with urea and sodium bicarbonate

Thepparath Ungsethaphand [1,3,*], Yuwadee Peerapornpisal [2] and Niwoot Whangchai [3]

[1] Biotechnology Program, Graduate School, Chiang Mai University, Chiang Mai 50200, Thailand

[2] Department of Biology, Faculty of Science, Chiang Mai University, Chiang Mai 50200, Thailand

[3] Faculty of Fisheries Technology and Aquatic Resources, Maejo University, Chiang Mai 50290, Thailand

* Corresponding author, e-mail: thorn@mju.ac.th

Received: 18 May 2009 / Accepted: 14 October 2009 / Published: 19 October 2009

Abstract: The cyanobacterium *Spirulina platensis* is an attractive source of valuable protein for both human and animal consumption. The conventional nitrogen source for *S. platensis* is nitrate. However, recent research has evaluated the potential of using animal waste as a low-cost nitrogen source. In this work, the cultivation of *S. platensis* was done using dry chicken manure (DCM), collected from a closed-system poultry house, as nitrogen source. The experiment was carried out in open concrete tanks with 100 litres of culture medium and an initial biomass concentration of 0.5 g/L. The culture media were prepared to test the effect of unsupplemented DCM, DCM supplemented with 2.0 mg/L of urea (DCM+U), and/or 40 mg/L of sodium bicarbonate (DCM+U+B or DCM+B). The best cellular growth and highest protein production were observed for *S. platensis* in the biomass harvested from the culture medium containing DCM supplemented with 2.0 mg/L of urea (DCM+U).

Keywords: *Spirulina*, chicken manure, urea, bicarbonate, nitrogen source

Introduction

Egg-laying chicken production is the top farm commodity in many areas of Thailand. Poultry producers must periodically clean their poultry houses to promote the animals' health and limit the build-up of wet manure [1]. It is well known that poultry manure can be used as an alternative source of fertiliser in fish ponds. It is economically beneficial to use chicken manure rather than chemical fertiliser, and this also reduces the environmental pollution of manure caused by inappropriate disposal

Maejo Int. J. Sci. Technol. **2009**, *3*(03), 379-387

[2]. Many chicken producers have integrated poultry houses with fish ponds to grow fish using poultry litter (manure plus spilled feed) without additional cost. Unfortunately, after the crisis of bird flu the Thai government has promoted the closed-system poultry house and discouraged integrated farming with chickens above fish ponds.

One of the possible acceptable ways to utilise farm manure is in the production of microalgae. The cyanobacterium *Spirulina platensis* is an attractive source of valuable proteins for both human and animal consumption. The conventional nitrogen source for *S. platensis* is nitrate. However, recent research has evaluated the potential of using animal waste as a low-cost nitrogen source [3-5]. These studies were focused mainly on the production of *Spirulina* from swine manure and waste, and there is only limited information available on utilisation of poultry manure. More recently, Ungsethaphand et al.[6] has shown that dry chicken manure (DCM) can supply the necessary nutrients for the culture of *S. platensis*. Costa et al. [7] reported that the addition of 1.125 mg/L of urea to Mangueira Lagoon water is beneficial to the growth of *S. platensis.* In the alkaline culture medium, urea is hydrolysed to ammonia, which can be toxic to microalgae in high concentration. However, urea addition by fed-batch process makes it possible to replace KNO_3 as nitrogen source in the culture media. On the other hand, the work on an industrial scale with addition of a constant amount of urea should be simpler [8]. The use of urea as a cheap source of ammonia could then be an interesting alternative to the traditional nitrate-based *S. platensis* culture.

Binaghi et al. [9] reported that *S. platensis* is a filamentous cyanobacterium able to form large colonies in surface water containing a high level of carbonates and bicarbonates. Among the nutrients of cultivation media, the inorganic carbon source is primarily responsible for the alkaline condition and is preferentially assimilated by cyanobacteria in the form of bicarbonate [10]. A concentration of bicarbonate lower than 0.1 M decreases the growth rate of *S. platensis* [11].

The aim of this work is to study the production of *S. platensis* using DCM supplemented with urea and sodium bicarbonate by fed-batch addition. The chemical composition of the *S. platensis* biomass is also investigated.

Materials and Methods

Microorganism

Spirulina platensis was obtained from the Faculty of Fisheries Technology and Aquatic Resources, Maejo University. The culture was routinely maintained in modified Zarrouk liquid medium [12].

Culture medium

The culture medium used was 2.0 kg of dry egg-laying chicken manure (DCM) collected from a closed-system house. The manure was suspended in 100 L of aerated tap water for 7 days before being sieved through a 30-mesh Tylor net. Sodium metabisulfite (5 mg/L) was added to prevent microbial contamination. After 24 h, 8.5 g/L of sodium bicarbonate was added before the beginning of the experiment.

Maejo Int. J. Sci. Technol. **2009**, *3*(03), 379-387

Experiment

The addition of urea and sodium bicarbonate to the culture was done by a fed-batch process. The nutrients were added in an aqueous solution to replace daily water evaporation using the following protocol:

(i) DCM (control): tab water was added every 24 h;
(ii) DCM+U: urea (2.0 mg/L) was added every 24 h;
(iii) DCM+B: sodium bicarbonate (40 mg/L) was every 24 h;
(iv) DCM+U+B: urea (2.0 mg/L) and sodium bicarbonate (40 mg/L) were added every 24 h.

Culture conditions

The experiment was carried out in open concrete tanks under daylight in a greenhouse and 27.8-34.3 ^{o}C temperature range. The depth of the cultures was always 15 cm with 100 L of culture medium. Each culture was agitated by aeration at a flux of 20 L/h provided by a diaphragm pump. The initial pH was adjusted to 9.5 ± 0.2 with 6M NaOH.

Inoculation

The inoculum was obtained by liquid culturing using a modified Zarrouk medium [12] at 32^{o}C with initial pH of 9.2. Cultivation was done in 500-ml Erlenmeyer flasks subjected to a moderate mixing provided by a small air pump operating at a rate of 0.023 L/min and illuminated by fluorescent lamps (36 w) in cycle of 12 h of light and 12 h of darkness. After seven days, the culture reached it exponential phase and the cells were harvested by filtration through a 62-µm mesh and washed thrice with a 0.8% NaCl solution to completely remove sodium nitrate. The cells were resuspended in the modified Zarrouk medium without nitrate and used as inoculum (500 mg/L concentration).

Analytical methods

The culture pH and temperature were monitored daily with a pH metre. Ammonia-nitrogen was determined by using standard phenate method described by APHA [13] and chlorophyll *a* was determined by measuring absorbances at 665 and 750 nm [13].

Biomass concentration was determined on alternate days by optical density (OD) determination at 560 nm (Hach instrument, Model DR2000) to produce a standard curve relating dry weight of *S. platensis* biomass to OD. This standard curve was subsequently used to determine the biomass of individual samples [14].

The dry weight of biomass was determined by filtration of sample (25 ml) through Whatman filter paper No.4 after washing with 3.0 N acetic acid to eliminate salt precipitate. The biomass obtained was then washed twice with 0.8% saline solution and dried at 80^{o}C for 4 h according to Olguin et al. [5].

The chemical composition of the dried biomass was determined according to AOAC methods [15]. Crude protein was determined by micro Kjeldahl method; total lipid by Soxhlet solvent extraction; and ash by combustion at 550^{o}C for 12 h.

Maejo Int. J. Sci. Technol. **2009**, *3*(03), 379-387

Statistical analysis

One-way ANOVA was used to test the effect of the culture media. Tukey's test was also applied to compare the means when a significance difference ($p < 0.05$) was detected by ANOVA.

Results and Discussion

The maximum cell concentration and chlorophyll *a* content were significantly different among treatments. The growth results (Tables 1-2) showed highest cellular concentration, chlorophyll *a* content and protein content of *S. platensis* when DCM+U medium was used. The addition of bicarbonate (DCM+B) gave only a slight increase in biomass while in DCM+U+B (added urea and bicarbonate) medium, there was actually a decrease in biomass. These results agree with those of Costa et al. [7], who found that the addition of urea and bicarbonate in Mangueira Lagoon water caused a decrease of biomass of *Spirulina*. Urea utilisation as a nitrogen source provides an energetic gain due to its spontaneous hydrolysis in the alkaline medium to ammonia, which is easily assimilated by *Spirulina* [8]. Costa et al. [7] reported that the highest biomass values were obtained in the treatment with 1.125 mg/l of added urea without addition of sodium bicarbonate. Danesi et al. [8] has shown that the use of urea as nitrogen source in *S. platensis* cultivation causes an increase in the biomass production as well as chlorophyll content. The DCM+U medium thus seems to be more appropriate to *S. platensis* cultivation for high-protein biomass utilisation in food and feed [16].

Table 1. Results of the cultivation of *S. platensis* grown on different media containing DCM

	DCM	DCM+U	DCM+B	DCM+U+B
Cells (mg/L dw) [a]	414.2±2.5 ^{a}	457.5±6.2 ^{b}	429.7±4.2 ^{ab}	409.7±2.9 ^{a}
Time (days) [b]	18	20	18	18
Chlorophyll *a* (mg/g)	3.02±0.04 ^{a}	3.33±0.08 ^{b}	3.07±0.07 ^{ab}	3.33±0.12 ^{b}

[a] Maximum cell concentration

[b] Time of achieving maximum cell concentration

Note: Means ± se in row with different superscripts are statistically different at significant level of 0.05 when compared by Tukey's test.

Table 2. Chemical composition (% dry weight) of *S. platensis* grown on different DCM media

	DCM	DCM+U	DCM+B	DCM+U+B
Protein	35.55±2.26 ^{a}	53.32±2.24 ^{b}	37.84±1.59 ^{a}	52.23±0.83 ^{b}
Lipid	4.86±0.99	4.53±0.20	2.64±0.50	3.92±1.07
Carbohydrate	38.89±3.44 ^{a}	20.77±3.91 ^{b}	40.87±0.86 ^{a}	25.04±2.05 ^{b}
Mineral	18.67±1.27	19.49±1.73	17.57±1.30	16.73±1.06
Fibre	2.02±0.67	1.89±0.10	1.08±0.02	2.07±0.50
Moisture	11.53±1.38	11.22±0.37	13.58±0.86	11.73±1.05

Note: Means ± se in row with the different superscripts are statistically different at a significant level of 0.05 when compared by Tukey's test.

Maejo Int. J. Sci. Technol. **2009**, *3*(03), 379-387

Figure 1 shows an apparent relationship between biomass concentration and chlorophyll *a* content. This observation is in agreement with the results reported by Rangel-Yagui et al. [17] who also observed similar relationship between urea addition and the production of biomass with higher chlorophyll content. Piorreck et al. [18] reported lower concentration of chlorophyll obtained from cultivation carried out with limited nitrogen concentration. The shading effect [17] on the other hand may have contributed to a higher concentration of chlorophyll *a* observed in the biomass obtained from cultivation with higher added nitrogen at a fixed light intensity. This yields higher a cellular concentration, which can generate a higher chlorophyll *a* biosynthesis rate in order to increase the efficiency of photon capture and thus compensate for the reduction of light intensity for the cells not located at the surface [19].

The significantly higher protein content was observed in the biomass of DCM+U and DCM+U+B media (Table 2). The increase in protein content was apparently due to the nitrogen level in the medium. Piorreck et al. [18] reported that increasing the nitrogen level in the nutrient medium leads to an increase in the biomass and protein content of *Spirulina.* Nitrogen is required for the synthesis of amino acids which make up proteins and other cellular components. Therefore, a lower urea concentration correspondingly gave a lower value of cellular proteins [20].

The lipid content was not significantly influenced by the different treatments (Table 2). According to Piorreck et al.[18], blue-green algae do not show any significant change in the percentage and composition of their lipids and fatty acids when grown at different concentrations of nitrogen. Danesi et al. [8] also verified that the lipid content in the *S. platensis* biomass is not influenced by the nitrogen source used.

According to Walach et al. [21], higher quantities of carbohydrates are synthesised when nitrogen availability is decreased while carbon availability is constant. These two factors together may explain the significantly higher production of carbohydrate in DCM and DCM+B treatments. Nitrogen deficiency has been found to stimulate the synthesis of all carbohydrate fractions (intracellular, capsular and soluble) in a cyanobacterium [22].

The temperature variation in this experiment (Figure 2) during the cultivation was close to the optimum range reported for *S. platensis* cultivation [8,23]. The pH change (Figure 3) did not show significant differences between the treatments. The cyanobacterium grew effectively in the medium leading to a progressive pH increase, in agreement with many authors [9,16,17]. This observation can be correlated with the carbon-source consumption. The bicarbonate ions, for example, are assimilated by the cyanobacteria and subsequently converted into carbon dioxide and carbonate. The carbon dioxide is utilised in photosynthesis and the carbonate is excreted into the medium. The increase in the pH of the system is due to the shift of the bicarbonate-carbonate equilibrium towards the carbonate [17]. No external contamination was detected, most likely because of the high alkalinity of the culture medium.

Maejo Int. J. Sci. Technol. **2009**, *3*(03), 379-387

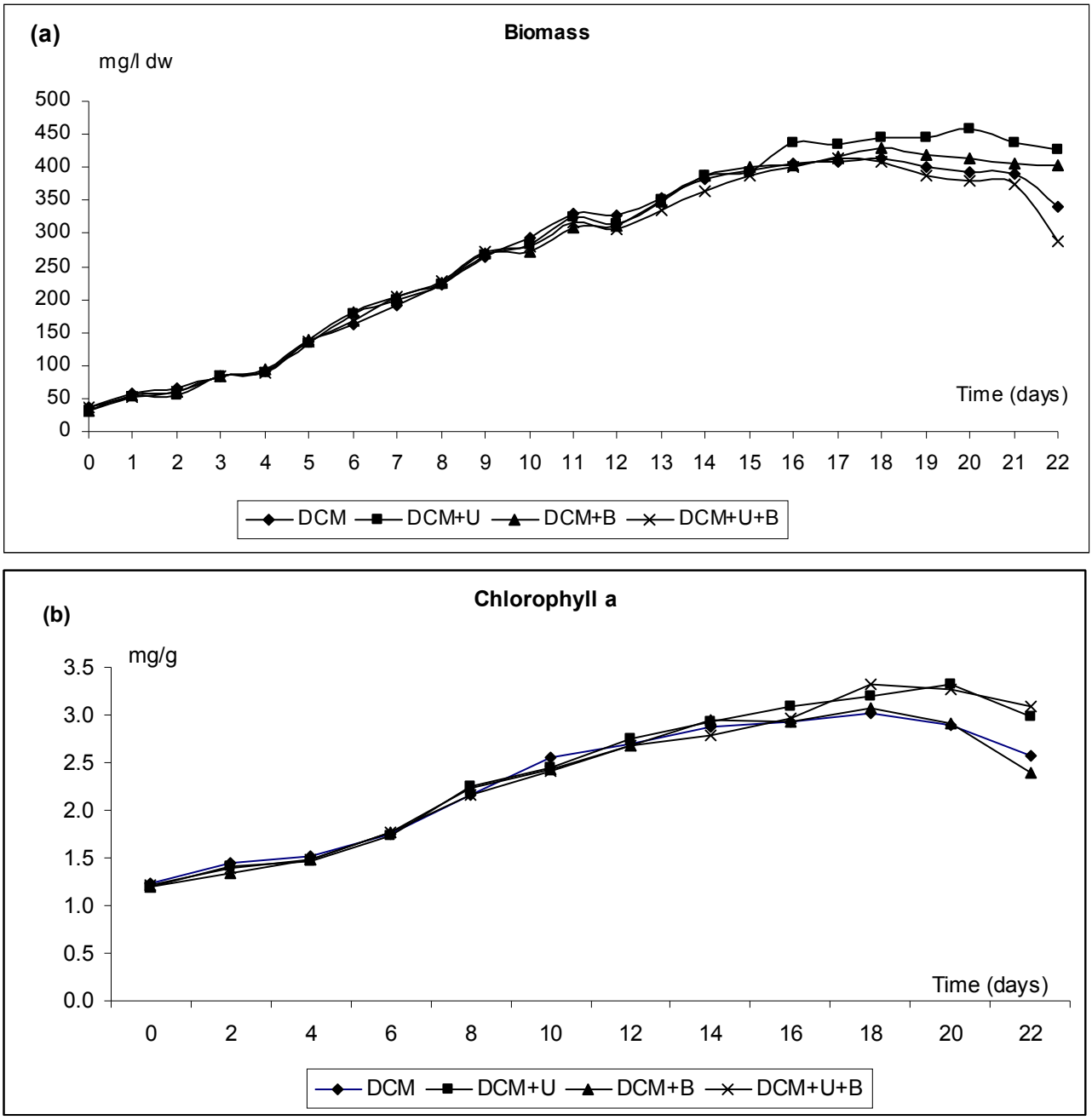

Figure 1. Profiles of biomass concentration (a) and chlorophyll *a* content (b) during the cultivation of *S. platensis* grown in different DCM media

Maejo Int. J. Sci. Technol. **2009**, *3*(03), 379-387

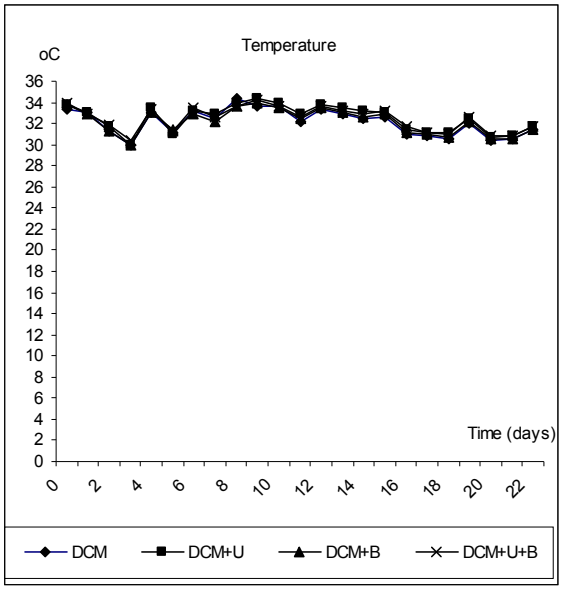

Figure 2. Temperature variation during the cultivation of *S. platensis* grown on different DCM media

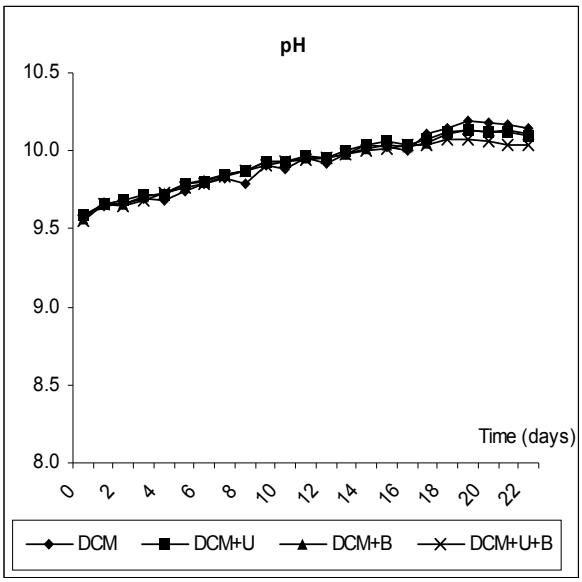

Figure 3. pH of culture during the cultivation of *S. platensis* grown on different DCM media

Conclusions

The fed-batch cultivation of *S. platensis* is feasible using dry chicken manure (2.0 kg/100 L) in the culture medium supplemented with urea (2.0 mg/L). This culture medium resulted in the best cellular growth and highest protein content. The potential of reducing production cost with the medium in a large-scale cultivation is also apparent.

Acknowledgement

Financial support from the Graduate School of Chiang Mai University in the form of a Ph.D fellowship (to T. U.) is gratefully acknowledged.

References

1. K. R. Sistani, G. E. Brink, S. L. McGowen, D. E. Rowe and J. L. Oldham, "Characterization of broiler cake and broiler litter, the by-products of two management practices", *Bioresour. Technol.*, **2003**, *90*, 27-32.
2. M. Z. Dong, X. Z. Hao, Y. J. Wang, Y. H. Dong and L. Cang, "Copper and Zn uptake by radish and pakchoi as affected by application of livestock and poultry manures", *Chemosphere*, **2005,** *59*, 157-175.

3. M. Gantar, Z. Obreht and B. dalmaeijia, "Nutrient removal and algal succession during the growth of *Spirulina platensis* and *Scenedesmus quadricanda* on swine wastewater", *Bioresour. Technol*., **1991**, *36*, 167-171.
4. R. O. Canizares, L. Rivas, C. Montes and A. R. Dominguez, "Aerated swine-wastewater treatment with K-Carrageenan-immobilized *Spirulina maxima*", *Bioresour. Technol.*, **1994,** *47*, 89-91.
5. E. J. Olguin, S. Galicia, O. Angulo-Guerrero and E. Hernandez, "The effect of low light flux and nitrogen deficiency on the chemical composition of *Spirulina* sp. (*Arthrospire*) grown on digested pig waste", *Bioresour. Technol.*, **2001**, *77*, 19-24.
6. T. Ungsethaphand, Y. Peerapornpisal, N. Whangchai and U. Sardsud, "Productivity and chemical composition of *Spirulina platensis* using dry chicken manure as nitrogen sources", Proceedings of the 19th Annual Meeting of the Thai Society for Biotechnology, **2007**, Bangkok, Thailand, pp. 43-48.
7. J. A. V. Costa, L. M. Colla and P. F. D. Filho, "Improving *Spirulina platensis* biomass yield using a fed-batch process", *Bioresour. Technol*, **2004**, *92*, 237-241.
8. E. E. G. Danesi, C. O. Rangel-Yagui, J. C. M. Carvalho and S. Sato, "An investigation of the effect of replacing nitrate by urea in the growth and production of chlorophyll by *Spirulina platensis*", *Biomass Bioenergy*, **2002**, *23*, 261-269.
9. L. Binaghi, A. Del Borghi, A. Lodi, A. Converti and M. Del Borghi, "Batch and fed-batch uptake of carbon dioxide by *Spirulina platensis*", *Process Biochem.*, **2003**, *38*, 1341-1346.
10. E. Huertas, O. Montero and L. M. Lubian, "Effect of dissolved inorganic carbon availability on growth, nutrient uptake and chlorophyll fluorescence of two species of marine microalgae", *Aquacult. Eng.*, **2000**, *22*, 181-187.
11. A. Richmond, S. Karg and S. Boussiba, "Effects of bicarbonate and carbon dioxide on the competition between *Chlorella vulgaris* and *Spirulina platensis*", *Plant Cell Physiol.*, **1982**, *23*, 1411-1417.
12. E. A. George, "Culture Centre of Algal and Protozoa. List of Strains 1976", 3rd Edn., Institute of Terrestrial Ecology, Natural Environment Research Council, Cambridge, **1976**.
13. APHA, "Standard Methods for the Examination of Water and Wastewater", 17th Edn., American Water Works Association and Water Pollution Control Federation, New York, **1989**.
14. A. Leduy and N. Therien, "An improved method for optical density measurement of the semi-microscopic blue algal *Spirulina maxima*", *Biotechnol. Bioeng.*, **1977**, *19*, 1219-1224.
15. AOAC, "Official Methods of Analysis", 14th Edn., Association of Official Analytical Chemists, Washington, DC, **1984**.
16. L. H. Pelizer, E. D .G. Danesi, C. de O. Rangel, C. E. N. Sassano, J. C. M. Carvalho, S. Sato and I. O. Moraes, "Influence of inoculum age and concentration in *Spirulina platensis* cultivation", *J. Food Eng.*, **2003**, *56*, 371-375.
17. C. de O. Rangel-Yagui, , E. D. G. Danesi, J. C. M. Carvalho and S. Sato, "Chlorophyll production from *Spirulina platensis*: Cultivation with urea addition by fed-batch process", *Bioresour. Technol*., **2004**, *92*, 133-141.

Maejo Int. J. Sci. Technol. **2009**, *3*(03), 379-387

18. M. Piorreck, K. H. Baasch and P. Pohl, "Biomass production, total protein, chlorophyll, lipids and fatty acids of freshwater green and blue-green algae under different nitrogen regimes", *Phytochem.*, **1984**, *23*, 207-216.
19. G. A. F. Hendry, "Chlorophyll and chlorophyll derivatives", in: "Natural Food Colorants" (Ed. G. A. F. Hendry and J. D. Houghton), Blackil Academic Professional, London, **1996**, pp.131-155.
20. C. M. Colla, C. O. R. Reinehr, C. Rcichert and J. A. V. Costa, "Production of biomass and nutraceutical compound by *Spirulina platensis* under different temperature and nitrogen regimes", *Bioresour. Technol.*, **2007,** *98*, 1489-1493.
21. M. R. Walach, M. Bazin and J. Pirt, "Computer control of carbon-nitrogen ratio in *Spirulina platensis*", *Biotechnol. Bioeng.*, **1984**, *29*, 520-528.
22. O. Fresnedo, O. and J. L. Serra, "Effect of nitrogen starvation on the biochemistry of *Phormidium laminosum* (Cyanophyceae)", *J. Phycol.*, **1992**, *28*, 786-793.
23. L. D. Zanchez-Luna, A. Converti, G. C. Tonini, S. Sato and J. C. M. Carvalho, "Continuous and pulse feeding of urea as a nitrogen source in fed-batch cultivation of *Spirulina platensis*", *Aquacult. Eng.*, **2004**, *31*, 237-245.

Maejo Int. J. Sci. Technol. **2009**, *3*(03), 388-399

Maejo International

Journal of Science and Technology

ISSN 1905-7873

Available online at www.mijst.mju.ac.th

Full Paper

Development of Job's-tears ice cream recipe

Waraluck Khongjeamsiri, Wiwat Wangcharoen*, Suthaya Pimpilai and Wichittra Daengprok

Faculty of Engineering and Agricultural Industry, Maejo University, Chiang Mai 50290, Thailand

*Corresponding author, e-mail: wiwat@mju.ac.th

Received: 29 May 2009 / Accepted: 9 October 2009 / Published: 20 October 2009

Abstract: Job's tears ice cream recipe was developed by varying proportions of Job's tears, sucrose, salt and coconut milk. Product positioning mapping was used to identify the sensory attributes that were drivers of preference, which appeared to be sweetness, smoothness, richness, and coconut milk and Job's-tears flavours of the product. Cluster analysis was used to differentiate consumers by their preference direction. Nutritional composition, antioxidant capacity and total phenolic content of the final product were also determined.

Key words: Job's-tears, ice cream, antioxidant capacity, product positioning map, cluster analysis

Introduction

Ice cream is a frozen product made from a combination of dairy products and one or more of the following ingredients: eggs, sugar, dextrose, corn syrup and honey, with or without flavouring and colouring, and with or without edible gelatin or vegetable stabiliser, and in the manufacture of which freezing has been accomplished by agitation of the ingredients [1]. The body and texture of ice cream is affected by many factors such as fat content, milk solid not fat content, type and relative amount of sweetening agent, total solid content, type and amount of stabiliser, temperature history of the ingredients, heat treatment of the mixture, temperature and pressure of homogenisation, rate of freezing and hardening, amount of overrun, and temperature fluctuation during storage and delivery [2]. The quantity of ingredients, including fat, milk solid not fat, sweeteners, stabilisers, and emulsifiers, is used for general classification of ice cream and related products [1, 3-5]. In many countries non-dairy fat is

Maejo Int. J. Sci. Technol. **2009**, *3*(03), 388-399

not permitted in ice cream and products made with non-dairy fat must be described by an alternative name. European Community countries permit the use of non-dairy fat but they apply the term "dairy" ice cream where all the fat is milk fat [4].

In Thailand, commercial ice cream products are now legally controlled by Ministry of Public Health Announcements Issue 222 (2001) and 257 (2002), which classify products into 5 categories, viz. dairy ice cream, modified fat ice cream, mixed ice cream, ice cream in liquid or dried or powder forms, and sweet and cold ice cream from non-dairy products [6-7]. Ice cream produced from non-dairy products is easily available in both commercialised and home-made styles. Coconut milk, obtained by squeezing coconut flesh that has been soaked in water, is a well-known raw material used for replacing dairy products in ice cream production [8]. Ice cream made from other liquid foods has been developed such as soy milk ice cream, brown rice ice cream [9-10] and fruit ice cream [11].

Job's-tears (*Coix lacryma-jobi*) is a kind of cereal used for both food [12-13] and Chinese and Indian medicine [14-16], although it is not widely consumed in Thailand. The potential to develop Job's-tears-based ice cream has been investigated by us [17]. Thus, this work is aimed to develop Job's-tears-based ice cream recipe which is accepted by the consumers as well as potentially healthful.

Materials and Methods

Ingredients

All ingredients used were commercial products. These were Job's-tears (Rai Tip brand), sucrose (Mitr Phol brand), salt (Prung Thip brand), coconut milk (Chaokoh brand) and glucose syrup (5 Star Elephant brand).

Study on optimal Job's-tears content

Job's-tears seeds were washed, soaked in water for 2 hours, boiled for 40 minutes and blended with water in a ratio of 1:2 (boiled seeds:water) by means of a blender. The blended mixture contained 13-15 % (w/w) of initial total solid (dry weight), which was subsequently adjusted by water addition to four concentrations, i.e. 6, 8, 10 and 12 % (w/w), used for preparing ice cream. Coconut milk, glucose syrup, sucrose and salt at 50, 32, 12 and 0.8 % (w/w) respectively of each diluted mixture were added. The concoction was mixed with the blender and heated at 80° C for 15 min, then cooled rapidly and stored overnight in the refrigerator. It was made into ice cream by means of a compressor ice cream maker (JCS Technic Line Co., Ltd.). The ice cream was packed and kept in the freezer at least 1 week before testing.

Study on concentration of sucrose and salt

The concentration of sucrose in the ice cream was varied at 12 and 20 % of the blended Job's-tears mixture while that of salt was varied at 0.4 and 0.8 %.

Study on quantity of coconut milk

The coconut milk quantity in the ice cream was varied at 50, 55, 60 and 65 % of the blended Job's-tears mixture.

Maejo Int. J. Sci. Technol. **2009**, *3*(03), 388-399

Sensory property measurement

One hundred consumers were requested to evaluate the sensory attributes of the products, viz. hardness, sweetness, saltiness, Job's-tears flavour, coconut milk flavour, richness, smoothness and aftertaste, together with their overall preference on each product by scoring each item on a scale of 1 to 10 (least to most).

Chemical analysis of the final product

Nutritional data, antioxidant capacity and total phenolic content of the final product were determined. Moisture, protein, fat, ash and crude fibre content were determined in accordance with AOAC methods [18], and carbohydrate content was calculated by subtraction. Antioxidant capacity was evaluated by 3 different methods, namely ferric reducing/antioxidative power (FRAP) assay [19], improved ABTS radical cation decolorisation assay [20] and DPPH free radical scavenging activity [21]. Total phenolic content was analysed by Folin-Ciocalteau micro method [22].

For the analysis of antioxidant capacity and total phenolic content, 2 grams of sample was added with 10 ml of 57% ethanol. The extraction was done by using a vortex mixer for 60 s. The mixture was filtered by Whatman No 1 filter paper and the filtrate was used as the extract sample.

Briefly of FRAP assay, 6 ml of working FRAP reagent (0.1 M acetate buffer:0.02 M $FeCl_3$:0.01 M TPTZ = 10:1:1) prepared daily was mixed with 20 µl of the extract sample. The absorbance at 593 nm was recorded after a 30-min incubation at 37 °C.

For ABTS assay, the $ABTS^+$ was produced by reacting 7 mM ABTS stock solution with 2.45 mM postassium persulphate (final concentration) and allowing the mixture to stand in the dark at room temperature for 12-16 hours before use. The $ABTS^+$ solution was diluted with deionised water and 95 % ethanol (1:1) to an absorbance of 0.70 ($\pm$ 0.02) at 734 nm. Twenty µl of the extract sample was mixed with 6 ml of the diluted $ABTS^+$ solution. The decrease of absorbance was recorded at 1 min after mixing.

In the case of DPPH assay, 400 µl of the extract sample was diluted to 5.4 ml using deionised water and 95 % ethanol (1:1) before 0.6 ml of 0.8 mM DPPH solution was added and the mixture shaken vigorously. The decrease of absorbance was recorded at 1 min after mixing. Vitamin C (0-40 µg) were used as standard, and results were reported as mg vitamin C equivalent per 100 grams of product.

To determine total phenolic content, 60 µl of the extract sample was diluted with deionised water to 4.8 ml before 300 µl of Folin-Ciocalteau reagent was added with shaking. After that, 900 µl of 20% sodium carbonate was added with mixing. The mixture was left at 40° C for 30 min before reading of the absorbance at 765 nm. Gallic acid (0-50 µg) was used as standard and results were reported as mg gallic acid equivalent per 100 grams of product.

Statistical analysis

Sensory-attribute rating scores of products in each step were reduced by principal component analysis (PCA) and its result was used to create the product positioning map for identifying sensory attributes that were drivers of preference. Overall preference data were analysed by cluster analysis to find out the different directions of consumer preference. Analysis of variance and Duncan's new

Maejo Int. J. Sci. Technol. **2009**, *3*(03), 388-399

multiple range test were applied to differentiate products by consumer preference. All statistical analysis was done by SPSS 16.0 Family.

Results and Discussion

Study on optimal Job's-tears content

Sensory attributes of ice cream produced from Job's-tears at 6, 8, 10, and 12 % are reduced to 3 principal components (PCs) with 52.1% variance explained (Figure 1). Product positioning maps created from 3 PCs show that products with more Job's-tears total solid were harder and stronger in Job's-tears flavour and aftertaste while those with less total solid were smoother. In addition, smoothness, richness, coconut milk flavour, sweetness and saltiness can be considered as drivers of preference for this step because their vectors are in the same direction of the overall preference vector, especially for smoothness (Figure 1). The smoothness of ice cream is not only due to ingredients but also to the process used in the manufacture [1]. Fats, sweeteners and stabilisers are ingredients influencing the texture of ice cream [2,4,5]. Temperature and pressure of homogenisation should be optimised while freezing and hardening processes have to be very rapid to provide small ice crystals and a smooth body of ice cream [2,3,5]. However, only used ingredients were studied to improve product acceptance in this experiment. The amounts of sugar, salt and coconut milk therefore were varied in further steps.

From 100 consumers, the mean overall preference scores of products with 6 and 8 % Job's-tears were significantly higher than those with 10 and 12 %. However, cluster analysis result show two different directions of consumer preference. Sixty consumers preferred the product with 8 % Job's-tears while forty preferred that with 12 % (Table 1). Thus, the former composition of Job's-tears was selected for producing the ice cream in the next step.

Table 1. Overall preference scores (mean $\pm$ standard deviation) of ice cream produced from 6, 8, 10, and 12 % Job's-tears

Content of Job's tears total solid	Whole consumer (n = 100)	Consumer group 1 (n_1 = 60)	Consumer group 2 (n_2 = 40)
6 % Total solid	$5.31^{a} \pm 2.13$	$5.65^{b} \pm 1.99$	$4.80^{b} \pm 2.25$
8 % Total solid	$5.59^{a} \pm 2.13$	$6.58^{a} \pm 1.79$	$4.10^{b} \pm 1.69$
10 % Total solid	$4.34^{b} \pm 2.07$	$3.89^{c} \pm 1.94$	$5.03^{b} \pm 2.10$
12 % Total solid	$4.66^{b} \pm 2.02$	$3.62^{c} \pm 1.57$	$6.20^{a} \pm 1.59$

Note : Means with different letters in the same column were significantly different ($p \leq 0.05$).

Maejo Int. J. Sci. Technol. **2009**, *3*(03), 388-399

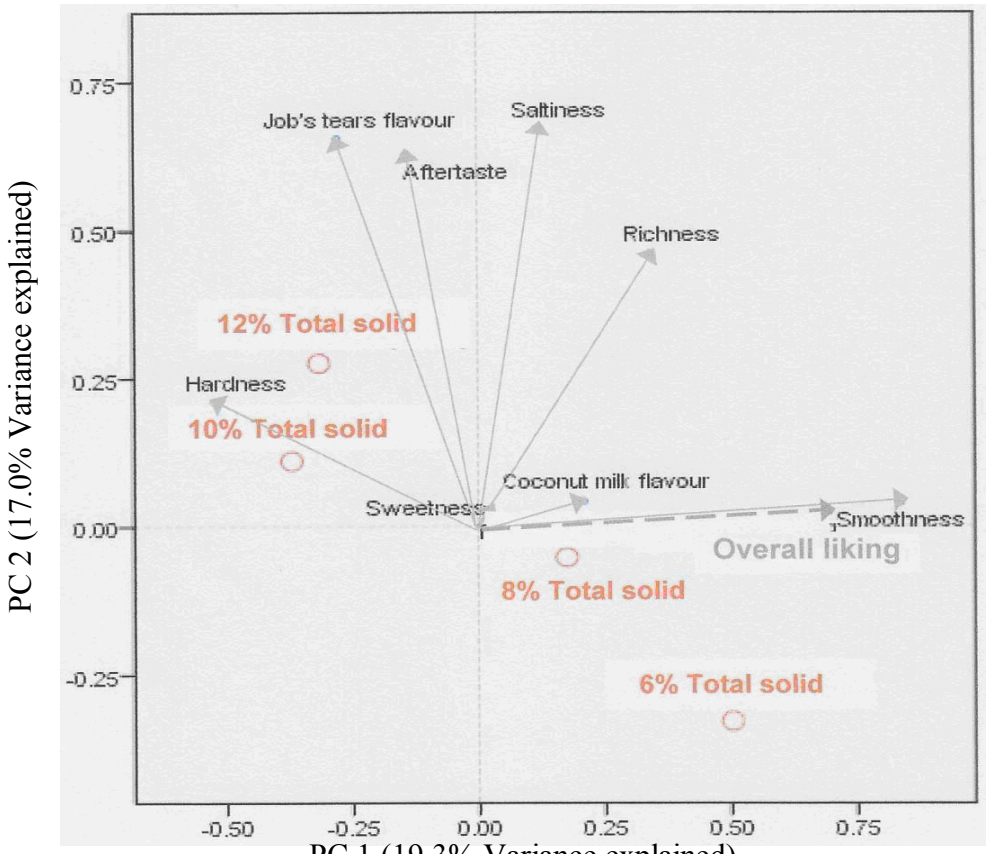

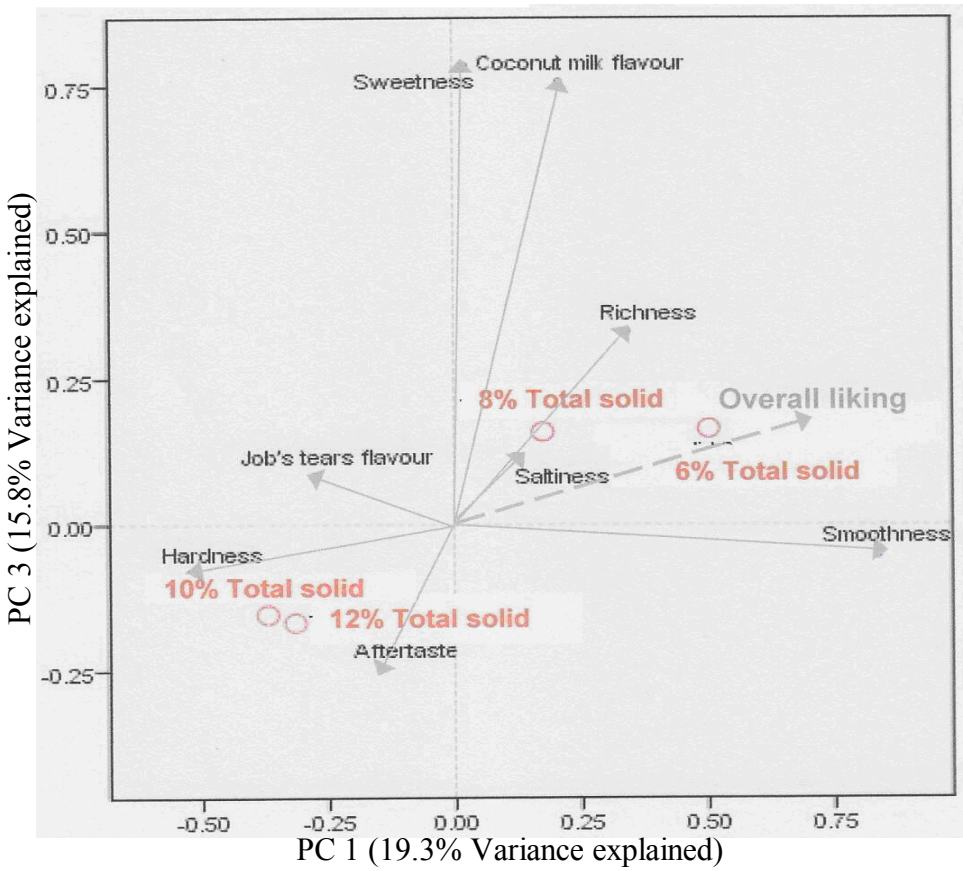

Figure 1. Product positioning maps of ice cream produced from 6, 8, 10 and 12 % Job's tears

Maejo Int. J. Sci. Technol. **2009**, *3*(03), 388-399

Study on concentration of sucrose and salt

Sucrose and salt were studied together because both of them affect the taste of the products. Sensory attributes from sucrose and salt were reduced to 3 PCs with 55.0 % variance explained. From their product positioning maps (Figure 2), the sweetness of products with 12 and 20 % sucrose was reduced by increasing the quantity of salt, while the saltiness of products with 0.8% salt was also reduced by the amount of sucrose added. This interaction is a physiological factor called suppression [23]. Drivers of product preference in this step seem to be smoothness, richness, coconut milk flavour and sweetness because their vectors are in the same direction of the overall preference vector. In this step, saltiness was not the driver of preference anymore because saltiness perception was suppressed by sweetness, and sweetness is one of the desired tastes for ice cream [5].

The mean overall preference scores from 100 consumers show that the products with 20% sucrose were preferred to the ones with 12 % sucrose (Table 2). However, different directions of consumer preference were found by cluster analysis. Sixty-five consumers preferred sweet products (20% sucrose + 0.4% salt > 20% sucrose + 0.8% salt > 12% sucrose + 0.4% salt > 12% sucrose + 0.8% salt), while 35 consumers preferred salty products (20% sucrose + 0.8% salt ≥ 12% sucrose + 0.8% salt ≥ 12% sucrose + 0.4% salt > 20% sucrose + 0.4% salt). Therefore, 20% sucrose and 0.4% salt were selected for producing Job's-tears ice cream in the next step.

Table 2. Overall preference scores (mean ± standard deviation) of ice cream produced from 12 and 20 % sucrose and 0.4 and 0.8 % salt

Sugar and salt concentration of product	Whole consumer (n = 100)	Consumer group 1 (n_1 = 65)	Consumer group 2 (n_2 = 35)
12 % Sucrose + 0.4 % Salt	4.85^{b} ± 2.27	4.86^{c} ± 2.15	4.83^{b} ± 2.51
12 % Sucrose + 0.8 % Salt	4.58^{b} ± 2.21	4.31^{d} ± 2.19	5.09^{ab} ± 2.23
20 % Sucrose + 0.4 % Salt	5.90^{a} ± 2.33	7.13^{a} ± 1.68	3.63^{c} ± 1.52
20 % Sucrose + 0.8 % Salt	5.61^{a} ± 2.18	5.49^{b} ± 2.16	5.83^{a} ± 2.23

Note : Means with different letters in the same column were significantly different ($p \leq 0.05$).

Maejo Int. J. Sci. Technol. **2009**, *3*(03), 388-399

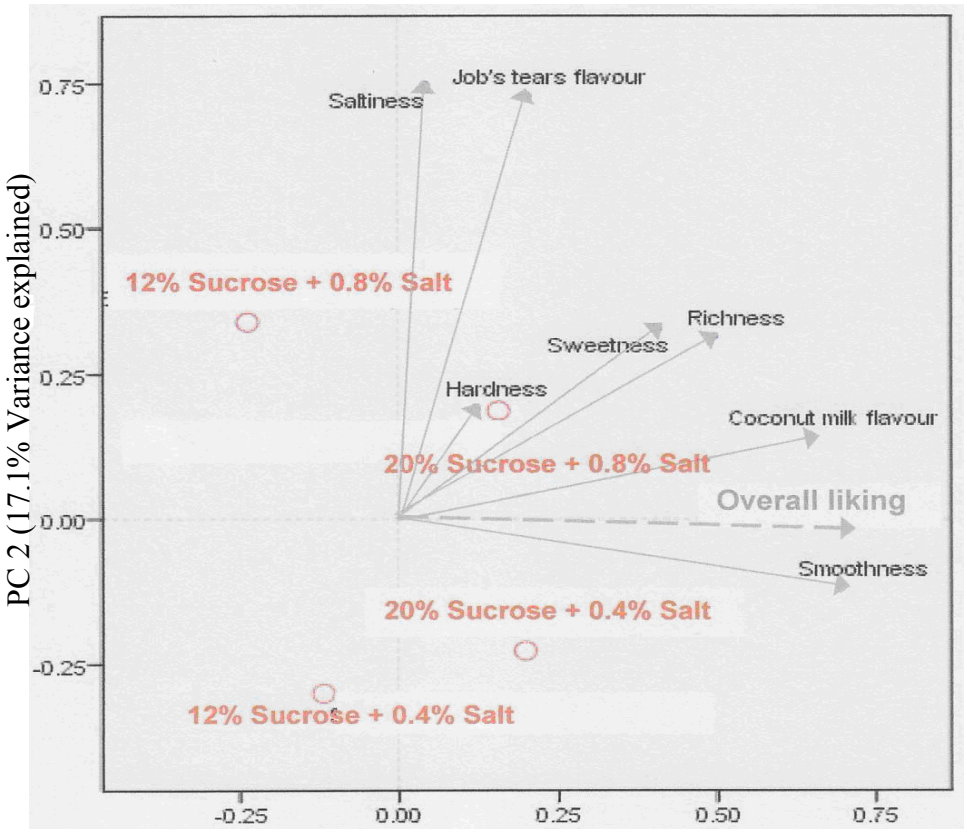

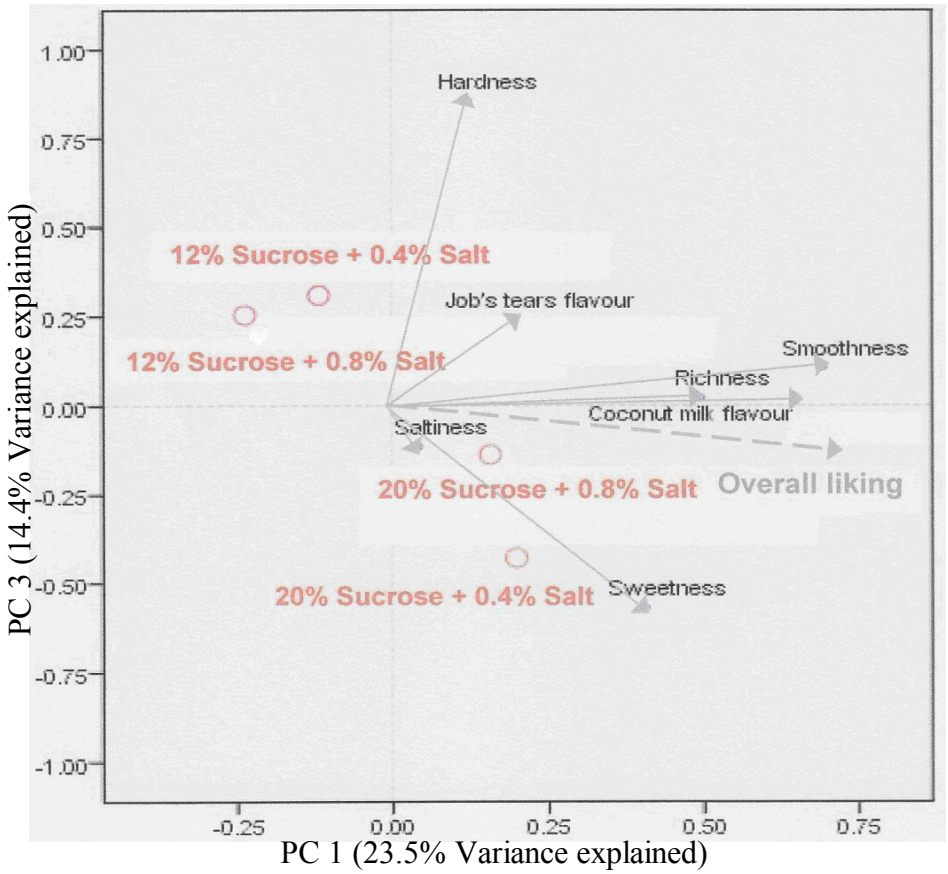

Figure 2. Product positioning maps of ice cream produced from 12 and 20% sucrose and 0.4 and 0.8% salt.

Maejo Int. J. Sci. Technol. **2009**, *3*(03), 388-399

Study on quantity of coconut milk

Sensory attributes of products with different quantities of coconut milk were reduced to 2 PCs with 43.2 % variance explained. The product positioning map (Figure 3) shows that products with high coconut milk quantity were richer, sweeter, smoother and stronger in coconut milk and Job's-tears flavours. Drivers of preference of products in this step seem to be smoothness, richness, coconut milk flavour, sweetness and Job's-tears flavour because their vectors are in the same direction of the overall preference vector. The mean overall preference scores of products from 100 consumers in this step are not significantly different ($p>0.05$), but cluster analysis could separate 100 consumers into two different groups (Table 3). Sixty-nine from 100 consumers preferred the product with 50% coconut milk while the rest preferred products with 60-65% coconut milk. This result agrees with the previous work [17] which found that only 36 from 100 consumers wanted more coconut milk in Job's-tears ice cream. Therefore, the product with 50% coconut milk was selected as the final product in this study.

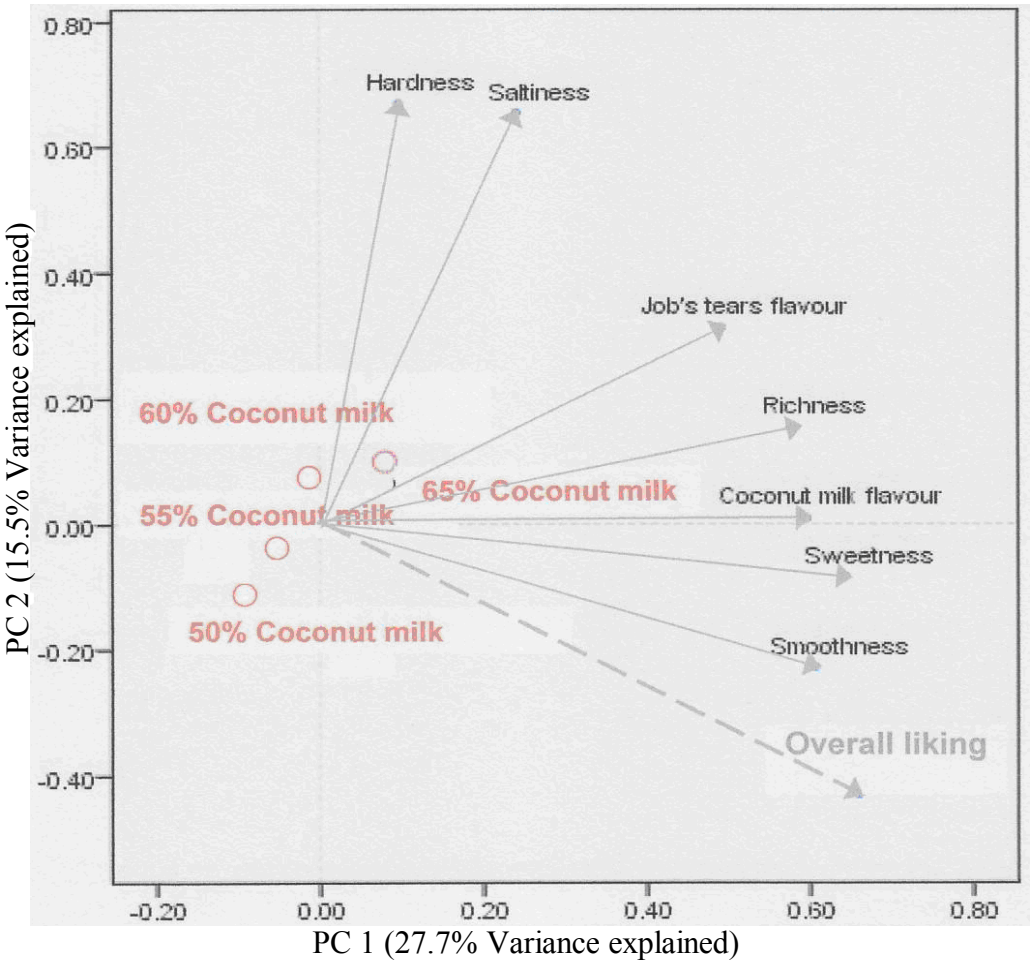

Figure 3. Product positioning map of ice cream with 50, 55, 60 and 65 % coconut milk

Maejo Int. J. Sci. Technol. **2009**, *3*(03), 388-399

Table 3. Overall preference scores (mean ± standard deviation) of ice cream with different quantities of coconut milk

Quantity of coconut milk in product	Whole consumer [ns] (n = 100)	Consumer group 1 (n_1 = 69)	Consumer group 2 (n_2 = 31)
50% Coconut milk	5.59 ± 2.14	6.52[a] ± 1.63	3.52[c] ± 1.64
55% Coconut milk	5.05 ± 2.13	4.67[b] ± 2.11	4.71[b] ± 2.03
60% Coconut milk	4.97 ± 2.05	5.09[b] ± 2.06	5.90[a] ± 1.97
65% Coconut milk	5.07 ± 2.05	4.70[b] ± 2.05	5.91[a] ± 1.82

Note : Means with different letters in the same column were significantly different ($p \leq 0.05$).
[ns] Means in this column were not significantly different ($p > 0.05$).

Chemical analysis of the final product

Nutritional data, antioxidant capacity and total phenolic content of the final product were shown in Table 4. Job's-tears ice cream in this study was higher in carbohydrate and crude fibre, but lower in protein, fat and ash compared to the regular ice cream reported by Nutrition Division [24]. However, its antioxidant capacity was very high. In this study, the antioxidant capacity of 100 grams of Job's-tears ice cream was equivalent to at least 47.12 mg of vitamin C, one of the antioxidant vitamins which participate in physiological, biochemical and cellular processes that inactivate free radicals or prevent free radical-initiated chemical reactions [25]. The antioxidant capacity of Job's-tears is due to six phenolic compounds, namely coniferyl alcohol, syringic acid, ferulic acid, syringaresinol, 4-ketopinoresinol, and mayuenolide [26]. The lowest antioxidant capacity value determined in this study (47.12 mg vitamin C equivalent/100 grams) is more than 75% of the daily value of vitamin C (about 60 mg) [27]. This information points to a very high antioxidant potential of Job's-tears ice cream.

Maejo Int. J. Sci. Technol. **2009**, *3*(03), 388-399

Table 4. Nutritional data, antioxidant capacity and total phenolic content (mean ± standard deviation) of Job's-tears ice cream

	Wet basis	Dry basis
Moisture (%w/w)	67.66 ± 0.36	-
Protein (%w/w)	1.00 ± 0.06	3.09 ± 0.17
Fat (%w/w)	0.48 ± 0.12	1.49 ± 0.38
Ash (%w/w)	0.34 ± 0.01	1.05 ± 0.03
Carbohydrate (%w/w)	30.52 ± 0.56	94.37 ± 0.39
Crude fibre (%w/w)	0.04 ± 0.01	0.10 ± 0.01
Antioxidant capacity		
FRAP (mg vitamin C equivalent per 100 grams of product)	47.12 ± 2.63	145.70 ± 8.13
ABTS (mg vitamin C equivalent per 100 grams of product)	228.54 ± 20.48	706.68 ± 63.32
DPPH (mg vitamin C equivalent per 100 grams of product)	251.38 ± 8.61	775.30 ± 26.62
Total phenolic content (mg gallic acid equivalent per 100 grams of product)	9.06 ± 0.07	28.01 ± 0.22

Conclusions

The developed Job's-tears ice cream recipe was preferred by 69% of the consumers. It consists of a mix containing 8% (w/w) Job's-tears total solid with added sucrose (20% of the mix), salt (0.4% of the mix) and coconut milk (50% of the mix), together with glucose syrup (32% of the mix). It is therefore composed of 4.0, 45.4, 9.9, 0.2, 24.7, and 15.8 % (w/w) of Job's tears total solid, water, sucrose, salt, coconut milk, and glucose syrup respectively. The resulting product may be rather high in carbohydrate and low in protein and fat. However, it is very high in antioxidant capacity and therefore potentially healthful.

Acknowledgement

This work was a research project supported by a grant from the Faculty of Engineering and Agro-Industry at Maejo University.

Maejo Int. J. Sci. Technol. **2009**, *3*(03), 388-399

References

1. C. H. Eckles, W. B. Combs and H. Macy, "Milk and milk products", Tata McGraw-Hill Publishing, New Delhi, **1979.**
2. J. Tobias, in "Dairy Technology and Engineering" (Ed. W. J. Harper and C. W. Hall), AVI Publishing, Connecticut, **1976**, Ch. 2.
3. V. A. Jones and W. J. Harper, in "Dairy Technology and Engineering" (Ed. W. J. Harper and C. W. Hall), AVI Publishing, Connecticut, **1976**, Ch.4.
4. A. H. Varnam and J. P. Sutherland, "Milk and Milk Products: Technology, Chemistry and Microbiology", Chapman and Hall, London, **1994**.
5. R. T. Marshall and W. S. Arbuckle, "Ice Cream", 5th Edn., Chapman and Hall, New York, **1996**.
6. Ministry of Public Health, Announcement Issue 222, "Ice cream", Ministry of Public Health, Bangkok, **2001.** (in Thai)
7. Ministry of Public Health, Announcement Issue 257, "Ice cream (Issue 2)", Ministry of Public Health, Bangkok, **2002**. (in Thai)
8. M. Moore, "Thai-style ice cream", Phuket Magazine Vol. 13.1 (no date), Retrieved December 15, 2007, from: http://www.phuketmagazine.com/html/PM%20Issues/Vol.13.1/Ice%20Cream-%20Thai%20Style.htm
9. K. Wongcharoenkit and M. Chuchom, **"**Soy milk ice cream**"**, Special Problem for Bachelor of Science Program in Food Science and Technology, **2005,** Maejo University, Thailand. (in Thai)
10. W. Wangcharoen, "Brown rice ice cream and soy milk ice cream", Workshop on "Processing of Health Food Products", **2007**, Maejo University, Thailand. (in Thai)
11. N. Tengmongkol (ed.), "Ice Cream", Sang Daad Publisher, Bangkok, **2004**. (in Thai)
12. A. Arber, "The Gramineae - a Study of Cereal, Bamboo, and Grass", Wheldon and Wesley, New York, **1965.**
13. A. Pink, "Gardening for the million", EText-No.11892**, 2004**, Retrieved February 20, 2007, from: http://www.gutenberg.org/etext/11892.
14. J. A. Duke and E. S. Ayensu, "Medicinal Plants of China", Reference Publications, Michigan, **1985.**
15. H. Yeung, "Handbook of Chinese Herbs and Formulas", Institute of Chinese Medicine, Los Angeles, **1985.**
16. R. N. Chopra, S. L. Nayar and I. C. Chopra, "Glossary of Indian Medicinal Plants" (including the supplement), Council of Scientific and Industrial Research, New Delhi, **1986.**
17. W. Khongjeamsiri, W. Wangcharoen, S. Pimpilai and W. Daengprok, "Preference direction study of Job's-tears ice cream", *Maejo Int. J. Sci. Technol*., **2007**, *1*, 137-144.
18. AOAC Internatioanl, "Official Method of Analysis of AOAC International", 17th Edn., Gaithersburg, Maryland, **2000**.
19. I. F. F. Benzie and J. J. Strain, "Ferric reducing / antioxidative power assay: direct measure of total antioxidant activity of biological fluids and modified version of simultaneous measurement of antioxidant power and ascorbic acid concentration", *Methods Enzymol.,* **1999**, *299*, 15-27.
20. M. J .T. J. Arts, G. R. M. M. Haenen, H. P. Voss and A. Bast, "Antioxidant capacity of reaction products limits the applicability of the Trolox equivalent antioxidant capacity (TEAC) assay" *Food Chem. Toxicol*., **2004**, *42*, 45-49.

Maejo Int. J. Sci. Technol. **2009**, *3*(03), 388-399

21. W. Brand-William, M. Cuelier and M. E. Berset, "Use of free radical method to evaluate antioxidant activity", *Lebensm. Wiss. Technol.*, **1995**, *28*, 25-30.
22. A. Waterhouse, "Folin-Ciocalteau micro method for total phenol in wine", (no date), Retrieved May 4, 2005, from: http://waterhouse.ucdavis.edu/phenol/folinmicro.htm.
23. M. Meilgaard, G. V. Civille and B. T. Carr, **"**Sensory Evaluation Techniques**"**, 3rd Edn., CRC press, Boca Raton, **1999**.
24. Nutrition Division, "Nutrient composition per 100 grams edible portion", Department of Health, Ministry of Public Health, Bangkok, **1987**. (in Thai)
25. U.S. FDA., "Food labeling; nutrient content claims: definition for 'high potency' and definition of 'antioxidant' for use in nutrient content claims for dietary supplements and conventional foods", Fed. Regist. 62:49868-49881, U.S. Food and Drug Administration, **1997**.
26. C. C. Kuo, M. C. Shih, Y. H. Kuo and W. Chiang, "Antagonism of free-radical-induced damage of adlay seed and its antiprolifrative effect in human histolytic lymphoma U237 monocytic cells", *J. Agric. Food Chem.*, **2001**, *49*, 1564-1570.
27. CFSAN., **"**Guidance for industry: a food labeling guide**"**, Center for Food Safety and Applied Nutrition, **2008**, Retrieved April 15, 2008, from: http://www.cfsan.fda.gov/guidance.html.

Maejo Int. J. Sci. Technol. **2009**, *3*(03), 400-407

Maejo International

Journal of Science and Technology

ISSN 1905-7873

Available online at www.mijst.mju.ac.th

Full Paper

Study on magnetic concentration of Nigerian Itakpe sinter concentrate to a Midrex-grade concentrate

Solomon A. Ola [1], Adewale O. Adeleke [2, *], Garba A. Usman [1], Anthony A. Odunaike [1], Shehu M. Kollere [3] and Paul O. Ajiboye [1]

[1] National Metallurgical Development Centre (NMDC), P.M.B. 2116, Jos, Nigeria
[2] Department of Materials Science and Engineering, Obafemi Awolowo University, Ile-Ife, Nigeria
[3] Raw Materials Research and Development Council, Abuja, Nigeria
* Corresponding author, e-mail: aoadeleke2002@yahoo.com

Received: 16 February 2009 / Accepted: 14 October 2009 / Published: 21 October 2009

Abstract: The sinter grade of the Nigerian Itakpe iron ore that assayed 63.63% Fe and 6.62% total acid gangue was subjected to both wet low-intensity magnetic separation (LIMS) and wet high-intensity magnetic separation (WHIMS) to upgrade it to Midrex-grade super-concentrate. Chemical analysis conducted on the super-concentrate samples from LIMS and WHIMS gave Fe content of 67.59% and 68.70%, and lower acid gangue of 1.55% and 3.22% respectively. However, screen distribution analysis results showed that the cumulative fractions passing 45-μm sieve were 0.88% and 0.38% for LIMS and WHIMS super-concentrates respectively. These results indicate that the Fe and acid content determined for both LIMS and WHIMS meets the requirement for a Midrex-grade super-concentrate, while the fractions of the concentrate passing 45-μm sieve are below the 30% upper limit for transportation to the reduction plant.

Key words: Itakpe iron ore, magnetic separation, Midrex-grade concentrate

Maejo Int. J. Sci. Technol. **2009**, *3*(03), 400-407

Introduction

Itakpe iron ore deposit, with an estimated reserve of about 200 million ton, was found in 1977. The deposit is embedded in the Itakpe Hill near Okene in the north-central Kogi State of Nigeria. The deposit extends approximately 3,000 m in length and includes about 25 layers of ferruginous quartzite. From a tectonic point of view, the Itakpe deposit is confined to the southern limb of a large Itakpe-Ajabanoko anticline with enclosing rocks and conformable ore layers striking sub-latitudinally and slightly bending to the north and dipping southward at angles ranging from 40° to 80° with local minor-fold complications. The deposit contains a mixture of magnetite and hematite with ratio varying throughout the deposit. The ore consists of coarse, medium and fine grained particles. The fine ores are located mainly in the eastern part of the deposit and in thin layers, while the coarse and medium ores are relatively mixed. However, the coarse ore predominates in the north and west of the central layers while the medium one does in the centre of the central layers. The average iron content of the ore deposit was determined to be approximately 35% [1].

The world production of direct reduced iron (DRI) has increased from 1 million ton in 1970 to 40 million ton currently. The Midrex process has accounted for over 60% of the annual worldwide DRI production [2]. Steelmaking slag contains calcium oxide, magnesium oxide, silica, alumina and other compounds in smaller concentrations. Pure silica has a very high viscosity, but the addition of other metal oxides, except alumina, reduces the viscosity. The preferred characteristic for DRI grade pellets is typically 67% (minimum) Fe and 3.0% (maximum) silica + alumina + titanium oxide [3].

A major determining factor in establishing an iron and steel plant is the availability of an iron ore deposit that can be economically upgraded for the intended processing route. The Itakpe iron ore deposit has been earmarked by the Federal Government of Nigeria to supply iron ore concentrate and super-concentrate for the blast furnace process at Ajaokuta and the Midrex-based direct iron reduction plant at Delta steel plant, Ovwian-Aladja respectively. The gravity concentration route currently installed at the National Iron Ore Mining Company (NIOMCO), Okene, was designed to produce iron ore concentrate for the Ajaokuta steel plant while the froth flotation route that requires imported chemical reagents was proposed to produce super-concentrate for Ovwian-Aladja. The aim of this research work is to investigate the possibility of using magnetic separation method to produce a Midrex-grade iron ore super-concentrate for use at the Delta steel plant.

Materials and Methods

Material

The sinter-grade concentrate was supplied for this work by the National Iron Ore Mining Company (NIOMCO), Itakpe, Kogi State of Nigeria. The concentrate was air-dried and representative samples were taken for grain-size distribution analysis and chemical composition analysis.

Maejo Int. J. Sci. Technol. **2009**, *3*(03), 400-407

Grain size distribution analysis

The sinter-grade iron ore, the feed and the magnetic concentrate were subjected to screen distribution analysis by a set of sieves. A stack of sieves with 100 g of the ore charged on the topmost sieve was clamped on the sieve shaker and shaken for 20 minutes. The weight retained on each sieve was then recorded.

Chemical composition analysis

The ore was subjected to chemical analysis. The iron (%Fe), alumina ($\%Al_2O_3$) and silica ($\%SiO_2$) content of the ore were determined by classical wet analysis as outlined by the National Metallurgical Development Centre [4].

Magnetic separation

The sinter-grade concentrate was first run through a wet low-intensity magnetic separator of 250 kg/hr capacity (manufactured by Boxmag-Rapid) to remove the ferro-magnetic material leaving a combination of gangue and para-magnetic material, which were directed to a wet high-intensity magnetic separator P40 of 250 kg/hr capacity (manufactured by Humboldt-Wedag, Germany) operating at 10,250 gauss for the separation of the para-magnetic material from the tailings. The concentrates of the wet low-intensity magnetic separation (LIMS) and the wet high-intensity magnetic separation (WHIMS) were combined to form the magnetic super-concentrate. The mass balance was done by taking samples with pulp-density cans at some points in the process line (Figure 3) and working out the corresponding weight % at each point.

Results and Discussion

The results obtained on the grain-size distribution and chemical composition analyses are presented in Tables 1-2 and 3-4 respectively, while the curves for the particle size distribution and the mass balance for the process are presented in Figures 1, 2 and 3.

From Tables 1-2, particle size distribution analyses gave, for sinter grade concentrate, LIMS super-concentrate and WHIMS super-concentrate: 62.67%, 63.22% and 57.43% passing 355-μm sieve size; 27.38%, 26.83% and 22.86% passing 180-μm sieve size; 2.12%, 2.79% and 1.54% passing 63-μm sieve size; and 0.65%, 0.88% and 0.38 passing 45-μm sieve size respectively. The highest undersizes of 63.22%, 2.79% and 0.88% (a total of 66.89% in the lower sieve range) on 355-μm, 63-μm and 45-μm sieves respectively were determined for LIMS as against 57.43%, 0.65% and 0.38% (a total of 58.46% in the lower sieve range) for WHIMS. The screen distribution results suggest that the LIMS super-concentrate consists generally of finer grain in comparison with the WHIMS super-concentrate.

Table 2 shows the sieve analyses for the super-concentrate produced from LIMS and WHIMS. It can be seen from the table that the 45-μm size materials consist of 0.88% and 0.38% of LIMS and

Maejo Int. J. Sci. Technol. **2009**, *3*(03), 400-407

WHIMS super-concentrates respectively. The results therefore show that the magnetic separation process is very effective for the production of super-concentrates from Itakpe iron ore. The fractions of the concentrates that passed the 45-μm sieve for both LIMS and WHIMS were very much lower than the upper limit of 30% required for the Middrex-grade super-concentrate used to produce pellets for direct reduction [5]. The plots of log % cumulative undersize against log sieve aperture size for LIMS and WHIMS in Figures 1 and 2 respectively are almost linear. The pattern of the curves obtained conforms to expectation [6].

Table 1. Grain-size distribution of Itakpe iron ore sinter grade concentrate

Sieve size (μm)	Weight % retained on sieve	Cumulative% undersize	Cumulative% oversize
-710	11.13	88.87	11.13
-500+355	11.81	77.06	22.94
-355+250	14.39	62.67	37.33
-250+180	18.50	44.17	55.83
-180+125	16.79	27.38	72.62
-125+90	13.00	14.38	85.62
-90+63	8.04	6.34	93.66
-63+45	4.22	2.12	97.88
-45	2.00	0.65	99.35

Note : - indicates sieve aperture undersize; + indicates sieve aperture oversize.

Table 2. Grain size distribution of Itakpe iron ore sinter and magnetic concentrates

Sieve size (μm)	Log sieve aperture	LIMS super-concentrate cumulative undersize (%)	Log % LIMS super-concentrate cumulative undersize	WHIMS super-concentrate cumulative undersize (%)	Log % WHIMS super-concentrate cumulative undersize
-500+355	2.70	78.53	1.90	nd	-
-355+250	2.55	63.22	1.80	57.43	1.76
-250+180	2.40	44.18	1.65	38.76	1.59
-180+125	2.26	26.83	1.43	22.86	1.36
-125+90	2.10	15.01	1.18	11.88	1.08
-90+63	1.95	7.37	0.87	5.19	0.72
-63+45	1.80	2.79	0.45	1.54	0.19
-45	1.65	0.88	-0.06	0.38	-0.42

Note : nd = not determined

- indicates sieve aperture undersize; + indicates sieve aperture oversize.

Maejo Int. J. Sci. Technol. **2009**, *3*(03), 400-407

Table 3. Chemical analysis results for Itakpe sinter concentrates at various size fractions

Parameter (%)	Itakpe sinter grade	Sieve fraction		
		- 180µm	- 500µm+180µm	+500µm
Fe	63.63	56.27	64.23	66.88
SiO_2	5.90	10.36	5.03	1.98
Al_2O_3	0.72	0.61	0.76	1.00
SiO_2+Al_2O_3	6.62	10.97	5.79	2.98

Table 4. Chemical analysis results for super-concentrates produced by magnetic separation

Parameter (%)	Itakpe sinter grade	LIMS super-concentrate	WHIMS super-concentrate
Fe	63.63	67.59	68.70
SiO_2	5.90	0.90	2.44
Al_2O_3	0.72	0.65	0.78
SiO_2+Al_2O_3	6.62	1.55	3.22

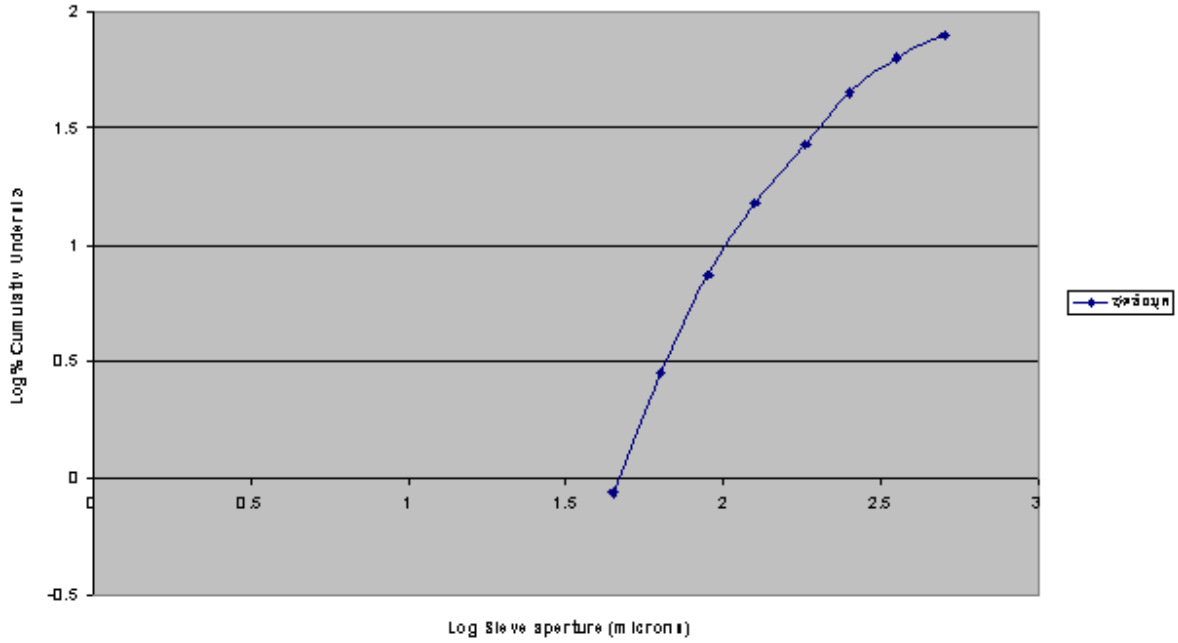

Figure 1. Plot of log % cumulative undersize against log sieve aperture size for LIMS

Maejo Int. J. Sci. Technol. **2009**, *3*(03), 400-407

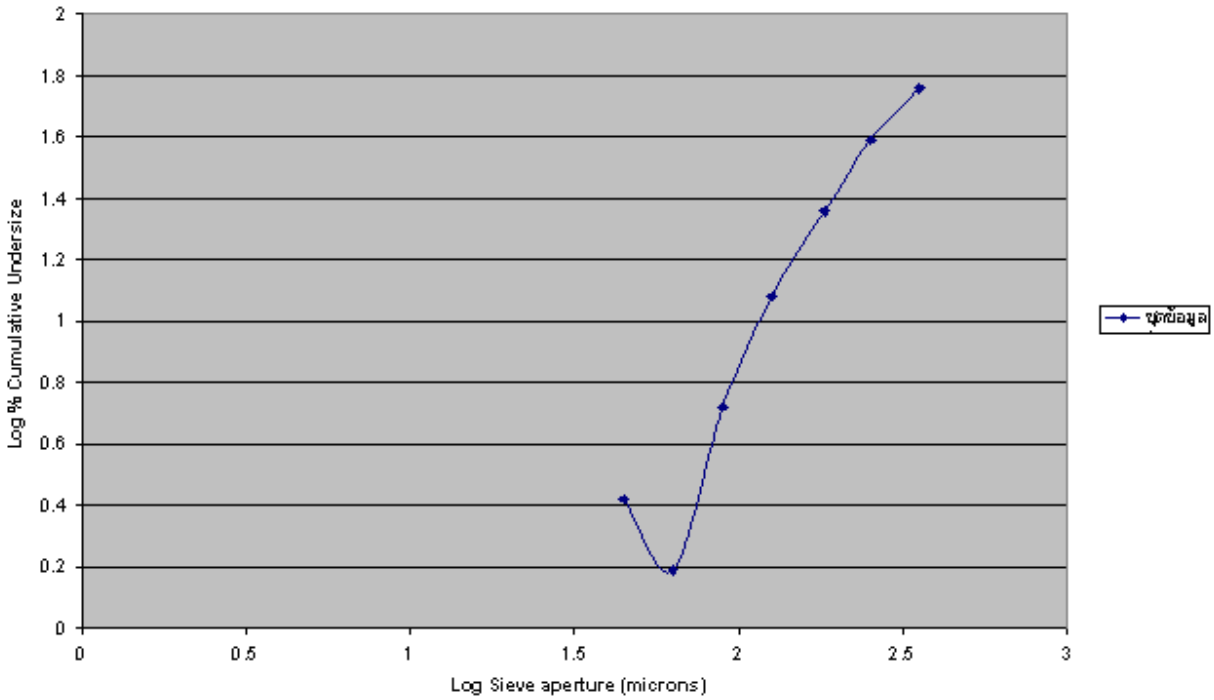

Figure 2. Plot of log % cumulative undersize against log sieve aperture size for WHIMS

The mass balance chart in Figure 3 shows that Itakpe sinter feed with 77% fractions passing through the 500-µm sieve was fed to the wet low intensity magnetic separator, which produced a ferromagnetic super-concentrate and a second product consisting of paramagnetics and gangue. The super-concentrate assayed 67.59% with the weight and iron recovery of 13.20% and 14.40% respectively, while the paramagnetic assayed 62.83% with the weight and iron recovery of 86.80% and 85.60% respectively. The WHIMS super-concentrate obtained from the paramagnetic assayed 68.70% with the weight and iron recovery of 78.73% and 84.91% respectively. These results show that the WHIMS concentrate had the highest iron content and recovery, while the paramagnetic yield of the Boxmag-Rapid wet low-intensity magnetic separation gave the lowest iron content. In general, the results indicate that the magnetic method successfully upgraded Itakpe iron ore to a super-concentrate grade [6].

Chemical analysis revealed iron content of 66.88%, 64.23% and 56.27% for +500µm, -500 µm+180µm and -180µm sieve fractions of sinter-grade iron ore respectively (Table 3). The average iron content determined for the sinter-grade ore was 63.63% (Table 4). The iron content of 66.88% and 64.23% for the coarse-size fractions of +500µm and -500µm+180µm exceeded the average iron content of 63.63%. However, the 56.27% iron content determined for the -180 µm fraction was lower than the average iron content. This suggests that the coarse fractions of the Itakpe sinter-grade ore were richer in iron than the fine-size fractions, and that such concentration method as gravity separation may be more economical in upgrading the Itakpe sinter-grade concentrate to a super-concentrate. The iron content determined for all the size fractions, except the -180µm one, was higher than the 63.22%

Maejo Int. J. Sci. Technol. **2009**, *3*(03), 400-407

present in the concentrate in use at the China Anshan iron and steel company. In addition, it exceeded the standard specification of 63% for use at the Ajaokuta steel plant blast furnace.

The determined acid oxides in term of silica and alumina were 2.98%, 5.79% and 10.97% for +500μm, -500μm+180μm and -180μm sinter-grade iron ore fractions respectively (Table 3), the average acid oxide content being 6.62% (Table 4). The acid content thus seemed to increase with decreasing sieve size, the coarser fraction of the sinter-grade concentrate containing less acid gangue than the finer fraction. The acid gangue content determined for all the size fractions as well as the representative sample was observed to exceed the upper limit of 3.0% for Midrex direct reduction process [6]. For some other standards, the total acid oxides include titanium oxide [3]. These analysis results indicate that Itakpe concentrate needs to be further upgraded to be useable in the Midrex direct reduction process.

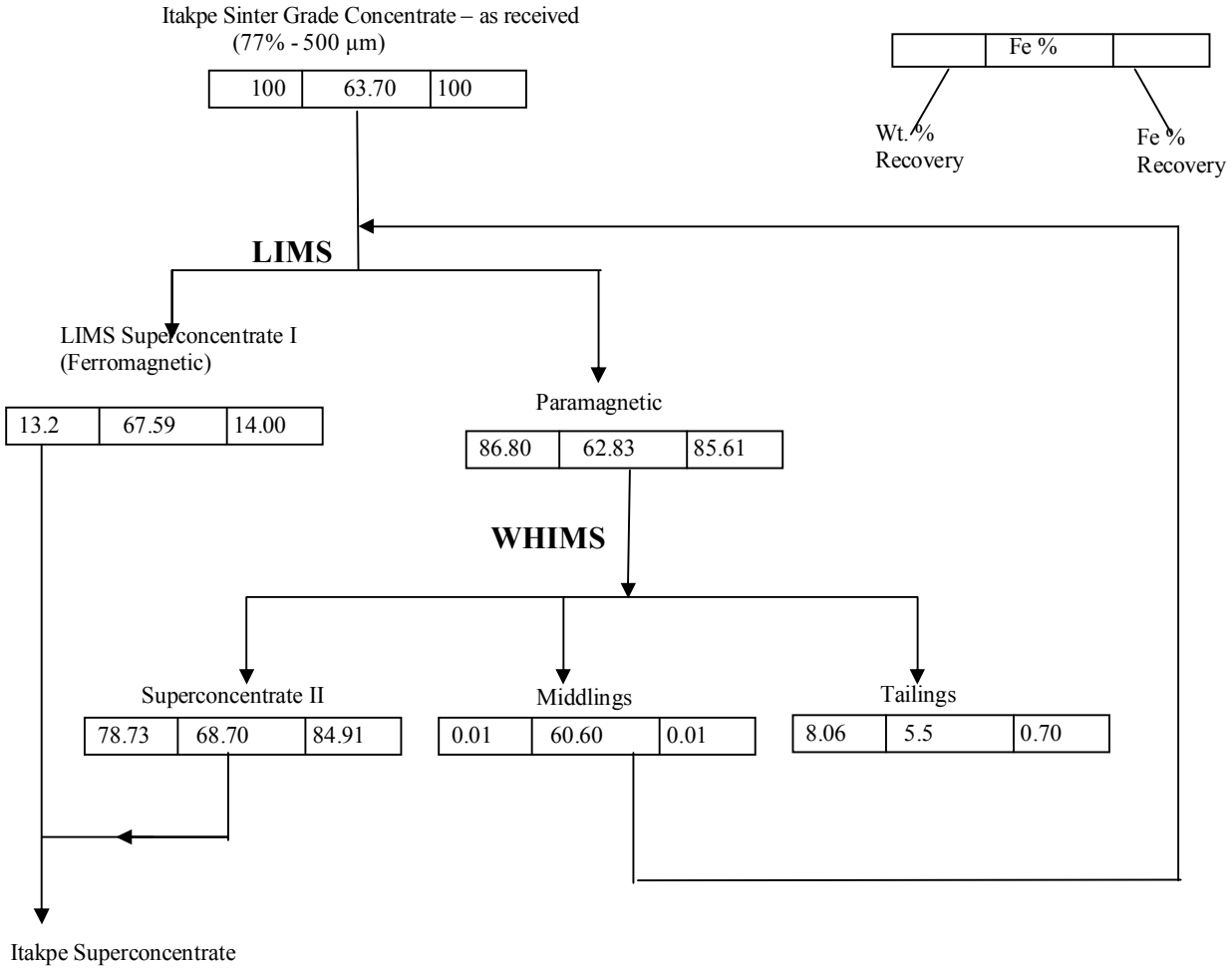

Figure 3. Mass balance for the production of Itakpe super-concentrates by magnetic separation.

Maejo Int. J. Sci. Technol. **2009**, *3*(03), 400-407

The chemical analysis result also indicated the content of iron and acid oxide at 67.59% and 1.55% respectively for LIMS super-concentrate, and at 68.70%, 3.22% respectively for WHIMS super-concentrate. This indicates that the magnetic concentrates satisfied the iron content (66-66.8%) required for the Midrex process while the acid oxide content (1.55-3.22%) fell below the upper limit of 3.5% for the Midrex process. Thus, LIMS and WHIMS Itakpe iron ore super-concentrates obtained met the chemical composition requirements for Midrex direct reduction.

Conclusions

The sinter grade of the Nigerian Itakpe iron ore that assayed 63.63% iron and 6.62% total acid gangue was successfully upgraded to super-concentrates by low intensity magnetic separation and wet high intensity magnetic separation with higher iron content of 67.59% and 68.70%, and lower acid gangue of 1.55% and 3.22% respectively. These figures meet the requirements for a Midrex-grade super-concentrate while the percentage of fractions of the concentrates passing through the 45-μm sieve fell below the upper limit of 30%. This should minimise dust loss during transport to the direct reduction plant.

Acknowledgements

The authors hereby acknowledge the approval and support of the National Metallurgical Development Centre, Jos, Nigeria, for carrying out this research work. We are particularly grateful to the Director General/CE, Engr. Garba Usman and the head of Analytical Services Department, Sir C.I.C Nwankwo, for their commitment to the completion and success of the series of tests carried out on the Itakpe ore.

References

1. P. U. Umunakwe, “Developing a new mine—The Itakpe case”, Proceedings of the Annual Conference of Nigeria Mining and Geosciences Society, **1985**, Jos, Nigeria.
2. http://www.midrex.com/uploads/documents/Direct Reduction Brochure1.pdf, Retrieved 1st November, 2008.
3. http://books.google.com/books?isbnn=0849366763, Retrieved 14th October, 2009.
4. "Modified Chemical Analyses Procedures for Iron Ores", National Metallurgical Development Centre, Jos, Nigeria, **1993**.
5. "Raw Materials and Products Specifications for Steel Industries", Federal Ministry of Mines, Power and Steel, Abuja, Nigeria, **1994**.
6. B. A. Wills, “Mineral Processing Technology”, 5th Edn., Pergamon Press, Oxford, **1992**.

Maejo Int. J. Sci. Technol. **2009**, *3*(03), 408-414

Maejo International

Journal of Science and Technology

ISSN 1905-7873

Available online at www.mijst.mju.ac.th

Full Paper

Novel method for heuristic modelling of flexible manufacturing systems

Payyalore R. Venkateswaran[1,*] P. R., Jayadeva Bhat[2] and S. Meenatchisundaram[1]

[1] Instrumentation and Control Engineering Department, Manipal Institute of Technology, Manipal 576 104 Karnataka, India

[2] Chemical Engineering Department, Manipal Institute of Technology, Manipal 576 104 Karnataka, India

* Corresponding author, e-mail: prv_i@yahoo.com

Received: 2 March 2009 / Accepted: 22 October 2009 / Published: 27 October 2009

Abstract: Flexible manufacturing systems (FMS) play an important role in industrial automation. They belong to a class of systems known as discrete event systems (DES) representing varying events with time. The modeling and control of such systems poses a challenge of handling uncertainties in resources and sequences for optimization. Presently the tools used for modeling such systems including Petri nets are constrained in the face of uncertainties in the system. A modified approach using new fuzzy logic formalism in Petri nets is proposed in this paper as a solution to overcome the problem. The utility of this formulation is that apart from the validity, it is adaptable to practical implementation in sequence controllers normally employed in FMS.

Keywords: flexible manufacturing system (FMS), fuzzy Petri nets, programmable logic controllers (PLC)

Introduction

The behaviour mapping of systems has undergone rapid change with advances in technology. The representation has become digital with state description of the behaviour. This manifestation is called discrete event systems (DES), exhibiting properties such as non-determinism, conflict and parallelism [1-3]. Supervisory control theory (SCT) [4-5] is chosen as a modeling paradigm and

Maejo Int. J. Sci. Technol. **2009**, *3*(03), 408-414

programmable logic controllers (PLC) [6-8] as an implementation tool for DES. This work investigates the use of fuzzy Petri nets in supervisory control and suggests a modified and improved version called fuzzy automation Petri net (FAPN) as a modeling tool. It presents a systematic approach to the synthesis of fuzzy-Petri-net-based supervisor for the forbidden state problem using supervisory design procedure. The controlled model of the system can be constructed from this FAPN net structure. The implementation uses the flexible manufacturing system (FMS) as an example of DES. The results can be interpreted and applied to high level manufacturing systems, where the role of the supervisor is to coordinate the control of multiple machines, or to low-level manufacturing systems where the control function is to switch on/off with respect to the dynamics between different valves.

Description of an FMS

The FMS shown in Figure 1 represents a packaging process that can be controlled by a programmable logic controller. In this application the objective is to control the speed of two conveyors which are used for packaging products. The strategy is to optimize the speed of a motor driven belt conveyor so that productivity in terms of packaging is achieved.

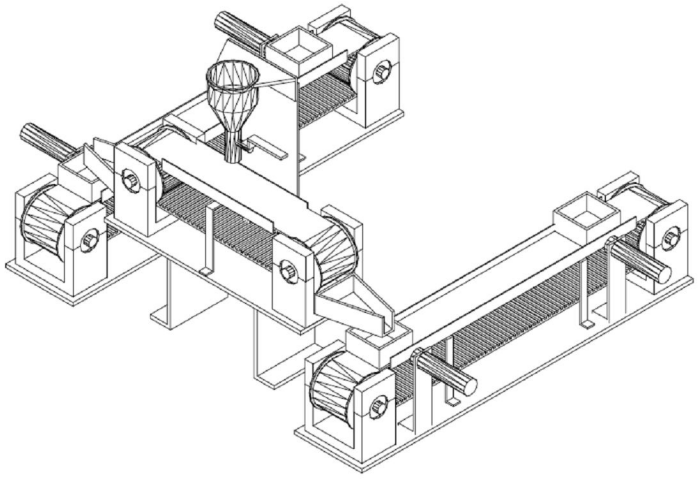

Figure 1. Schematic picture of the FMS considered for operation

Products are carried at irregular intervals in both the right conveyor (C_R) and left conveyor (C_L). The speeds of both conveyors are controllable. The processes in the conveyors C_R and C_L are identical and are as follows. Both conveyors are started together and the system will wait for a signal from either the sensor in C_R (designated as S_R) or the sensor in the C_L (designated as S_L). Suppose S_R (a box is detected on conveyor R) occurs (if not it will check for left conveyor), the hopper feed conveyor is moved towards right (HCR). Now if the box has arrived at the box detector of the right conveyor D_R (D_R occurs), the hopper valve is opened (V_1). The valve remains open for a time T and then it is closed (V_0). The conveyors are again started and the flow starts. In the case that the box is detected first at conveyor L (S_L occurs), the same sequence is followed at the left conveyor. The most important thing to note here is that in the time interval A_1 (i.e. the interval between the instant S_R occurs and D_R occurs), a control action needs to be such that both C_R and C_L are controlled. The same

Maejo Int. J. Sci. Technol. **2009**, *3*(03), 408-414

procedure is true for the other cycle. This system represents a typical conveyor system of a process of the manufacturing system.

Controller Synthesis using the Inhibitor Arc Method

Fuzzy automation Petri net (FAPN) is a variant of automation Petri net (APN) in the work of Greene [9] and Uzam [10], and is used to capture the uncontrolled behaviour of the system. The representation of the system using FAPN is as in Figure 2. This is derived as a result of literature review [11-14]. There are fifteen places, P = {p_0, p_2… p_{14}}, and ten transitions, T = {t_1, t_2… t_{10}}, with firing conditions defined as: χ_1=I0.0, χ_2=I0.0 (same on/off switch for both conveyors for simultaneous operation), χ_3 = I0.1, χ_4 = I0.2, χ_5 = I0.3, χ_6 = I0.4, χ_7 = I0.5 and χ_8 = I0.6, associated with them for the first eight transitions respectively. The last two of the transitions are defined by timers. If there is a token in p_0, then the conveyor is said to be in *on* status. If in transition, the token is passed to p_2 then the left conveyor is in *off* status. Similarly, the presence of token in places p_1 and p_3 define the *on* and *off* status respectively of the right conveyor. A token in the place of p_4 or p_5 indicates the presence of box sensed at the entry of either the left or the right conveyor as can be seen in Figure 2. . A token in place of p_9 or p_{10} indicates the running of the hopper feed conveyor (HFC) towards the left or right of the conveyor as in Figure 2. The hopper feed valve (HFV) status is indicated by places p_{11} and p_{12}.

The initial conditions for the system are the conveyors (C_L and C_R) switched off, the HFC idle, the HFV closed and the buffer of C_L and C_R full. Conveyors C_L and C_R can be started with a start switch. Whenever a box is detected at the entry of either conveyor, the hopper feed conveyor if ready should start moving towards that particular conveyor. In the case that the hopper feed conveyor is already engaged, it should wait till the operation gets completed. The box travels to the filling station where it gets filled through the hopper and then finally gets dispatched.

The reachability diagram for the system can be considered in two phases. The first one is said to be an uncontrolled FAPN model where the flow of events is unregulated and is shown in Figure 3. There are 57 arcs representing the firing of transitions in the uncontrolled model and there are 19 nodes, M = {M_0,M_1…M_{18}}, representing all possible markings reachable from the initial marking M_0. The events χ ={χ_1, χ_2…χ_8} represents the firing of the corresponding transitions T ={t_1, t_2 … t_{10}}. All time delays associated with the transitions are implied although not indicated. “Bad states” in a reachability diagram will happen under two circumstances: (i) the states are not reached as per specifications identified as forbidden-state specifications, and (ii) the states are in conflict with the constraints of the system parameters. Initially, the system specifications are considered for defining the “bad states”. Such system specifications are called forbidden-state specifications and are denoted as follows:

(i) The boxes should not leave the conveyor without getting filled.
(ii) The hopper feed conveyor should not respond to transition without completing the current operation.
(iii) The hopper feed conveyor should not run till the conveyor in which the box is detected is stopped.

Maejo Int. J. Sci. Technol. **2009**, *3*(03), 408-414

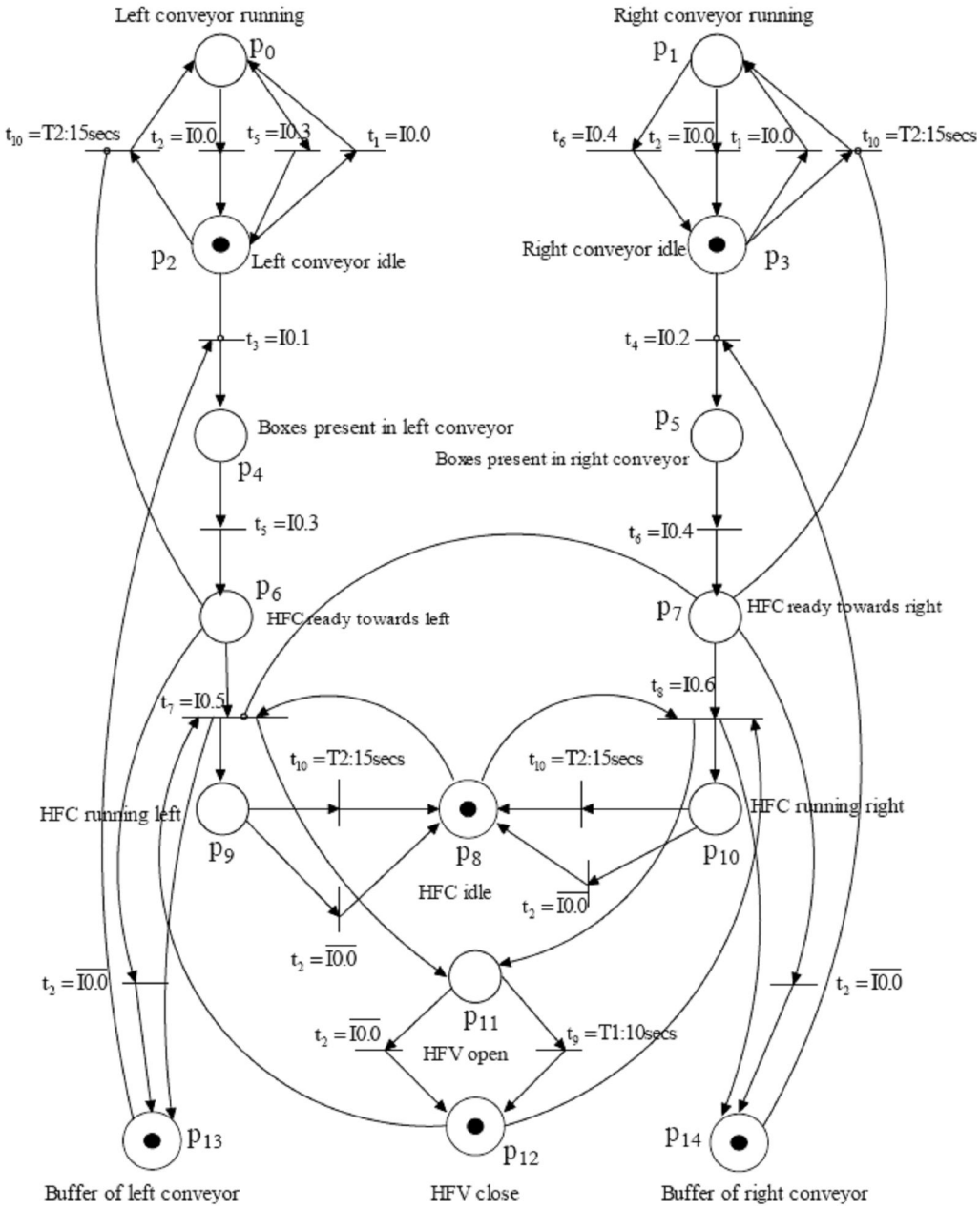

Figure 2. FAPN model of a flexible manufacturing system (FMS)

To identify the system with respect to its specifications, all of these specifications are considered. In addition, the constraints imposed on the system due to operating/working conditions are also considered. The states which do not agree to any of these specifications are eliminated in the reachability diagram. When a state is removed, the transitions that lead to it become redundant and lose their meaning. Consequently all the transitions leading to/from "bad states" are also eliminated. For example, let us consider a case of M_{14}=[2,3,6,7,8,12]. Here all the conveyors are in the idle state. This indicates that all the conveyors are idle simultaneously inferring that no useful work is done in the system. This must be prevented from happening although it is not against specifications per se. Thus, apart from M_0, the states M_9, M_{10}, M_{11} and M_{14} in which all the conveyors become idle are to be

Maejo Int. J. Sci. Technol. **2009**, *3*(03), 408-414

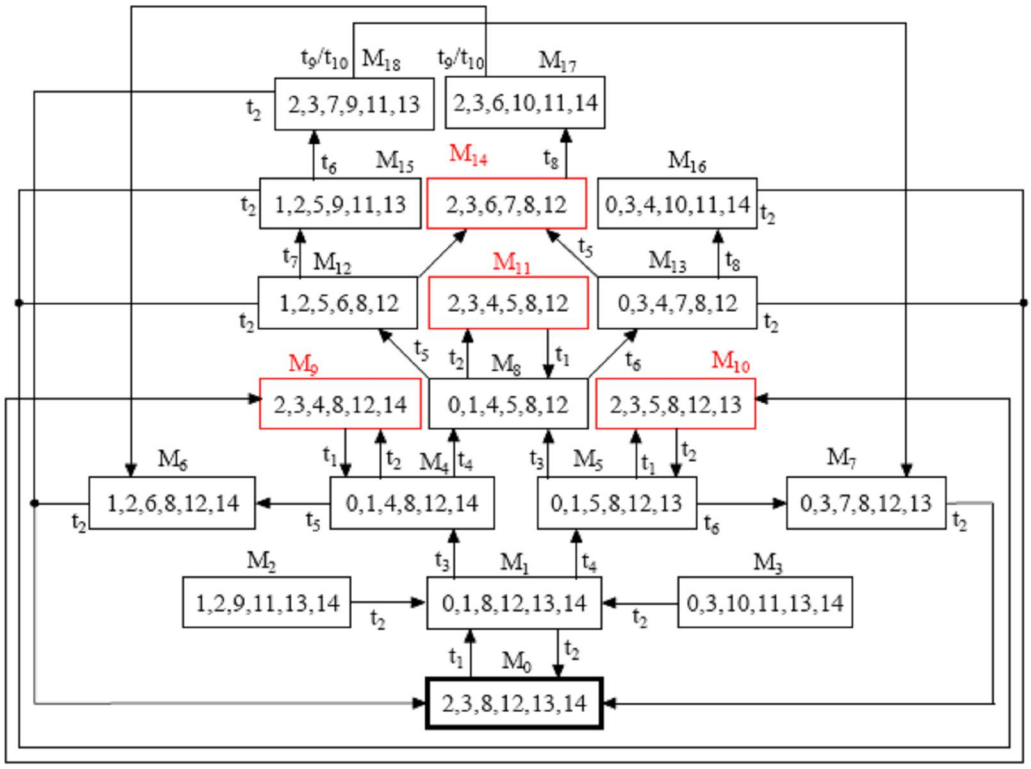

Figure 3. Reachability diagram of the FAPN model

removed from the reachability diagram. This includes all transitions terminating and originating from the individual states. In addition, there is a state called M_{16}, which when reached in the system does not lead anywhere. This is because there is no transition that originates at M_{16}. Therefore, it should be made sure that M_{16} does not occur. If M_{16} is to be removed, then as a natural extension, M_{13} is also to be removed. Similarly, for states M_2 and M_3, there are no input transitions. They cannot happen in the flow of the system. The final diagram makes sure that for all defined states, there is a sequence which will be followed to complete the operation. By following the above sequences, the following objectives will be achieved:

1. If there is no sign of machine starving or blocking, then keep the production surplus close to zero. In other words, produce at a rate more or less equal to demand.
2. If an undesirable event (upstream or downstream buffer full or empty) is about to occur, then ignore surplus levels and try to prevent starting or blocking by increasing or decreasing the production rate accordingly.

Results and Discussion

The implementation was with a prototype conveyor system in the PC Instrumentation Laboratory of Manipal Institute of Technology, Manipal, India. A Siemens PLC (CPU 226) was used to control the process and Step 7 Version 4.0 was used as the software interface for the PLC. If all possible states in the system are to be considered, there will be an exponential increase in the reachability diagram resulting in state space explosion problem. The effects of the state explosion problem on the conventional methods are twofold. The first one is that the computation of the

Maejo Int. J. Sci. Technol. **2009**, *3*(03), 408-414

supervisor becomes very difficult as the system becomes bigger. The second effect is that the bigger the system is, the bigger is the number of places and transitions required as the supervisors. However, this problem was overcome by the inclusion of the system modeling using FAPN. The representations of states became linguistic in nature and hence eliminated the exact number replica of states in a system. In addition, the supervisors obtained were correct by construction. For implementation, the supervisors obtained were converted into ladder logic diagrams (LLD) to be implemented on any PLC. The design was based on the premise that the DES considered are controllable and observable and the result can be extended into a wide array of DES. The summary of all the approaches are presented in Table 1. The applications of these methods could range into different types of DES exhibiting unique characteristics of uncertainty, vagueness and imprecision. Thus, all modern systems classified into the domain of DES can be included as systems of interest for implementation.

Table 1. Performance review of methods for FMS

	Ladder logic method [15]	Inhibitor arc method [15]	Enabling arc method [15]	Fuzzy automation petri net method
Number of places used	NA	14	14	12
Number of transitions used	NA	14	14	10
Number of LLD rungs proposed	15	Infinite	Infinite	140

Conclusions

A formal design of fuzzy-Petri-net-based complied supervisors for DES control problem and their efficient implementation are a challenging problem. In this paper, a flexible manufacturing system was used to illustrate the applicability, strengths and drawbacks of the design techniques using fuzzy Petri nets. It is proved by experimentation that application of fuzzy in modelling and programming for discrete event systems is useful in handling uncertainties. Since the derivation of the formalism is generic in nature, it can be applied to a wide distribution of DES. In addition, the problem of state space explosion is eliminated by using fuzzy automation Petri nets (FAPN). The design was based on the premise that the DES considered are controllable and observable and the result can be extended into a wide array of DES.

References

1. A. Hellgren, "Modeling and implementation aspects of supervisory control", Technical Report No.350L, Control and Automation Laboratory, Department of Signals and Systems, Chalmers University of Technology, Sweden, **2000**.

Maejo Int. J. Sci. Technol. **2009**, *3*(03), 408-414

2. G. Cohen, D. Dubois, J. P. Quadrat and M. Viot, "A linear system theoretic view of discrete event processes and its use for performance evaluation in manufacturing", *IEEE Trans. Autom. Control*, **1985**, *AC-30*, 210-220.
3. R Valette, J. Cardoso and D. Dubois, "Monitoring manufacturing systems by means of Petri nets with imprecise markings", IEEE International Symposium on Intelligent Control, September **1989**, Albany, NY, USA, pp. 233-238.
4. P. J. Ramadage and W. M. Wonham, "Supervisory control of a class of discrete event processes", *SIAM J. Control Optim.*, **1987**, *25*, 206-230.
5. P. J. Ramadage and W. M. Wonham, "The control of discrete event systems", *Proc. IEEE*, **1989**, *77*, 81-98.
6. A. Taholakian and W. M. M. Hales, "PN↔PLC: A methodology for designing, simulating and coding PLC based control systems using Petri nets", *Int. J. Product. Res.*, **1997**, *35*, 1743-1762.
7. M. Courvoisier, R. Valette, J. M. Bigou and P. Esteban, "A programmable logic controller based on a high level specification tool", Proceedings of IEEE Conference on Industrial Electronics, **1983**, Amsterdam, pp. 174-179.
8. R. Valette, "A Petri net based programmable logic controller", in "Computer Applications in Production and Engineering (CAPE'83)" (Ed. E. A. Warman), North-Holland Publishing Co., Amsterdam, **1983**, pp. 103-116.
9. J. Greene, "Petri net design methodology for sequential control", *Meas. Control*, **1989-1990**, *22*, 288-291.
10. M. Uzam, "Petri net supervisory control of discrete event systems and their ladder logic diagram implementation", *PhD. Thesis*, **1998**, University of Salford, UK.
11. S. S. Peng, "Ladder diagram and Petri-net based discrete event control design methods", *IEEE Trans. Syst. Man Cybern. Part C Appl. Rev.*, **2004**, *34*, 523-531.
12. R. David and H. Alla, "Petri nets for modeling of dynamic Systems: A survey", *Automatica*, **1992**, *30*, 175-202.
13. T. Cao and A. C. Sanderson, "Modeling of sensor based robotic task plans using fuzzy Petri nets", Proceedings of the 4th International Conference on Computer Integrated Manufacturing and Automation Technology, **1994**, Troy, NY, USA, pp.73-80.
14. M. Hanna, "Determination of product quality from an FMS cell using fuzzy Petri nets", *Proc. IEEE*, **1994**, *2*, 2002-2007.
15. P. R. Venkateswaran, "Fuzzy logic supervisory control of discrete event systems", *PhD. Thesis*, **2008**, Manipal University, India.

Maejo Int. J. Sci. Technol. **2009**, *3*(03), 415-425

Maejo International

Journal of Science and Technology

ISSN 1905-7873

Available online at www.mijst.mju.ac.th

Full Paper

Characterisation of chitosan solubilised in aqueous formic and acetic acids

Esam A. El-hefian*, Abdul H. Yahaya and Misni Misran

Department of Chemistry, University of Malaya, 50603 Kuala Lumpur, Malaysia

* Corresponding author, e-mail: eelhefian@yahoo.com

Received: 24 May 2009 / Accepted: 28 October 2009 / Published: 3 November 2009

Abstract: The intrinsic viscosity of chitosan (MW 7.9 x 10^5 g mol^{-1}) having a high degree of deacetylation and solubilised in aqueous formic and acetic acids was determined at room temperature. Contact angle and conductivity of the chitosan solutions were also studied. The values of critical coagulation concentration (CCC) were then obtained from the plots of contact angle or conductivity versus concentration.

Keywords: chitosan, intrinsic viscosity, contact angle, conductivity, critical coagulation concentration

---

Introduction

Chitosan is an amino-sugar-containing polysaccharide usually obtained by alkaline deacetylation of chitin from crab and shrimp shells [1-2]. This fibril biopolymer is composed of β-(1$\rightarrow$4)-2-amino-2-deoxy-D-glucopyranose units (glucosamine units). It is a non-toxic, biocompatible and biodegradable polymer [3-4]. It has been widely used in diverse fields ranging from waste management to food processing, medicine and biotechnology [5-11].

The physical [12], chemical [13] and biological [14-15] properties of chitin and chitosan depend mainly on two parameters: degree of deacetylation (DD) and molecular weight distribution, both of which are affected by the source of chitin and the method of preparation. The DD also plays a significant role in affecting the molecular weight of chitosan. A lower DD leads to a higher molecular weight. Chitosan is very difficult to dissolve in water, alkaline solutions or common organic solvents. This is due to the formation of intermolecular hydrogen bonds of its molecules. However, it is soluble to some extent in dilute aqueous acid solutions. This is mainly

Maejo Int. J. Sci. Technol. **2009**, *3*(03), 415-425

due to the presence of amino groups in its molecular structure which get protonated in the aqueous acid solution rendering it soluble [16]. Thus, in the preparation of a solution of chitosan, an aqueous organic acid is always used as solubilising agent. The level of solubility of chitosan in dilute acids depends on its molecular weight and DD.

Viscosity is an important factor in the conventional determination of molecular weight of chitosan and its commercial applications. Chitosan viscosity is found to decrease with increased time of the demineralisation step in its preparation [17]. Bough et al. [18] found that in the treatment of chitin to make chitosan, deproteinisation with 3% NaOH and elimination of the demineralisation step decrease the viscosity of the final chitosan product. No et al. [19] demonstrated that chitosan viscosity is considerably affected by physical treatments (grinding, heating, autoclaving, ultrasonicating, but not freezing) and chemical treatments (e.g. ozone), wherein it decreases with an increase in treatment time and temperature. Kim et al. [20] noted a sharp decrease in chitosan viscosity in some organic acid solutions (40-60% in one day). However, the viscosity of chitosan solution stored at 4^{o}C was found to be relatively stable [19]. No et al. [21] reported a decrease in the viscosity of chitosan (1% chitosan in 1% acetic and/or lactic acid solution) with increased storage time and temperature. The decrease in viscosity recorded over time was related to the partial degradation of chitosan by the organic acid solutions. However, reports that relate the viscosity of chitosan to the type of solubilising organic acid solution are barely found in the literature [16].

A number of reports are found in the literature regarding conductivity studies of chitosan solutions [22-24], although this is not the case for the contact angle of chitosan solutions. Instead, reports are easily available for contact angles of liquids on films of pure chitosan or chitosan associated with other polymers [25-28].

It has been demonstrated that the type of acid used as a solvent of chitosan has an effect on the properties of chitosan [29-32]. This makes it necessary to understand the behaviour of the chitosan solution before using this polymer. The present work therefore reports on the investigation of the viscosity, contact angle and conductivity chitosan solubilised in dilute aqueous solutions of two organic acids (formic acid and acetic acid). A study of such kind is very essential before further exploring the compatibility of chitosan with other polymers in order to obtain blends for making films for various applications.

Materials and methods

Materials

Shrimp-derived chitosan sample with DD > 95% (defined by UV method [33]) was purchased from the chitin-chitosan laboratory at National University of Malaysia. Organic acids, viz. formic acid (98-100%, from Scharlau) and acetic acid (99.5%, from R & M Chemicals) were used as received. Distilled water was used to prepare all solutions. Freshly prepared solutions were used in all experiments.

Maejo Int. J. Sci. Technol. **2009**, *3*(03), 415-425

Preparation of acid solutions of chitosan

A stock solution of chitosan was prepared by adding chitosan (0.1 g) to 100 mL of each acid solution (0.1 M) and heating the mixture at 40-50°C with continuous stirring for 24 h. Each one of the solubilised solutions (0.1g/100mL) was then diluted to the desired concentration.

Methods

The molecular weight of chitosan was determined by gel permeation chromatography equipped with a Waters 1515 HPLC pump and a 2414 Refractive index detector. The column used was PL Aquagel-OH 30 (8 μm, 300 × 7.5 mm) and the solvent used was 1% acetic acid. The chromatograph was calibrated with polystyrene standards.

Viscosity measurements were conducted using a Ubbelohde-type viscometer (Fisher, Germany). The viscometer was connected to a visco-clock (Schott Visco clock) to record the time of solution passing through the two marks of the viscometer automatically. Every value recorded was an average of 4 measurements.

The relative viscosity, η_r, for a diluted polymer solution can be calculated from:

$$\eta_r = \frac{\eta}{\eta_o} = \frac{t}{t_o}$$

where η and η_o are the viscosities of polymer solution and the pure solvent respectively, t is the outflow time of the polymer solution and t_o is the outflow time for the pure solvent.

The specific viscosity, η_{sp}, was given by the relative increment in the viscosity of the polymer solution to the viscosity of the solvent as follows:

$$\eta_{sp} = \frac{(\eta - \eta_o)}{\eta_o} = \eta_r - 1$$

The reduced viscosity (viscosity number), η_{red}, is the specific viscosity per unit concentration C and was given by:

$$\eta_{red} = \frac{\eta_{sp}}{C} = \frac{(\eta_r - 1)}{C}$$

The intrinsic viscosity, $[\eta]$, can be determined from the reduced viscosity (η_{red}), which equals $\frac{\eta_{sp}}{C}$, or from the inherent viscosity, η_{inh}, which equals $\frac{\ln \eta_r}{C}$, by extrapolation to zero concentration [34]. To obtain an accurate value of the intrinsic viscosity of the chitosan solution, therefore, its average extrapolated value to C = 0 from the linear graphs of $\frac{\ln \eta_r}{C}$ and $\frac{\eta_{sp}}{C}$ versus concentration was taken.

The contact angle of the chitosan solution was measured using the contact angle measuring system G40 (Krüss gmbh., Hamburg, Germany) at room temperature. The measurement was done on microscope slides (25.4×76.2 mm, 1-1.2 mm thick). Each slide was cleaned before use by soaking in ethanol overnight. The average contact angle of both sides of the drop was taken into consideration. The average value of contact angle of water on the slide was 42°. Sample volume used was 1 μL and the measurement time was 1.5 minutes.

Maejo Int. J. Sci. Technol. **2009**, *3*(03), 415-425

Conductivity measurements were carried out using the Orion Model 105 conductivity metre. The actual conductivity reading was obtained by multiplying the observed conductance reading by the cell constant (K), which was equal to 1.0 cm^{-1} in this case. Calibration was done with standard potassium chloride solution. The equivalent conductivity is defined as:

$$\Lambda\ (ohm^{-1}\ m^2\ kg^{-1}) = \frac{k\ (ohm^{-1}m^{-1})}{C\ (kg\ m^{-3})}$$

where Λ is equivalent conductivity, k is conductivity and C is concentration.

Results and Discussion

Determination of molecular weight

The molecular weight of chitosan used in this work was found to be 7.9 x 10^5 g mol^{-1}. This value was somewhat higher than some of those reported in the literature. For example, it was higher than that reported by Ladet et al. (5.5 $\times 10^5$ g mol^{-1}) [35]. This is acceptable, however, since the molecular weight of chitosan depends on such factors as source of raw material and method of preparation.

Determination of viscosity

Figures 1 and 2 show the plots of $\frac{\ln \eta_r}{C}$ and $\frac{\eta_{sp}}{C}$ versus concentration for chitosan in the solubilising aqueous formic acid and acetic acid respectively. The two values of $[\eta]$ were obtained by linearly extrapolating the two graphs to $C = 0$ (Y-intercept). The data of intrinsic viscosity obtained are presented in Table 1, together with the values of coefficients $k_1$and k'_1, which were calculated from the slopes of the graphs. As can be seen, chitosan solubilised in acetic acid records a higher value of intrinsic viscosity. However, this value is lower than that in propionic acid reported by us earlier [36]. This behaviour may be related to the acid strength of the solubilising acid and the molecular volume of the solvated anion of chitosan.

It can also be observed that the intrinsic viscosity of chitosan in formic or acetic acid increased with the increase in the concentration of chitosan solution—a normal viscosity behaviour, in contrast to that determined in propionic acid [36]. Similar normal behaviour in the apparent viscosity of chitosan in aqueous organic acids was reported for pH varied between 2-5 [37]. Values of the coefficients k_1 and k'_1 were also found to be in agreement with those reported in the literature [38,39].

Maejo Int. J. Sci. Technol. **2009**, *3*(03), 415-425

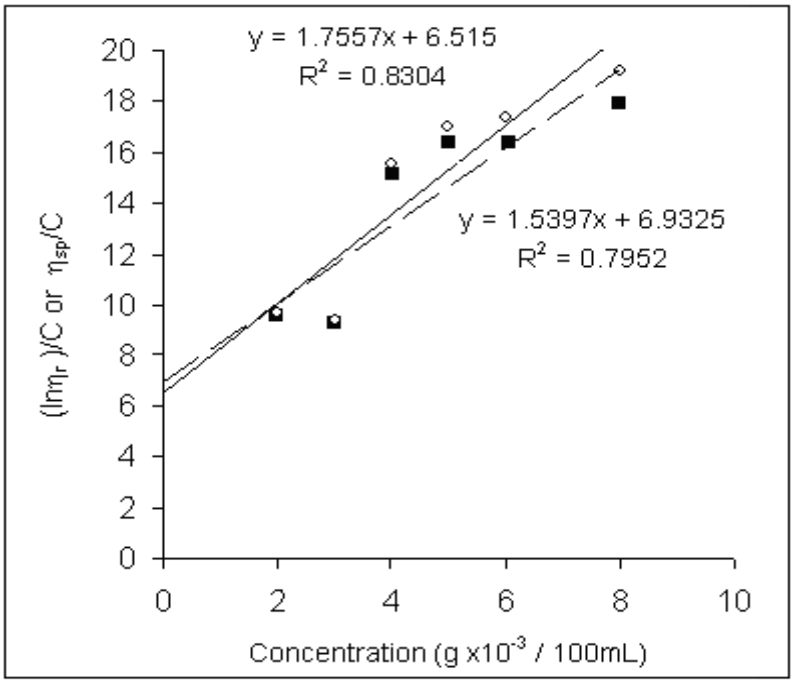

Figure 1. $\frac{\ln \eta_r}{C}$ (solid line) and $\frac{\eta_{sp}}{C}$ (dash line) of chitosan in formic acid solution versus concentration

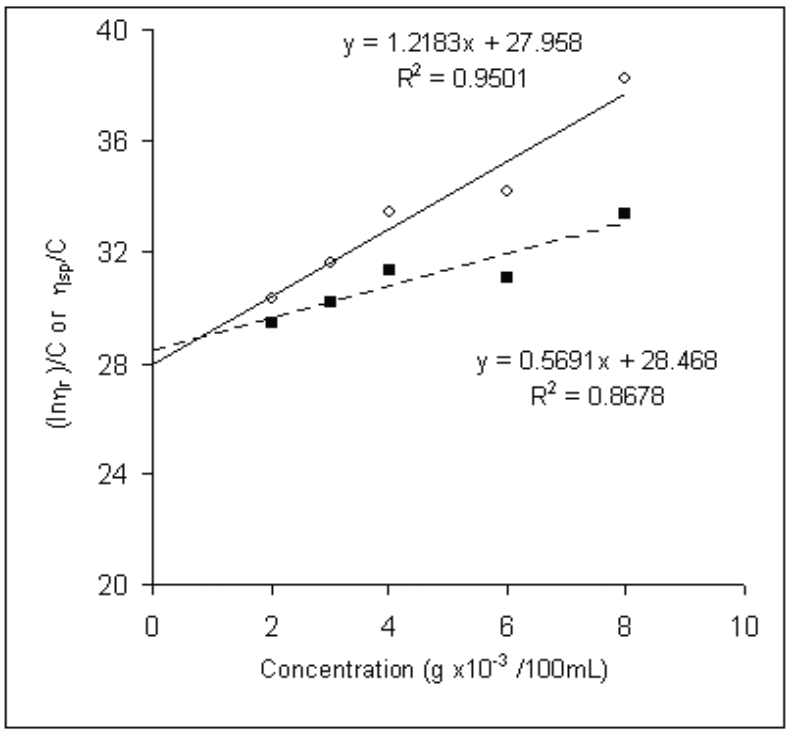

Figure 2. $\frac{\ln \eta_r}{C}$ (solid line) and $\frac{\eta_{sp}}{C}$ (dash line) of chitosan in acetic acid solution versus Concentration

Maejo Int. J. Sci. Technol. **2009**, *3*(03), 415-425

Table 1. Values of $[\eta]$ ($cm^3\ g^{-1} x\ 10^2$), k_1 and k'_1 for chitosan in different solvents

Viscosity parameter	Formic acid	Acetic acid	Propionic acid*
$[\eta]$ (mean ± SD)	6.723 ± 0.294	28.213 ± 0.360	37.679 ± 0.340
k_1	0.032	0.702×10^{-3}	0.785×10^{-3}
k'_1	0.041	1.558×10^{-3}	0.487×10^{-3}

* Quoted from previous study [36] for comparison

Determination of contact angle

The average of contact angle is plotted as a function of concentration (Figures 3-4). Increase in the contact angle (decreas in $\cos\theta$) with increasing concentration of the solution may be linked to the departure from pure water (decrease in wettability) as the ratio of chitosan to water increases. However, a critical coagulation concentration (CCC) is reached, beyond which the contact angle becomes more or less independent of concentration [36,40]. The values of the CCC are about 9.5×10^{-5} and 7×10^{-5} g L^{-1} for chitosan in formic acid and acetic acid solutions respectively. These values are similar to that already reported for chitosan in propionic acid solution (4.5×10^{-5} g L^{-1}) [36].

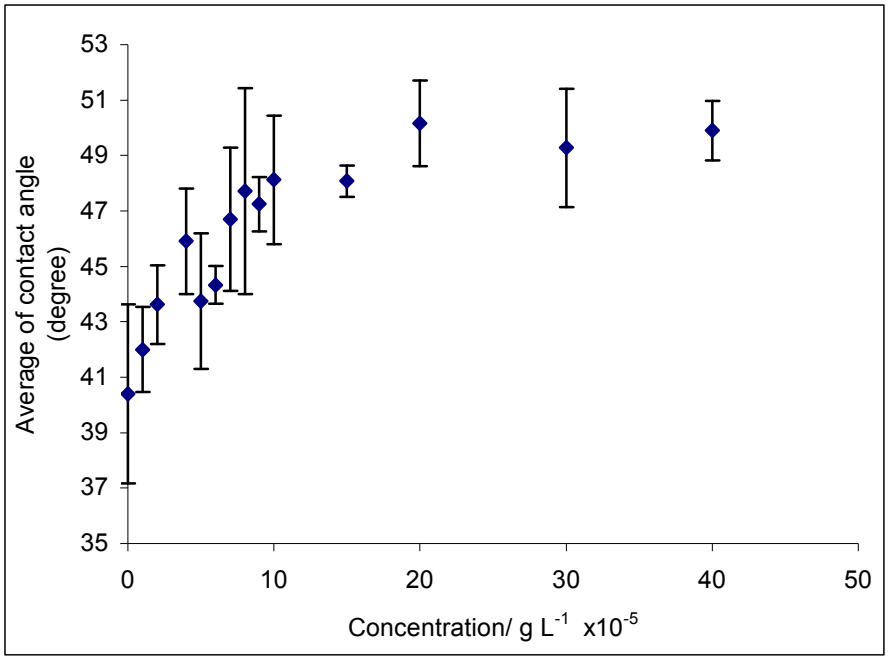

Figure 3. Contact angle of chitosan in 0.02 M formic acid solution versus concentration

Maejo Int. J. Sci. Technol. **2009**, *3*(03), 415-425

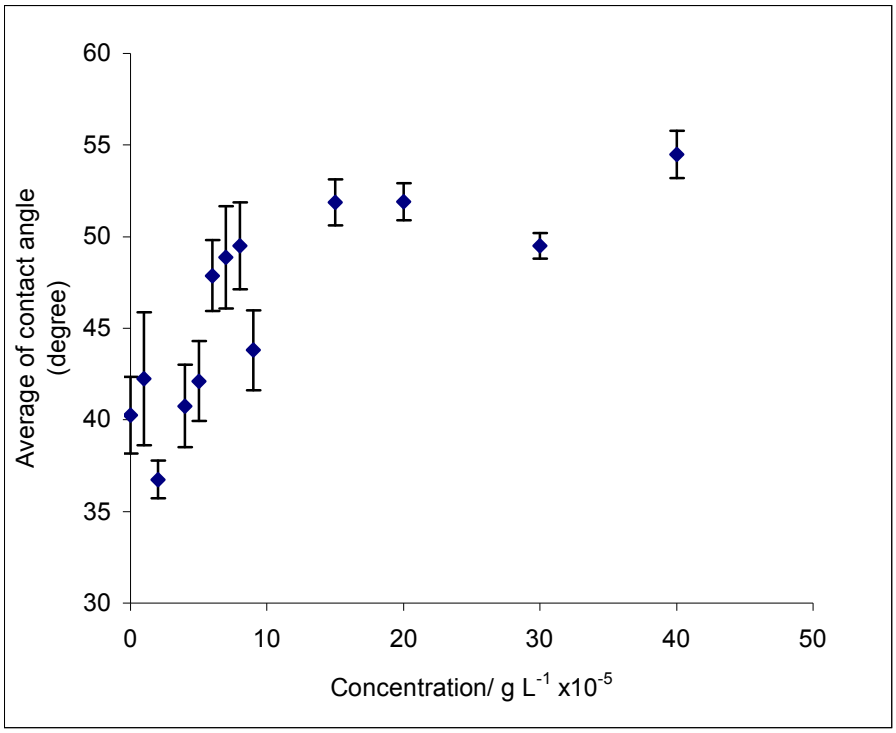

Figure 4. Contact angle of chitosan in 0.02 M acetic acid solution versus concentration

Determination of conductivity

Figures 5-6 show the correlation between equivalent conductivity and concentration. Equivalent conductivity decreases rapidly with increasing concentration until a CCC is reached, beyond which it decreases very gradually (almost constant)[36,41]. This behaviour is thought to be due to the decrease in ionic mobility of the polymer as concentration increases. Aggregation may have also occurred although probably not significantly. From this profile, the CCC values estimated (by noting a pronounced discontinuity in the curve) are 1×10^{-5} and 4×10^{-5} g L^{-1} for chitosan in 0.02 M formic acid and 0.02 M acetic acid respectively.

Maejo Int. J. Sci. Technol. **2009**, *3*(03), 415-425

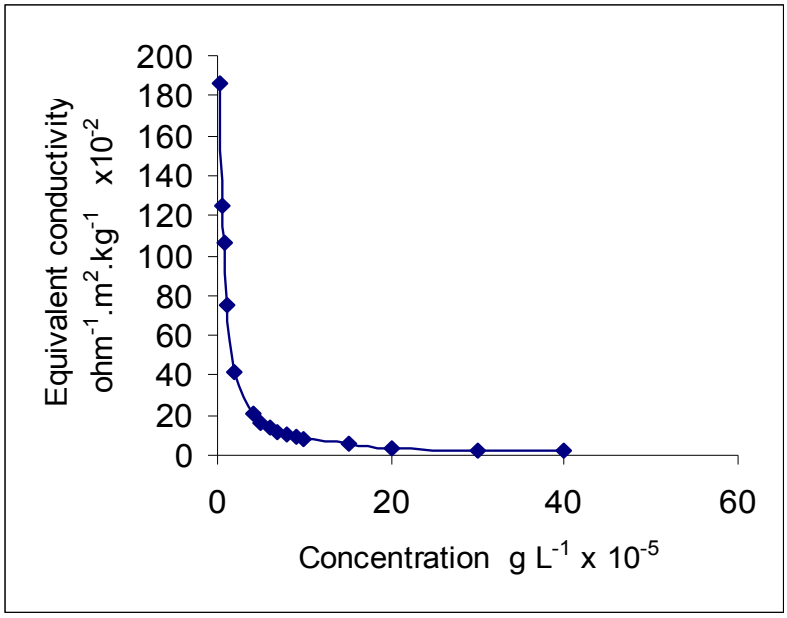

Figure 5. Equivalent conductivity of chitosan in 0.02 M formic acid solution versus concentration

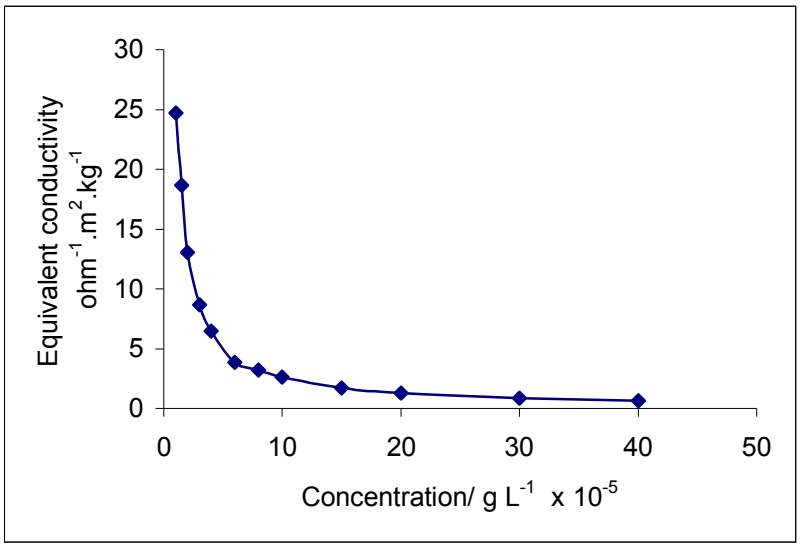

Figure 6. Equivalent conductivity of chitosan in 0.02 M acetic acid solution versus concentration

Conclusions

The intrinsic viscosity of chitosan with a molecular weight of 7.9 x 10^5 g mol^{-1} was 6.723 ± 0.294 and 28.213 ± 0.360 cm^3 g^{-1} in aqueous formic and acetic acids respectively. Contact angle of the chitosan solutions was found to increase initially with increase of the chitosan concentration up to a critical coagulation concentration (9.5×10^{-5} and 7×10^{-5} g L^{-1} in 0.02 M formic and acetic acids respectively). Conductivity of the chitosan solutions was found to decrease initially rapidly with

Maejo Int. J. Sci. Technol. **2009**, *3*(03), 415-425

increase of the chitosan concentration up to a critical coagulation concentration (1×10^{-5} and 4×10^{-5} g L^{-1} in 0.02 M formic acid and acetic acids respectively).

References

1. R. A. A. Muzzarelli, "Natural Chelating Polymers", Pergamon Press, London, **1973**, pp.83-95.
2. H. I. Bolker, "Natural and Synthetic Polymer: an Introduction", Marcel Dekker, New York, **1974**, pp.106-109.
3. G. Borchard and H. E. Junginger, "Modern drug delivery applications of chitosan*", Adv. Drug Del. Rev.*, **2001**, *52*, 139-144.
4. J. Karlsen and O. Skaugrud, "Excipient properties of chitosan", *Manuf. Chem.*, **1991**, *62***,** 18-19.
5. S. Sabnis and L. H. Block, "Improved infrared spectroscopic method for the analysis of degree of *N*-deacetylation of chitosan", *Polym. Bull.*, **1997**, *39*, 67-71.
6. S. Hirano and Y. J. J. Noishiki, "The blood compatibility of chitosan and *N*-acylchitosans", *Biomed. Mater. Res.*, **1985**, *19*, 413-417.
7. O. Pillai and R. Panchagnula, "Polymers in drug delivery", *Curr. Opin. Chem. Biol*., **2001**, *5*, 447-451.
8. E. Khor and L. Y. Lim, "Implantable applications of chitin and chitosan", *Biomaterials,* **2003***, 24*, 2339-2349.
9. S. Yuan and T. J. Wei, "New contact lens based on chitosan/gelatin composites", *Bioact. Compat. Polym.*, **2004**, *19*, 467-479.
10. Y. W. Cho, Y. N. Cho, S. H. Chung and W. Ko, "Water-soluble chitin as a wound healing accelerator", *Biomaterials*, **1999**, *20*, 2139-2145.
11. G. Crini, "Non-conventional low-cost adsorbents for dye removal: a review", *Bioresour. Technol.*, **2006**, *97*, 1061-1085.
12. S. Mima, M. Miya, R. Iwamoto and S. Yoshikawa, "Highly deacetylated chitosan and its properties", *J. Appl. Polym. Sci.,* **1983***, 28*, 1909-1917.
13. H. Miyoshi, K. Shimahara, K. Watanabe and K. Onodera, "Characterization of some fungal chitosans", *J. Biosci. Biotechnol. Biochem. Ed.*, **1992**, *56*, 1901-1905.
14. K. Nishimura, S. Nishimura, N. Nishi, I. Saiki, S. Tokura and I. Azuma, "Immunological activity of chitin and its derivatives", *Vaccine*, **1984**, *2*, 93-99.
15. K. Nishimura, S. Nishimura, N. Nishi, F. Numata, Y. Tone, S. Tokura and I. Azuma, "Adjuvant activity of chitin derivatives in mice and guinea pigs", *Vaccine*, **1985,** *3*, 379-384.
16. M. Hamdine. M. C. Heuzey and A. Begin, "Effect of organic and inorganic acids on concentrated chitosan solutions and gels", *Int. J. Biol. Macromol.*, **2005**, *37*, 134-142.
17. M. N. Moorjani, V. Achutha and D. I. Khasim, "Parameters affecting the viscosity of chitosan from prawn waste", *J. Food Sci. Technol.*., **1975**, *12*, 187-189.
18. W. A. Bough, W. L. Salter, A. C. M. Wu and B. E. Perkins, "Influence of manufacturing variables on the characteristics and effectiveness of chitosan products. I. Chemical composition, viscosity, and molecular-weight distribution of chitosan products", *Biotechnol. Bioeng.*, **1978**, *20***,** 1931-1943.

19. H. K. No, S. D. Kim, D. S. Kim, S. J. Kim and S. P. Meyers, "Effect of physical and chemical treatments on chitosan viscosity", *J. Korean Soc. Chitin Chitosan*, **1999**, *4*, 177-183.
20. B. S. Kim, K. B. Han, O. B. Rhee, J. W. Lee and H. D. Jo, "Effects of solvent on the viscosity of chitosan solution", Proceedings of the 8th International Chitin and Chitosan Conference and 4th Asia-Pacific Chitin and Chitosan Symposium, September 21-23, **2000**, Yamaguchi, Japan, pp. 105-106.
21. H. K. No, S. H. Kim, S. H. Lee, N. Y. Park and W. Prinyawiwatkul, "Stability and antibacterial activity of chitosan solutions affected by storage temperature and time", *Carbohydr. Polym.*, **2006**, *65*, 174–178.
22. O. V. Bobreshova, O. V. Bobylkina, P. I. Kulintsov, G. A. Bobrinskaya V. P. Varlamov and S. V. Nemtsev, "Conductivity of aqueous solutions of low-molecular chitosan", *Russ. J. Electrochem.*, **2004**, *40*, 694–697.
23. Q. x. Li , B. z. Song , Z. q. Yang and H. l. Fan, "Electrolytic conductivity behaviors and solution conformations of chitosan in different acid solutions", *Carbohydr. Polym.*, **2006**, *63*, 272–282.
24. J. Y. Cho, M. C. Heuzey, A. Be´gin and P. J. Carreau, "Viscoelastic properties of chitosan solutions: Effect of concentration and ionic strength", *J. Food Eng.*, **2006**, *74*, 500–515.
25. M. Cheng, J. Deng, F. Yang, Y. Gong, N. Zhao and X. Zhang, "Study on physical properties and nerve cell affinity of composite films from chitosan and gelatin solutions", *Biomaterials*, **2003**, *24*, 2871–2880.
26. V. Tangpasuthadol, N. Pongchaisirikul and V. P. Hovena, "Surface modification of chitosan films. Effects of hydrophobicity on protein adsorption", *Carbohydr. Res.*, **2003**, *338*, 937–942.
27. T. Çaykara, A. Alaslan , M. S. Eroglu and O. Gu¨ven, "Surface energetics of poly(N-vinyl-2-pyrrolidone)/chitosan blend films", *Appl. Sur. Sci.*, **2006**, *252*, 7430–7435.
28. C. H. Chen, F. Y. Wang, C. F. Maoa, W. T. Liao and C. D. Hsieh, "Studies of chitosan: II. Preparation and characterization of chitosan/poly(vinyl alcohol)/gelatin ternary blend films", *Int. J. Biol. Macromol.*, **2008**, *43*, 37–42.
29. P. Tengamnuay, A. Sahamethapat, A. Sailasuta and A. K. Mitra, "Chitosans as nasal absorption enhancers of peptides: Comparison between free amine chitosans and soluble salts", *Int. J. Pharm.*, **2000**, *197*, 53–67.
30. I. Orienti, T. Cerchiara, B. Luppi, F. Bigucci, G. Zuccari and V.Zecchi, "Influence of different chitosan salts on the release of sodium diclofenac in colon-specific delivery", *Int. J. Pharm.*, **2002**, *238*, 51–59.
31. G. C. Ritthidej, T. Phaechamud and T. Koizumi, "Moist heat treatment on physicochemical change of chitosan salt films", *Int. J. Pharm.*, **2002**, *232*, 11–22.
32. Z. Q. Yang, B. Z. Song, Q. X. Li and H. L Fan, "Effects of surfactant and acid type on preparation of chitosan microcapsules", *China Particuol.*, **2004**, *2*, 70–75.
33. R. A. A. Muzzarelli and R. Rochetti, "Determination of the degree of acetylation of chitosans by first derivative ultraviolet spectrophotometry", *Carbohydr. Polym.*, **1985**, *5*, 461–472.
34. M. L. Huggins, "The viscosity of dilute solutions of long-chain molecules. IV. Dependence on concentration", *J. Am. Chem. Soc.*, **1942**, *64*, 2716–2718.
35. S. Ladet, L. David and A. Domard, "Multi-membrane hydrogels", *Nature*, **2008**, *452*, 76-79.

Maejo Int. J. Sci. Technol. **2009**, *3*(03), 415-425

36. E. A. El-hefian, R. A. Khan and A. Yahaya, "Some physical properties of chitosan in propionic acid solutions", *Maejo Int. J. Sci. Technol.*, **2007**, *1*, 178-183.
37. R. H. Chen, W. C. Lin and J. H Lin, "Effects of pH, ionic strength, and type of anion on the rheological properties of chitosan solutions", *Acta Polym.*, **1994**, *45*, 41-46.
38. S. H. Maron and R. B. Reznik, "A new method for determination of intrinsic viscosity", *J. Polym. Sci. Ed. Part A-2: Polym. Phys.*, **1969**, *7*, 309-324.
39. D. J. Streeter and F. F. Boyer, "Viscosities of extremely dilute polystyrene solutions", *J. Polym. Sci*., **1953**, *14*, 5-14.
40. V. D. Dolzhikova, O. A. Soboleva and B. D. Summ, "Contact angles as indicators of micellization", *Colloid J.*, **1997**, *59*, 309-312.
41. D. Attwood and A. T. Florence, "Surfactant Systems, Their Chemistry, Pharmacy and Biology", Chapman and Hall, London, **1983,** pp. 469-566.

Maejo Int. J. Sci. Technol. **2009**, *3*(03), 426-433

Maejo International

Journal of Science and Technology

ISSN 1905-7873

Available online at www.mijst.mju.ac.th

Full Paper

Approximate solution of variational problems by an iterative decomposition method

Omotayo A. Taiwo [1,*] and Olutunde S. Odetunde [2]

[1] Department of Mathematics, University of Ilorin, P.M.B. 1515, Ilorin, Nigeria
[2] Department of Mathematical Sciences, Olabisi Onabanjo University, Ago - Iwoye P.M.B. 2002, Ago-Iwoye, Nigeria
* Corresponding author, e-mail: oataiwo2002@yahoo.com

Received: 27 May 2009 / Accepted: 12 October 2009 / Published: 11 November 2009

Abstract: A numerical method is presented for solving variational problems. The solution of an ordinary differential equation which arises from a variational problem is solved using the method. The solution is presented in the form of a fast convergent infinite series, the components of which are easily evaluated. Numerical examples are presented and results compared with exact solutions to show efficiency and accuracy.

Key words: variational problems, iterative decomposition, error

Introduction

In several problems arising in mathematics, mechanics, geometry, mathematical physics, other branches of science and even economics, it is necessary to minimise or maximise a certain functional. Because of the important role of this class of problems, considerable attention has been given to them. These problems are called variational problems [1, 2, 3].

The simplest form of a variational problem is given as:

$$V[y(x)] = \int_{x_0}^{x_1} F(x, y(x), y'(x))dx \qquad (1)$$

where V is the functional for which we need an extremum. To find the extremum of V, the boundary points of the admissible curve are of the following forms:

Maejo Int. J. Sci. Technol. **2009**, *3*(03), 426-433

$$y(x_0) = \alpha, \quad y(x_1) = \beta \tag{2}$$

Several popular methods have been applied to solve variational problems. One of the most popular methods is the direct method, in which the variational problem is regarded as a limiting case of a finite number of variables. The direct method of Ritz and Galerkin has been applied for this class of problems [4, 1]. A piecewise constant solution was obtained using the Walsh series method [1]. Some orthogonal polynomials have been used to obtain continuous solutions of variational problems. The work of Hwang and Shih [2] is an example of this method. The Fourier series are applied by Razzaghi and Razzaghi [3] to obtain continuous solutions of variational problems. Taylor series are used for the same purpose [5, 3]. The necessary condition for the solution of equation (1) is to satisfy the Euler-Lagrange equation:

$$F_y - \frac{d}{dx}F_{y'} = 0 \tag{3}$$

with the boundary conditions (2). If the solution of the Euler-Lagrange equation satisfies the boundary bonditions, it is unique, and this unique extremal will be the solution of the given variational problem [4]. Therefore, another approach for solving the problem (1) is to find the solution of the ordinary differential equation (3) which satisfies the boundary conditions (2). The general form of the variational problem given by equation (1) is

$$V[y_1, y_2, \ldots, y_n] = \int_{x_0}^{x_1} F(x, y_1, y_2, \ldots, y_n, y_1', y_2', \ldots, y_n')dx \tag{4}$$

with the given boundary conditions for all functions:

$$\begin{aligned} &y_1(x_0) = \alpha_1 \quad y_2(x_0) = \alpha_2, \ldots, y_n(x_0) = \alpha_n \\ &y_1(x_1) = \beta_1, \quad y_2(x_1) = \beta_2, \ldots, \quad y_n(x_1) = \beta_n \end{aligned} \tag{5}$$

The Euler-Lagrange equation (3) then takes the form of a system of second order differential equations:

$$F_{yi} - \frac{d}{dx}F_{yi} = 0, \qquad i = 1, 2, \ldots, n \tag{6}$$

with boundary conditions given by equation (5).

When the functional are dependent on higher-order derivatives, the variational problem is defined as:

$$V[y(x)] = \int_{x_0}^{x_1} F\left(x, y(x), y'(x), y''(x), \ldots, y^{(n)}(x)\right)dx \tag{7}$$

with the boundary conditions given as:

$$\begin{aligned} &y(x_0) = \alpha_0, y'(x_0) = \alpha_1, y''(x_0) = \alpha_2, \ldots, y^{(n-1)}(x_0) = \alpha_{n-1} \\ &y(x_1) = \beta_0, \; y'(x_1) = \beta_1, \; y''(x_1) = \beta_2, \ldots, y^{(n-1)}(x_1) = \beta_{n-1} \end{aligned} \tag{8}$$

The function y(x) which extremises the functional given by equation (7) must then satisfy the Euler-Poisson equation:

$$F_y - \frac{d}{dx}F_{y'} + \frac{d^2}{dx^2}F_{y''} + \ldots + (-1)^n \frac{d^n}{dx^n}F_{y^{(n)}} = 0 \tag{9}$$

Maejo Int. J. Sci. Technol. **2009**, *3*(03), 426-433

Equation (9) with boundary conditions (8) forms a 2n-point boundary value problem, and its solution extremises (7).

In the present work, we find the solution of variational problems by applying an iterative decomposition method. The method being presented is useful for solving problems which can be written in the form:

$$y = P(y) + f \tag{10}$$

where y is unknown, P is a non-linear operator and f is a given function. Equations of the form (10) occur in a wide variety of problems in the applied sciences. The proposed method searches for a solution in the form of a series, by decomposing the non-linear operator into a series, the terms of which are calculated recursively.

Iterative Decomposition Method

Consider the Euler-Lagrange equation (3). For the completion of the iterative decomposition, we can write equation (3) as:

$$L(y) - N(y) = f \tag{11}$$

for $x_0 \leq x \leq x_1$, where $L = \frac{d^2}{dx^2}$ is the second-order derivative operator, N is a nonlinear operator which contains differential operators of order less than two, and f is a given function. Suppose the inverse operator L^{-1} exists and can be taken as the two-fold definite integral of the following form:

$$L^{-1}(\cdot) = \int_{x_0}^{x}\int_{x_0}^{t_2}(\cdot)\,dt_1\,dt_2 \tag{12}$$

Applying the inverse operator L^{-1} to both sides of (11) , we have

$$L^{-1}L(y) = L^{-1}N(y) + L^{-1}f \tag{13}$$

Thus, we have

$$y(x) - y(x_0) - xy'(x_0) = L^{-1}N(y) + L^{-1}f \tag{14}$$

Thus, by the decomposition procedure, we construct the unknown function y(x) as the sum of the components of a decomposition series. The equation (14) is of the form:

$$y(x) = K(y) + c \tag{15}$$

where c is a constant and K denotes the nonlinear term on the RHS of (14).

It is convenient to find the solution of (15) in series form as:

$$y(x) = \sum_{i=0}^{\infty} y_i \tag{16}$$

We decompose the nonlinear operator K as:

$$K(y) = K(y_0) + \sum_{i=0}^{\infty}\{K(\sum_{j=0}^{i} y_j) - K(\sum_{j=0}^{i-1} y_j)\} \tag{17}$$

From equations (16) and (17), equation (15) is equivalent to

Maejo Int. J. Sci. Technol. **2009**, *3*(03), 426-433

$$\sum_{i=0}^{\infty} y_i = c + K(y_0) + \sum_{i=0}^{\infty}\left\{K(\sum_{j=0}^{i} y_j) - K(\sum_{j=0}^{i-1} y_j)\right\} \quad (18)$$

We then define the following iterative scheme:

$$y_0(x) = c$$

$$y_1(x) = K(y_0)$$

$$y_2 = K(y_0 + y_1) - K(y_0)$$

$$\vdots$$

$$y_{n+1} = K(y_0 + y_1 + y_2 + \cdots + y_n) - K(y_0 + y_1 + y_2 + \cdots + y_{n-1}) \quad (19)$$

Substituting the components y_i of (19) in (16) gives the solution of the equation.

Numerical Experiments

We now apply the decomposition method discussed in the previous section to solving some variational problems and then compare the solutions with the known exact solution of each problem.

Example 1

We consider the variational problem:

$$\min V = \int_0^{\pi/2}((y'')^2 - y^2 + x^2)dx \quad (20)$$

which satisfies the conditions:

$$y(0) = 1, \quad y'(0) = 0, \quad y\left(\frac{\pi}{2}\right) = 0, \quad y'\left(\frac{\pi}{2}\right) = -1 \quad (21)$$

The exact solution of this problem is $\cos x$.

The corresponding Euler-Poisson equation is:

$$y^{(iv)} - y = 0 \quad (22)$$

We can put equation (22) in operator form as:

$$Ly = y \quad (23)$$

where $L = \frac{d^4}{dx^4}$

Applying the iterative decomposition method, we have

$$y(x) = 1 + \frac{Ax^2}{2!} + \frac{Bx^3}{3!} + L^{-1}(y) \quad (24)$$

where A = y (0) and B = y'(0).

Maejo Int. J. Sci. Technol. **2009**, *3*(03), 426-433

Then

$$y_0 = 1 + \frac{Ax^2}{2!} + \frac{Bx^3}{3!}$$

$$y_1 = L^{-1} = \frac{x^4}{4!} + \frac{Ax^6}{6!} + \frac{Bx^7}{7!}$$

$$y_2 = L^{-1}(y_0 + y_1) - L^{-1}(y_0) = \frac{x^8}{8!} + \frac{Ax^{10}}{10!} + \frac{Bx^{11}}{11!}$$

$$y_3 = \frac{x^{12}}{12!} + \frac{Ax^{14}}{14!} + \frac{Bx^{15}}{15!}$$

$$y_4 = \frac{x^{16}}{16!} + \frac{Ax^{18}}{18!} + \frac{Bx^{19}}{19!} \qquad (25)$$

$$y_5 = \frac{x^{20}}{20!} + \frac{Ax^{22}}{22!} + \frac{Bx^{23}}{23!}$$

Summing the terms of equations (25) gives

$$y(x) = 1 + \frac{Ax^2}{2!} + \frac{Bx^3}{3!} + \frac{x^4}{4!} + \frac{Ax^6}{6!} + \frac{Bx^7}{7!} + \frac{x^8}{8!} + \frac{Ax^{10}}{10!} + \frac{Bx^{11}}{11!} + \frac{x^{12}}{12!} + \frac{Ax^{14}}{14!} + \frac{Bx^{15}}{15!} + \frac{x^{16}}{16!} + \frac{Ax^{18}}{18!} + \frac{Bx^{19}}{19!} + \frac{x^{20}}{20!} + \frac{Ax^{22}}{22!} + \frac{Bx^{23}}{23!} \qquad (26)$$

Applying the boundary conditions (21) to equation 26, we obtain the values of the constants:

$$A = -1.000000001 \; and \; B = 2.000000004E-09$$

Then y(x) is approximated as:

$$\begin{aligned} y(x) = 1 &- 0.5x^2 + (3.33333334E-10)x^3 + 0.041666666x^4 \\ &- (1.38888889E-03)x^6 + (3.968253976E-13)x^7 \\ &+ (2.48015873E-05)x^8 - (2.755731925E-07)x^{10} \\ &+ (5.010421687E-17)x^{11} + (2.087675699E-09)x^{12} \\ &- (1.147074561E-11)x^{14} + (1.529432749E-21)x^{15} \\ &+ (4.779477332E-14)x^{16} - (1.561920698E-16)x^{18} \\ &+ (1.644127053E-26)x^{19} + (4.110317623E-19)x^{20} \\ &- (8.896791401E-22)x^{22} + (7.736340357E-32)x^{23} \end{aligned} \qquad (27)$$

Table 1 gives the approximate values of y(x) for some points in the interval $0 \leq x \leq \frac{\pi}{2}$ and compares the approximate solution with the exact solution at those points. The very small errors generated by our decomposition approximation can be observed. Errors of less than 10E-10 are written as zero. In fact better accuracy is possible if more terms of the approximation series are taken. Recall that for the current problem, only five terms of the series have been taken to generate our approximate solution.

Maejo Int. J. Sci. Technol. **2009**, *3*(03), 426-433

Table 1. Approximate values by iterative decomposition method (IDM) vs. exact values of y(x) in Example 1

y / x	Exact	IDM Approximate	Error
0	1.000000000	1.000000000	0.000000000
$\frac{\pi}{20}$	0.98768834	0.98768834	5.95E-10
$\frac{\pi}{10}$	0.951056516	0.951056515	1.295E-09
$\frac{3\pi}{20}$	0.891006524	0.891006524	1.88E-10
$\frac{\pi}{5}$	0.809016994	0.809016994	3.75E-10
$\frac{\pi}{4}$	0.707106781	0.707106781	1.86E-10
$\frac{3\pi}{10}$	0.587785252	0.587785252	2.93E-10
$\frac{7\pi}{20}$	0.453990499	0.453990499	7.37E-10
$\frac{2\pi}{5}$	0.309016994	0.309016994	3.71E-10
$\frac{9\pi}{20}$	0.156434465	0.156434465	3.60E-11
$\frac{\pi}{2}$	0.000000000	-4.73732750E-09	4.74E-09

Example 2

Consider the variational problem [6]:

$$\min v = \int_0^1 \left(y(x) + y'(x) - 4e^{3x}\right)^2 dx \tag{28}$$

with given boundary conditions:

$$y(0) = 1, \quad y(1) = e^3 \tag{29}$$

The corresponding Euler-Lagrange equation is found to be:

Maejo Int. J. Sci. Technol. **2009**, *3*(03), 426-433

$$y''(x) - y(x) - 8e^{3x} = 0 \tag{30}$$

with the same boundary conditions as (29).

The exact solution of this problem is $y = e^{3x}$. Using the operator form of (28), we have

$$Ly = y + 8e^{3x} \tag{31}$$

Thus,

$$y(x) = 1 + Ax + L^{-1}(8e^{3x}) + L^{-1}(y(x)) \tag{32}$$

Using the previous decomposition procedure,

$$\sum_{n=0}^{\infty} y_n(x) = 1 + Ax + L^{-1}(8e^{3x}) + L^{-1}(\sum_{k=0}^{\infty} y_{k-1}(x)) \tag{33}$$

Then,

$$y_0(x) = \frac{1}{9} + Ax - \frac{8}{3}x + \frac{8}{9}e^{3x}$$

$$y_1(x) = -\frac{8}{81} - \frac{8}{27}x + \frac{x^2}{18} + \frac{Ax^3}{6} - \frac{4x^3}{9} + \frac{8}{81}e^{3x}$$

$$y_2(x) = -\frac{8}{729} - \frac{8x}{243} - \frac{4x^2}{81} - \frac{4x^3}{81} + \frac{x^4}{216} + \frac{Ax^5}{120} - \frac{x^5}{45} + \frac{8}{729}e^{3x}$$

$$y_3(x) = -\frac{8}{6561} - \frac{8x}{2187} - \frac{8x^2}{1458} - \frac{4x^3}{729} - \frac{x^4}{243} - \frac{x^5}{405} + \frac{x^6}{6480} + \frac{Ax^7}{5040} - \frac{x^7}{1890} + \frac{8}{6561}e^{3x}$$

and so on. Then the four-term approximation of y(x) is given as:

$$y(x) = \frac{1}{6561} + Ax - \frac{6560}{2187}x + \frac{x^2}{1458} + \frac{Ax^3}{6} - \frac{364x^3}{729} + \frac{x^4}{1941} + \frac{Ax^5}{120} - \frac{2x^5}{81} + \frac{x^6}{6480} + \frac{Ax^7}{5040} - \frac{x^7}{1890} + \frac{6560}{6561}e^{3x} \tag{34}$$

To evaluate the constant A, we impose the boundary condition at x=1 on the approximate solution (34). Then we obtain A= 3.00003101. The approximation is then given as:

$$\begin{aligned} y(x) = {} & (1.524157903E-04) + (4.88257E-04)x + (6.858710562E-04)x^2 \\ & + (6.9104E-04)x^3 + (5.144032922E-04)x^4 + (3.11222E-04)x^5 \\ & + (1.543209877E-04)x^6 + (6.61437189E-04)x^7 \\ & + (0.999847584)e^{3x} \end{aligned} \tag{35}$$

Table 2 gives a comparison of the exact solution with approximation of the solution at points $x \epsilon [0,1]$. From this example it is obvious that the decomposition algorithm can be considered an efficient method. A better approximation to the solution of the problem may be achieved by taking more components of y(x), as shown in example 1.

Maejo Int. J. Sci. Technol. **2009**, *3*(03), 426-433

Table 2. Approximate values by iterative decomposition method (IDM) vs. exact values of y(x) in Example 2

x	Exact	IDM Approximate	Error
0.0	**1.000000000**	**0.999999999**	**1.000000E-09**
0.1	**1.349858808**	**1.349861914**	**3.106000E-06**
0.2	**1.8221188**	**1.822120252**	**1.451610E-06**
0.3	**2.459603111**	**2.459612688**	**9.576590E-06**
0.4	**3.320116923**	**3.32013064**	**1.371726E-05**
0.5	**4.48168907**	**4.481709836**	**2.076566E-05**
0.6	**6.049647464**	**4.049683533**	**3.606826E-05**
0.7	**8.166169913**	**8.166241**	**7.108743E-05**
0.8	**11.02317638**	**11.02332391**	**1.475294E-04**
0.9	**14.87973172**	**14.88003464**	**3.029109E-04**
1.0	**20.08553692**	**20.08613453**	**5.976101E-04**

Conclusions

The iterative decomposition algorithm is used for the solution of the ordinary differential equations which arise from variational problems. It is noteworthy that this method does not require the discretisation of the variables .The implementation of the method is straightforward, requiring no restrictive assumptions or linearisation techniques.

References

1. I. M. Gelfand and S. V. Fomin, "Calculus of Variations", Prentice-Hall, New Jersey, **1963**.
2. C. Hwang and Y. P. Shih, "Laguerre series direct method for variational problems", *J. Opt. Theory Appl.*, **1983**, *39*, 143-149.
3. M. Razzaghi and M. Razzaghi, "Fourier series direct method for variational problems", *Int. J. Control.*, **1988**, *48*, 887-895.
4. L. Elsgolts, "Differential Equations and the Calculus of Variations", Mir, Moscow, **1977**.
5. V. D. Geijji and H. Jafari, "An iterative method for solving nonlinear functional equations", *J. Math. Anal. Appl.*, **2006**, *316*, 753-763.

Maejo Int. J. Sci. Technol. **2009**, *3*(03), 434-445

Maejo International

Journal of Science and Technology

ISSN 1905-7873

Available online at www.mijst.mju.ac.th

Short Article

Effect of temperature on sucrose penetration and browning reactions in longan aril during osmotic dehydration

Wiwat Wangcharoen

Faculty of Engineering and Agricultural Industry, Maejo University, Chiang Mai 50290, Thailand

E-mail: wiwat@mju.ac.th

Received: 12 July 2009 / Accepted: 13 November 2009 / Published: 20 November 2009

Abstract: Sucrose penetration and browning reactions in longan aril during osmotic dehydration at various temperatures were examined by measurement of total soluble solid and colour parameter (b*) of longan aril. Mathematical modelling and Arrhenius equation were used to express the changes during the process and the effect of temperature respectively. Parabola models ($Y = a_0 + a_1X + a_2X^2$) were fitted to the set of total soluble solid data where a_0 is the initial total soluble solid and X is the soaking time, because the rate of increase in total soluble solid of longan aril during osmotic dehydration was high in the initial period and gradually decreased until the system reached equilibrium. Linear models ($Y = a_0 + a_1X$) were fitted to the set of b* values where a_0 is the initial value and X is the soaking time. Mathematical equations were created for predicting response values at any temperature ranging from 30 to 90 °C, but the predicted values were slightly lower than the experimental ones.

Keywords: longan, sucrose penetration, browning reactions, osmotic dehydration, mathematical modelling, Arrhenius equation

Introduction

Longan (*Dimocarpus longan* (Lour.) Steud), commonly called Dragon's-eye in English and Lamyai in Thai, is reported to have originated in north-eastern India, Burma or south China in Yunan province [1]. In Thailand, it is generally grown in Chiang Mai and Lamphun provinces. Many cultivars including Daw, See Chompoo, Haew, Biew Kiew, Dang Klom and Bai Dam are grown [1-3], but Daw

Maejo Int. J. Sci. Technol. **2009**, *3*(03), 434-445

is the major cultivar which is grown for food processing supply. Approximately 30% of all produce is used for fresh consumption in the whole country, 20% for export, 40% for dried longan production, and 10% for longan canning process [4]. Longan fruits are brownish, globose to ovoid, and 1.5-2.5 cm in diameter. The skin is thin without protuberances. The aril is white, translucent and sweet with a mild aromatic spiciness [1]. The nutritional composition of a 100 g edible portion of longan consists of 71 calories, 81.0 g moisture, 15.6 g carbohydrate, 1.0 g protein, 1.4 g fat, 0.3 g crude fibre, 0.03 mg vitamin B1, 0.14 mg vitamin B2, 0.3 mg niacin, 56 mg vitamin C, 23 mg calcium, 36 mg phosphorus and 0.4 mg iron [5].

Due to the surplus of longan produce, a number of processes for preserving longan have been developed [6-7]. Osmotic dehydration by soaking the fruit flesh in a concentrated sugar solution is a common process used for fruit preservation. Mass transfer during osmotic dehydration can be divided into two periods, viz. an initial period with a high rate of water removal and solute penetration, followed by a period with a decreasing rate of water removal and solute penetration [8]. The temperature of the process can affect the rate of mass transfer [8] and such reactions as browning reactions [9-10]. To understand the effect of temperature on mass transfer and browning reactions during osmotic dehydration, the knowledge of thermodynamics and kinetics is required. Thermodynamics explains the driving force, the energy and entropy changes and the direction of reaction, while kinetics expresses the speed at which a reaction proceeds. Basically, mathematical models are used to determine the change and speed of reaction, while Arrhenius equation is used to show how the reaction speed is affected by temperature as well as to derive the activation energy of reactions [11].

This work aims to express the effect of temperature on sucrose penetration and browning reactions during osmotic dehydration of longan aril by using mathematical modelling and Arrhenius equation to explain the changes of total soluble solid and b* colour parameter of samples.

Materials and Methods

Osmotic dehydration

Logan aril (Daw) was purchased from a local fruit canning company. It was blanched in boiling water for 1 min before soaking in 70°Brix sucrose solution (longan aril:sucrose solution = 1:1) at room temperature (30$\pm$5 °C) for 24 hours. The whole process was repeated at 50, 60, 70, 80 and 90 °C. Total soluble solid (in °Brix) and colour parameter b* of longan aril were recorded before soaking and then every 4 hours. Total soluble solid was measured by a set of portable refractometers (Models FG 103/113, FG 104/114 and FG 106/116: Beijing Zhongjin Tech Metallurgical Equipment Corp., China), and colour parameter b* was measured by a JUKI Tri-stimulus colorimetre, Model JC801 (Colour Techno System Corp., Japan).

Data analysis and modelling

The experiment at each temperature was done in triplicate. Means of total soluble solid and b^* values were obtained from seven measurements. Mathematical models were applied to describe the

Maejo Int. J. Sci. Technol. **2009**, *3*(03), 434-445

changes of recorded data at each temperature and the speed of changes was calculated. The constant (pre-exponential factor or frequency factor) and the activation energy (E_a) of each change in the Arrhenius equation were determined and used to create mathematical models for predicting values of total soluble solid and b* at any temperature ranging from 30 to 90 °C. The linear regression between predicted and experimental values was done to compare their values.

Results and Discussion

Sucrose penetration

The increase in total soluble solid in longan aril expresses the penetration of sucrose from the concentrated sucrose solution. The gain in total soluble solid of longan aril, the initial value before immersion in the sugar solution being at 17.4±0.5°Brix, is shown in Figure 1. Parabola models, $Y = a_0 + a_1X + a_2X^2$, where a_0 is initial total soluble solid of longan aril, a_1 is initial rate of increase, a_2 is acceleration and X is soaking time, can fit this phenomena. The rate of increase in total soluble solid could be estimated from the first-order differential equation of the parabola model [11]: $dY/dX = dY/dt = a_1 + 2a_2X$. The rates of increase in total soluble solid were high at the initial period and gradually decreased until they became the small plus or minus values (Table 1) when the water activity of both the sucrose solution and the product reached equilibrium [8].

From the Arrhenius equation: $k = Ae^{-Ea/RT}$, the constant (A) and the activation energy (E_a) can be determined by taking the natural logarithms of both sides of the above equation to yield a linear equation: $\ln k = \ln A + (-E_a/R)(1/T)$, where ln A is the Y-axis intercept and $(-E_a/R)$ is the slope. In this experiment, five linear equations could be created for soaking time at 0, 4, 8, 12 and 16 hours (Figure 2). The equation for soaking time at 20 and 24 hours could not be created because the value of ln k where k was a minus value could not be determined. However, only 2 linear equations at 0 and 4 hours were needed to create the parabola equations for predicting values at any temperature in the experimental range since the value of a_1 and a_2 could be obtained from those two equations (Tables 2-3). The linear regression between the predicted and experimental values could be created and it was found that the predicted values were slightly lower (0.9 time) than the experimental ones (Figure 3).

Maejo Int. J. Sci. Technol. **2009**, *3*(03), 434-445

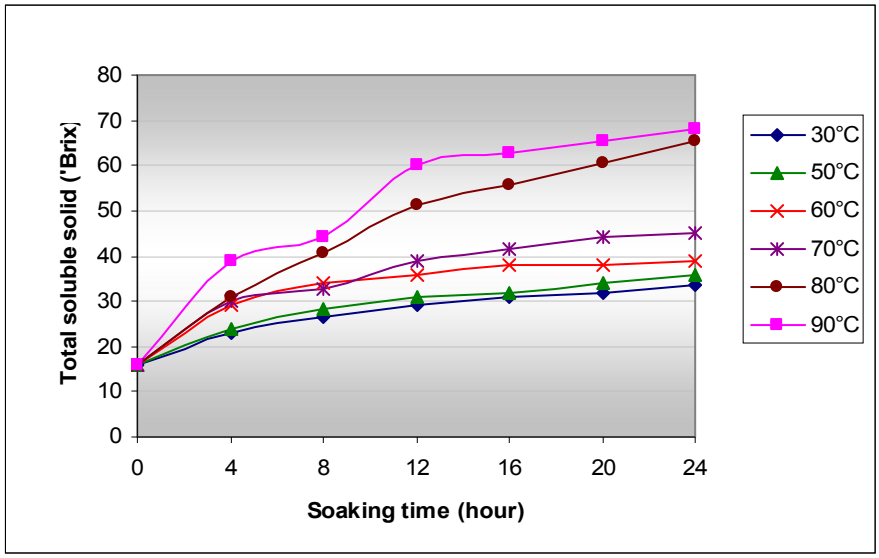

(a)

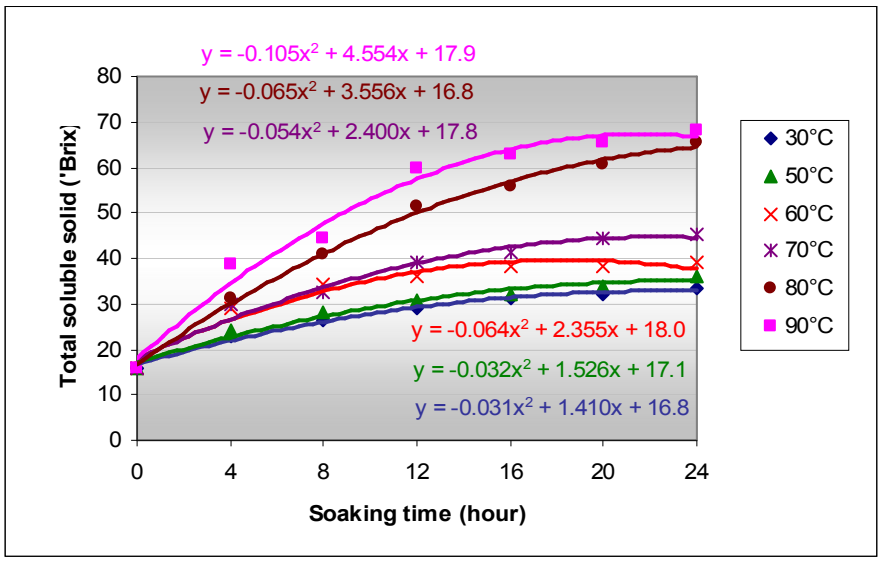

(b)

Figure 1. Changes of total soluble solid in longan aril during osmotic dehydration: (a) raw data, (b) mathematical fit

Maejo Int. J. Sci. Technol. **2009**, *3*(03), 434-445

Table 1. Change in rate of increase (°Brix /hour) in total soluble solid of longan aril during osmotic dehydration

Temperature	Soaking time (hour)						
(°C)	0	4	8	12	16	20	24
30	1.410	1.162	0.914	0.666	0.418	0.170	-0.078
50	1.526	1.270	1.014	0.758	0.502	0.246	-0.010
60	2.266	1.754	1.242	0.730	0.218	-0.294	-0.806
70	2.330	1.898	1.466	1.034	0.602	0.170	-0.262
80	3.556	3.036	2.516	1.996	1.476	0.956	0.436
90	4.554	3.714	2.874	2.034	1.194	0.354	-0.486

Note: Values are calculated by first-order differential equation: $dY/dX = a_1 + 2a_2X$, where X is soaking time.

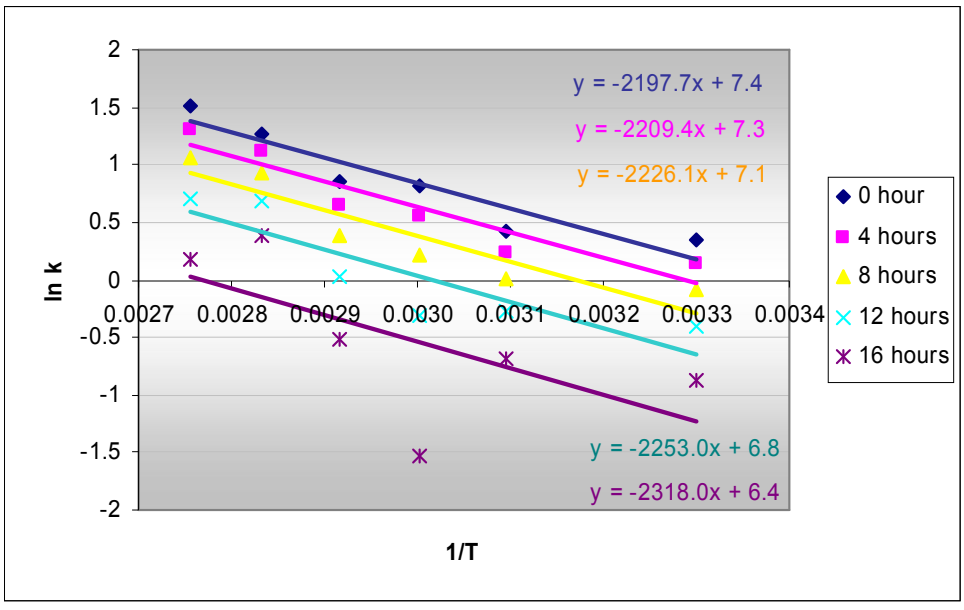

Figure 2. Linear Arrhenius equations from total soluble solid data of longan aril during osmotic dehydration

Maejo Int. J. Sci. Technol. **2009**, *3*(03), 434-445

Table 2. Parameters for creating the parabola equation for prediction of total soluble solid in longan aril at any temperature (30-90 °C) during osmotic dehydration

Soaking time (hour)	Y-axis intercept, ln A	Slope, $-E_a/R$	A	E_a (kJ mol^{-1})	a_1, $Ae^{-Ea/RT}$	a_2, $(Ae^{-Ea/RT} - a_1)/2X_1$
0	7.4	-2197.7	1636.0	18.3	$1636.0e^{-2197.7/T}$	
4	7.3	-2209.4	1480.3	18.4		$(1480.3e^{-2209.4/T} - a_1)/2X_1$

Note: T is temperature in Kelvin.
X_1 is the first recorded time after process was started and it was equal to 4 in this experiment.
Parabola equation used: $Y = a_0 + a_1X + a_2X^2$, where a_0 is the initial total soluble solid of longan aril.

Table 3. Mathematical models for predicting soluble solid in longan aril during osmotic dehydration at temperature ranging from 30 to 90 °C

Temperature (°C)	Model
30	$Y = -0.04X^2 + 1.40X + a_0$
40	$Y = -0.05X^2 + 1.35X + a_0$
50	$Y = -0.06X^2 + 2.16X + a_0$
60	$Y = -0.08X^2 + 2.64X + a_0$
70	$Y = -0.09X^2 + 3.18X + a_0$
80	$Y = -0.11X^2 + 3.80X + a_0$
90	$Y = -0.13X^2 + 4.49X + a_0$

Note: X is soaking time; a_0 is the initial total soluble solid of longan aril.

Maejo Int. J. Sci. Technol. **2009**, *3*(03), 434-445

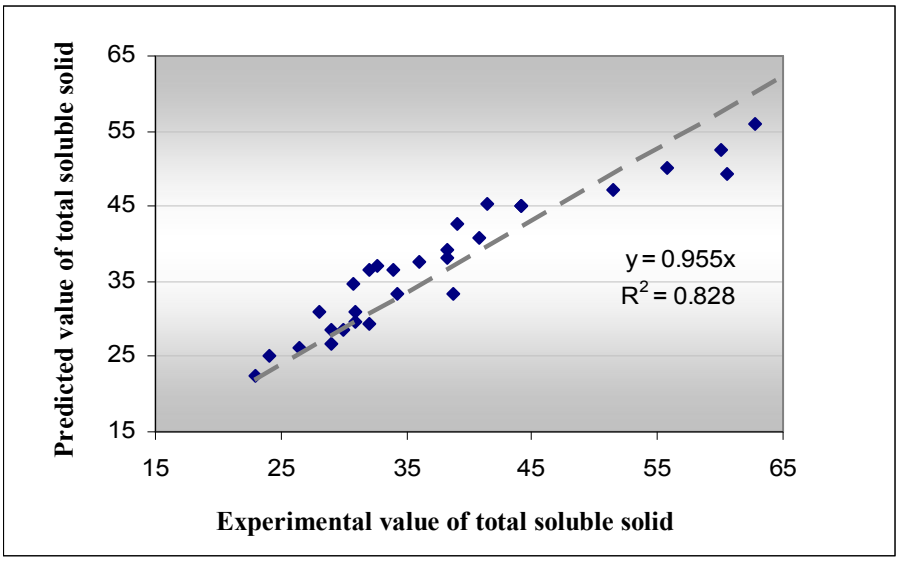

Figure 3. Linear regression between predicted and experimental values of total soluble solid

Browning reactions

Browning reactions in this study were nonenzymatic browning reactions which might be Maillard reaction and ascorbic acid browning since reducing sugar, protein and ascorbic acid were found in longan aril [5]. Maillard reaction is that between carbonyl groups (from reducing sugars, aldehydes, ketones, lipid oxidation products) and amino compounds (lysine, glycine, peptides, amines, ammonia, proteins) [12], while ascorbic acid browning is the thermal decomposition of ascorbic acid [13].

The colour parameter, b*, is one of the international standards for colour measurement adopted by the Commission Internationale d' Eclairage (CIE) in 1976. Parameter b* is a chromatic component which ranges from -120 (blue) to 120 (yellow) [14], and it has been used to express the brownness of fruit wines [15]. In this study the parameter b* was used to measure the browning reactions occurring during osmotic dehydration. The initial value of b* was 3.4 $\pm$ 0.3, which was increased when high temperatures (over 50 °C) were used (Figure 4), since nonenzymatic browning reactions are time and temperature dependent and are obviously faster at a higher temperature [9]. Linear models, $Y = a_0 + a_1X$, were fitted to this data set where a_0 is the initial value of b*, a_1 is its rate of increase and X is soaking time. The constant (A) and the activation energy (E_a) could be determined from a linear Arrhenius equation (Figure 5 and Table 4), and linear equations for predicting the value of b* during the process at any temperature ranging from 30 to 70 °C were created (Table 5). The predicted values were regressed against experimental values whereupon it was found that the predicted values were slightly smaller (0.9 time) than the experimental ones (Figure 6).

Maejo Int. J. Sci. Technol. **2009**, *3*(03), 434-445

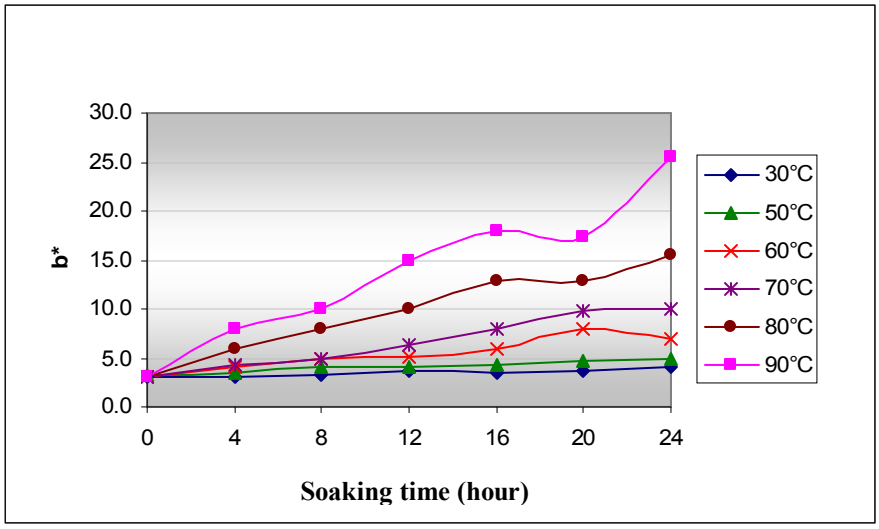

(a)

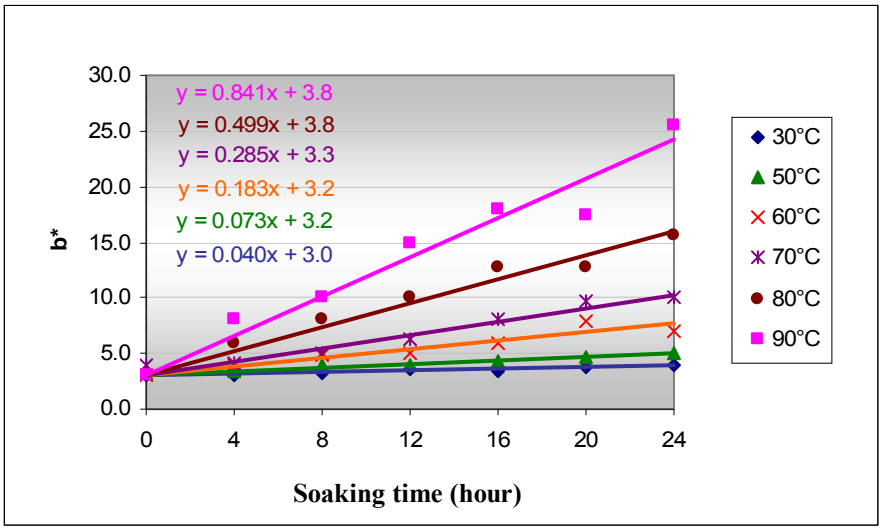

(b)

Figure 4. Changes of parameter b* of longan aril during osmotic dehydration: (a) raw data, (b) mathematical fit

Maejo Int. J. Sci. Technol. **2009**, *3*(03), 434-445

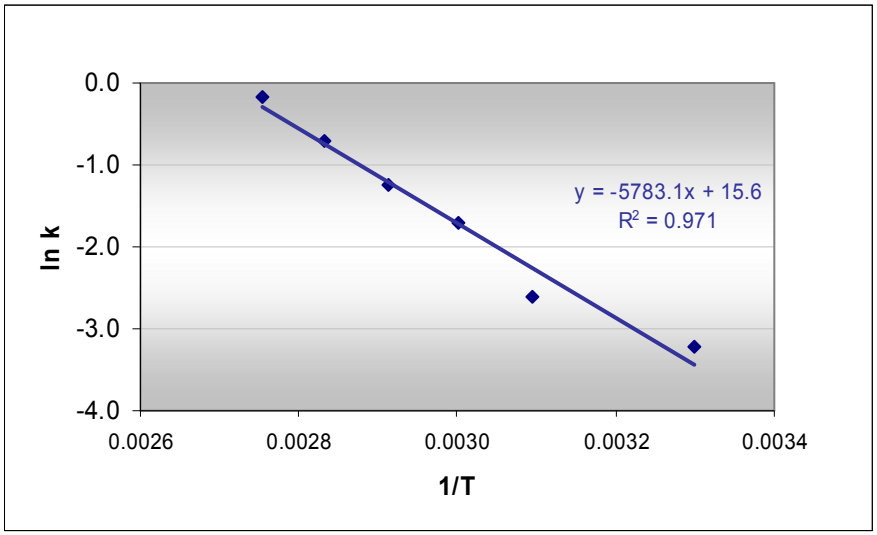

Figure 5. A linear Arrhenius equation from b* values of longan aril during osmotic dehydration

Table 4. Parameters for creating the linear equation to predict values of b* of longan aril at 30-90 °C during osmotic dehydration

Y-axis intercept, ln A	Slope, $-E_a/R$	A	E_a (kJ mol^{-1})	a_1, $Ae^{-Ea/RT}$
15.6	-5783.1	5,956,538.0	48.1	$5{,}956{,}538.0e^{-5783.1/T}$

Note: T is temperature in Kelvin.
Linear models used: $Y = a_0 + a_1X$, where a_0 is the initial value of b*

Maejo Int. J. Sci. Technol. **2009**, *3*(03), 434-445

Table 5. Mathematical models for predicting parameter b* of longan aril during osmotic dehydration at 30-90 °C

Temperature (°C)	Model
30	$Y = 0.03X + a_0$
40	$Y = 0.06X + a_0$
50	$Y = 0.10X + a_0$
60	$Y = 0.17X + a_0$
70	$Y = 0.29X + a_0$
80	$Y = 0.46X + a_0$
90	$Y = 0.72X + a_0$

Note: X is soaking time; a_0 is initial value of b*.

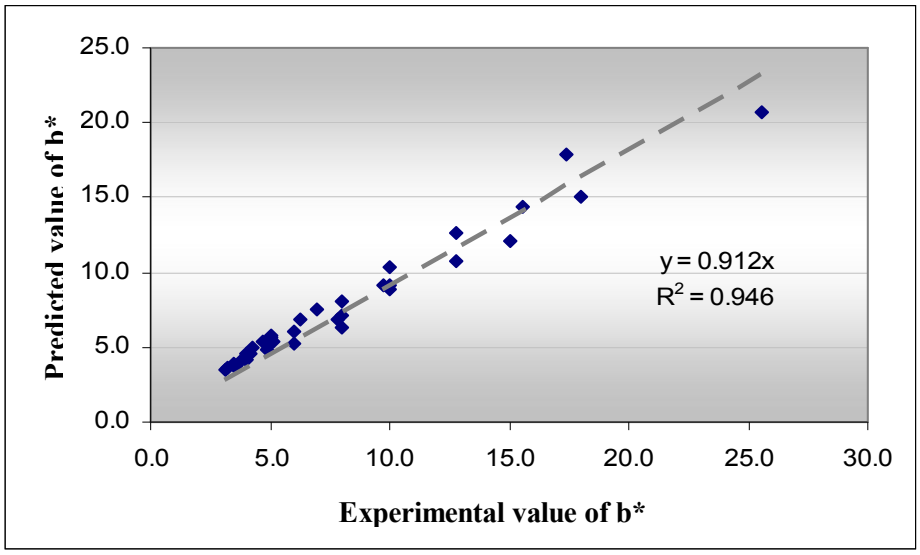

Figure 6. Linear regression between predicted and experimental values of b*

Conclusions

This study has shown how to express the effect of temperature on two phenomena, i.e. sucrose penetration and browning reactions, during osmotic dehydration of longan aril by using mathematical modelling and Arrhenius equation. The results allow researchers to predict response values during the process at any temperature in the experimental range, which could be useful for a process control when

Maejo Int. J. Sci. Technol. **2009**, *3*(03), 434-445

the final total soluble solid of longan aril is set or the initial total soluble solid of longan aril is changed, or when it is necessary to change the temperature of process. However, the result of this work is applicable only when a 70 °Brix sucrose solution is used. More experimentation is needed for other sucrose concentrations.

Acknowledgement

This work was a part of the research project supported by a grant from the Office of Agricultural Research and Extension at Maejo University.

References

1. H. Y. Nakasone and R. E. Paull, "Tropical Fruits", Cab International, Wallingford, **1998.**
2. S. Kunasak, "Study on special characteristics of longan cultivar", Special Problem, **1996**, Maejo Institute of Agricultural Technology, Chiang Mai. (in Thai)
3. M. Parwin, "Longan", Document no.76, Agricultural Communication Division, Department of Agricultural Extension, Ministry of Agriculture and Cooperatives, Bangkok (no date). (in Thai)
4. P. Armonthip, "Miracle…longan", Agricultural Communication Division, Department of Agricultural Extension, Ministry of Agriculture and Cooperatives, Bangkok (no date), Retrieved January 20, 2006, from: http://www.doae.go.th/report/last/bt81.htm (in Thai)
5. Nutrition Division, "Nutrient composition per 100 grams edible portion", Department of Health, Ministry of Public Health, Bangkok, **1987**. (in Thai)
6. A. Rattana, "Handbook for extension of storage life of fresh longan and commercial processing", The Thailand Research Fund, Bangkok, **2000**. (in Thai)
7. Office of Technology Promotion and Transfer, "Lamyai", Ministry of Science and Technology, Bangkok, **2003**, Retrieved January 20, 2006, from: http://www.ttc.most.go.th/journal/food/lamyai.htm (in Thai)
8. G. V. Barbosa-Cánovas and H. Vega-Mercado, "Dehydration of Foods", Chapman and Hall, New York, **1996**.
9. N. L. Pennington and C. W. Baker, "Sugar, a User's Guide to Sucrose", Van Nostrand Reinhold, New York, **1990**.
10. J. M. Deman, "Principle of Food Chemistry", 3rd Edn., Springer Science + Business Media, Inc., New York, **1999**.
11. M. A. J. S. van Boekel and L. M. M. Tijskens, in "Food Process Modeling" (Ed. L. M. M. Tijskens, M. L. A. T. M. Hertog and B. M. Nicoaï), Woodhead Publishing Ltd., Cambridge, **2001,** Ch.3.
12. M. Namiki, "Chemistry of maillard reaction: recent studies on the browning reaction mechanism and the development of antioxidant and mutagens", *Adv. Food Res.*, **1988**, *32*, 116-170.
13. B. L. Wedzicha, "Chemistry of Sulphur Dioxide in Foods", Elsevier Applied Science Publishers, London, **1984**.

Maejo Int. J. Sci. Technol. **2009**, *3*(03), 434-445

14. S. E. Papadakis, S. Abdul-Malek, R. E. Kamdem and K. L. Yam, "A versatile and inexpensive technique for measuring color of food" *Food Technol.*, **2000**, *54*, 48-51.
15. Y. H. Kalkan, "Evaluation of colour parameters and antioxidant activities of fruit wines", *Int. J. Food Sci. Nutrit.*, **2006**, *57*, 47-63.

Maejo Int. J. Sci. Technol. **2009**, *3*(03), 446-458

Maejo International

Journal of Science and Technology

ISSN 1905-7873

Available online at www.mijst.mju.ac.th

Full Paper

FTIR and chemometric tools for the classification of Thai wines

Vannajan S. Lee[1,*], Panthip Tue-ngeun[1], Patrinee Traisathit[2], Sukon Prasitwattanaseree[2], Piyarat Nimmanpipug[1] and Jeerayut Chaijaruwanich[3]

[1]Computational Simulation and Modelling Laboratory (CSML), Department of Chemistry and Centre for Innovation in Chemistry, Faculty of Science, Chiang Mai University, Chiang Mai, 50200,Thailand

[2]Department of Computer, Faculty of Science, Chiang Mai University, Chiang Mai, 50200, Thailand

[3]Department of Statistics, Faculty of Science, Chiang Mai University, Chiang Mai, 50200, Thailand

[*] Corresponding authors, e-mail: vannajan@gmail.com (V. S. Lee); patrinee@gmail.com (P. Traisathit)

Received: 23 June 2009 / Accepted: 26 November 2009 / Published: 27 November 2009

Abstract: A simple and rapid Fourier transform infrared (FTIR) spectroscopic method was developed to determine the content in wines without sample preparation or use of organic solvents. This research aimed at classifying seven Thai wines from various regions by employing both instrumental and statistical analysis. FTIR spectra in the region between 650-4000 cm^{-1} were characterised and used for multivariate chemometric analysis by principal component analysis (PCA), discriminant analysis (DA) and hierarchical cluster analysis (HCA). Application of PCA to FTIR data revealed the pattern and relationship of each brand or trademark. Thai wines were effectively distinguished by DA according to their trademarks and can be divided into four main groups according to HCA. All of the multivariate analyses yield similar conclusions that Thai wines cannot be clearly classified in terms of geographical origin. However, additional samples may provide further insight into the geographical distribution of Thai wines.

Keywords: Thai wines, authentication, chemometrics, multivariate analysis, FTIR spectroscopy

Maejo Int. J. Sci. Technol. **2009**, *3*(03), 446-458

Introduction

The application of spectroscopic techniques in the study of the origin and differentiation of drink products has developed considerably in recent years [1, 2]. The advantage of these techniques lies in the almost complete lack of sample preparation required, which makes them especially rapid to apply.

In order to develop methods of classification and differentiation, spectra are treated with chemometric techniques that permit characterisation and subsequent construction of models. With regard to analysis methods of constituents in wine, a number of reports appear in the literature such as high performance liquid chromatography (HPLC) for the determination of phenolic acids [3], gas chromatography (GC) for the analysis of aroma compounds in wine [4], GC-MS (mass spectrometry) for trifluoroacetylated glycocides [5], nuclear magnetic resonance (NMR) for determination of minor compounds [6], Fourier transform infrared (FTIR) spectroscopy for the differentiation and classification of wines and brandies during their ageing process [7], and inductively coupled plasma optical emission spectroscopy (ICP-OES) for fast analysis of a number of elements of the periodic table [8]. There seems to be a problem, however, with treating a large quantity of data. Fortunately, chemometric methods can be used to solve such multivariate data analysis problems [9, 10]. The use of chemometric tools in data analysis, together with recent advances in computer technology which simplify complex mathematical calculations, leads to the development of multivariate data analysis as a powerful tool in the evaluation of food quality [11].

Wine production from many kinds of fruits has bloomed in Thailand under the One Tambon One Product project (the OTOP project), which also resulted in the formation of the Thai Wine Association in 2004, exactly ten years after the first Thai grape wine was launched. The Kingdom's leading wine producers set up the association to join forces and immediately established winemaking quality standards and labelling requirements for Thai grape wines. Members adhere to the Thai Wine Charter, which is in line with international standards. The objective is to create awareness and enhance the image of Thai wines, both in the domestic and international markets, and to educate Thai people about Thai grape wines and the health benefits associated with moderate wine drinking. The wineries are mostly located in the northern and north-eastern parts of Thailand as shown in Figure 1.

The purpose of this research is to associate some Thai red and white wines by FTIR data using multivariate analyses. Chemometric techniques were used to discriminate between very similar chemical components from which several groups could ideally be determined. Such methods are particularly suited for working with large data sets and may be used to classify Thai wines into distinct groups by the correlation of measurement data.

Maejo Int. J. Sci. Technol. **2009**, *3*(03), 446-458

Figure 1. The location of wineries in Thailand. a) Chiang Rai province, b) Pichit province, c) Saraburi province, d) Nakornrachasima province, and e) Loei province

Materials and Methods

Samples

All Thai wines used in this study were commercial samples from the 2001-2004 vintage. Wine samples studied from different growing regions in Thailand are presented in Table 1, which included 2 white wines and 5 red wines belonging to three varieties, i.e. Shiraz, Chenin Blanc and a combination of 90% Shiraz and 10% Tempranillo. Two red Australian wines from the 2002-2003 vintage were also investigated for comparison.

FTIR analysis

A Perkin-Elmer FT-IR Spectrometre (Spectrum GX Series) equipped with a deuterated triglycine sulfate detector was used for FTIR analysis. The sampling station was equipped with an overhead horizontal attenuated total reflectance (ATR) accessory with multiple reflection comprising transfer optics within a chamber through which infrared radiation was directed to a detachable ATR zinc selenide crystal mounted in a shallow trough for sample containment [12-14]. The zinc selenide crystal was used to obtain data in the range of 650-4000 cm^{-1} with a resolution of 4.00 cm^{-1}. Single beam spectra (4000–650 cm^{-1}) of the samples were obtained (Figure 2) and corrected against the background spectrum of the zinc selenide crystal. The ATR crystal was carefully cleaned with water between measurements and dried with nitrogen gas after each experiment to ensure the best possible sample spectra. Commercial wines were used directly in

Maejo Int. J. Sci. Technol. **2009**, *3*(03), 446-458

Table 1. Details of Thai wines under study

Code No.	Trademark	Type	Variety	Geographical region	Area in the map
1	Chateau de Loei	White	Chenin Blanc	Upper north-eastern Thailand (Loei province)	e
2	Chateau des Brumes	White	Chenin Blanc	Lower north-eastern Thailand (Nakornrachasima province)	d
3	Chateau de Loei	Red	Shiraz	Upper north-eastern Thailand (Loei province)	e
4	Chateau des Brumes	Red	Shiraz	Lower north-eastern Thailand (Nakornrachasima province)	d
5	Shala One	Red	Shiraz	Lower northern Thailand (Pichit province)	b
6	Lumphaya	Red	Shiraz	Central Thailand (Saraburi province)	c
7	Khao Yai	Red	Shiraz (90%) + Tempranillo (10%)	Lower north-eastern Thailand (Nakornrachasima province)	d
8	Rothbury	Red	Shiraz	New South Wales, Australia	-
9	Bilyara	Red	Shiraz	South Australia	-

200-µl ATR cell samples with the same temperature condition (24°C) as used for the Thai wines. Each wine sample was rerecorded 5 times for the multivariate analysis.

Data analysis

A data matrix was constructed with a column representing wine samples (45 objects) and rows corresponding to wavenumber (3350 variables) (Table 2). These variables, called 'features', formed a 'data vector' which represented a wine sample. Data vectors belonging to the same group were analysed. These groups were then termed a 'category'. The chemometric tools used in this work were as follows.

Principal component analysis [15]

Principal component analysis (PCA), carried out with MATLAB 6.1 (MATLAB Inc, 1999), was mainly used for data reduction to identify a small number of factors that explain most of the variance observed in a much larger number of manifest variables. Such methods attempt to identify factors that explain the pattern of correlations within a set of observed variables. This permits a primary evaluation of the in-between category similarity and is very useful for visual inspection of complex data matrices. The information is compressed into a few components or directions in the

Maejo Int. J. Sci. Technol. **2009**, *3*(03), 446-458

Table 2. Tabulation of FT-IR spectral transmittance of wine samples

Sample	Wavenumber (cm^{-1})										
	4000	**3999**	**3998**	**3997**	**3996**	……	**654**	**653**	**652**	**651**	**650**
W_Loei_1	93.365	93.361	93.353	93.342	93.327	……	84.760	85.633	87.039	90.230	97.292
W_Loei_2	93.130	93.116	93.104	93.096	93.094	……	79.567	85.731	90.890	93.440	96.536
W_Loei_3	93.028	93.016	93.008	93.003	92.998	……	73.313	79.884	86.343	92.315	100.290
W_Loei_4	92.923	92.917	92.913	92.907	92.897	……	71.122	76.368	83.804	92.426	101.020
W_Loei_5	92.771	92.759	92.751	92.745	92.738	……	74.166	79.460	85.981	92.150	98.865
⋮ ⋮	⋮ ⋮	⋮ ⋮	⋮ ⋮	⋮ ⋮	⋮ ⋮	⋮ ⋮	⋮ ⋮	⋮ ⋮	⋮ ⋮	⋮ ⋮	⋮ ⋮
R_Bil_1	88.688	88.667	88.647	88.627	88.611	……	71.892	74.851	78.913	86.166	95.696
R_Bil_2	88.661	88.648	88.632	88.615	88.605	……	77.723	82.574	86.118	89.754	91.862
R_Bil_3	88.555	88.534	88.509	88.483	88.465	……	75.671	78.856	81.372	86.707	93.761
R_Bil_4	88.483	88.468	88.450	88.432	88.421	……	73.875	78.342	81.689	87.657	94.456
R_Bil_5	88.375	88.355	88.325	88.294	88.271	……	61.891	66.941	73.799	86.505	101.727

multivariate space. The first two of the principal components (PCs) of the wine data can be determined as follows:

$$PC1 = v1_1X_1 + v1_2X_2 + \ldots + v1_pX_p$$

$$PC2 = v2_1X_1 + v2_2X_2 + \ldots + v2_pX_p$$

where $PC1$, $PC2$ are the first and second principal component scores;
X_j is the observed variable of FTIR spectra at wavenumber j (j = 1, …, 3350);
$v1_j$ is the eigenvector of the first principal component for variable j;
$v2_j$ is the eigenvector of the second principal component for variable j.

Discriminant analysis [16]

Discriminant analysis (DA) is a technique for classifying a set of observations into predefined classes. The main purpose of discriminant function analysis is to predict group membership based on a linear combination of the interval variables. The procedure begins with a set of observations where both group membership and the values of the interval variables are known. The end result of the procedure is a model that allows prediction of group membership when only the interval variables are known. The second purpose of discriminant function analysis is to understand the data set, as a careful examination of the prediction model that results from the procedure can give insight into the relationships between group membership and the variables used to predict group membership. This technique is a widespread parametric method for classification purposes that assumes a priori knowledge of the number of classes and the sample class membership. The model is built based on a set of observations by which the classes are known. The technique constructs a set of linear functions of the predictors, known as discriminant functions (L), such that

$$L = b_1x_1 + b_2x_2 + \ldots + b_nx_n + c$$

where the b's are discriminant coefficients, the x's are the predictor variables and c is a constant.

Maejo Int. J. Sci. Technol. **2009**, *3*(03), 446-458

These discriminant functions are used to predict the class of a new observation. For a k class problem k discriminant functions are constructed. Given a new observation, all the k discriminant functions are evaluated and the observation is assigned to class i if the i^{th} discriminant function has the highest value. In our study we used all PCs as the input matrix. The DA was performed using SPSS 10.0 (SPSS Inc, 1999).

Hierarchical cluster analysis [17]

A general approach to cluster analysis is hierarchical cluster analysis (HCA) [18], the purpose of which is to group together objects or records that are 'close' to one another. The cluster method of complete linkage and the distance measured by the Euclidean squared distance were used. The dendrogram is a tree-like plot where each step of hierarchical clustering is represented as a fusion of two branches of the tree into a single one. The branches represent clusters obtained from each step of hierarchical clustering. The HCA was done using SPSS 10.0 (SPSS Inc, 1999).

Results and Discussion

Characterisation of FTIR spectra

Figure 2 presents the FTIR spectra of different Thai wines showing absorbance bands at 3264 cm^{-1} (O−H stretching), 2984 cm^{-1} (C–H stretching), 2123 cm^{-1} (C≡N stretching), 1636 cm^{-1} (C=C stretching), 1454 cm^{-1} (CH_2−methylene group), 1328 cm^{-1} (CH_3−methyl group), 1044 cm^{-1} (C−OH stretching), and 900-690 cm^{-1} (=C−H out of plane (oop) bending). The spectra of all wines showed similar peaks. Most wines contain water, alcohols, aldehydes, glycerol, sorbitol, mannitol, sulfites, amino acids, esters, minerals, phenols, sugars, organic acids such as tartaric, malic and citric acids, as well as volatile acids as common ingredients [19]. Similarity of the major ingredients gave rise to similar peak positions in the ATR spectra of the Thai wines studied. The broad peak found at 3264 cm^{-1} is mainly due to the stretching vibration of O-H bond of water, whereas the 2884 cm^{-1} peak is most likely due to the stretching vibration of bonds from multiple constituents of the wines. These vibrations include C–H stretching of hydrocarbons, O–H stretching of carboxylic acids and most importantly asymmetric stretching vibration of C–H bonds of methyl (–CH_3) groups. Acids give wine the sour or sharp note that enhances flavour when in balance with other components. Of the three organic acids that originate in grapes, tartaric acid is prevalent as the base measure of total acidity in wine, followed by malic and citric acids. Three other acid, namely succinic, lactic and acetic acids (the volatile acids), are produced by fermentation. The region between 1000 and 2200 cm^{-1} contains five peaks at 1044, 1328, 1454, 1636 and 2123 cm^{-1}, which can be correlated with the C−OH stretching, CH_3 bending, CH_2 bending, C=C stretching and C≡N stretching of the groups in compounds such as, phenols, alcohols, aldehydes, higher alcohols, polyols, acids, sugars, volatile acids and amino acids. The full spectrum of peaks was used for the chemometric analysis of the wines.

Maejo Int. J. Sci. Technol. **2009**, *3*(03), 446-458

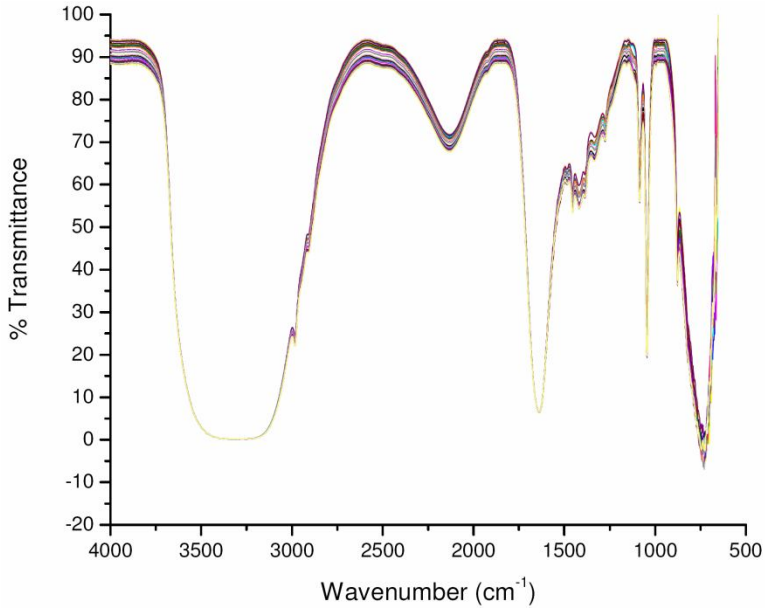

Figure 2. FT-IR spectra of different Thai wines

Principal component analysis

PCA allows the visualisation of the information in the data set in a few principal components while retaining the maximum possible variability within that set. The scores for each sample on the first two principal components, which contain 67.3% of the total variance, are represented in Figure 3. On the first principal component at the bottom left of the graph, the majority of the samples are the white wine of Chateau des Brumes, which has a higher negative score than the white wine of Chateau de Loei. The red wine samples fell into the same area on the right of the PC plots. Chateau des Brumes, Shala One, and Lumphaya were quite clearly distinguishable according to their own trademarks, whereas the red and white wines of Chateau de Loei could not be distinctly classified. PC1 and PC2 might differentiate better if the variance explained was high (more than 80%). Such overlap represents the closer relationship between these two wines which come from the same province and share the same trademark of Chateau de Loei. It can be seen that the samples of Australian red wines (Rothbury and Bilyara) at the top right of the graph are separated from the remaining samples. The Thai wine closely located near the Australian wine is the reserve red Khao Yai. A combination of 90% Shiraz (red) and 10% Tempranillo (white) varieties in Khao Yai was used in the wine production. The cluster of samples found on the right of PC1 may be due to the higher percentage of red wine variety. The first principal component is therefore most likely related to the wine type, i.e. white or red wine. Although no classification or grouping of wine by geographical origin is clearly seen in the plot, the grouping can be more related to the wine trademark and variety. The Shiraz's are grouped together towards the right while the Chenin Blanc's are located on the left. For the second principal component, it can be seen that the samples of red wine of Chateau de Loei have higher scores than the white wine of the same vineyard; however, they can be grouped in the same cluster. It can be concluded that using these first two principal components, we can clearly distinguish among the wine samples according to their brand or trademark. Although the wines of different brands or trademarks were of the same

Maejo Int. J. Sci. Technol. **2009**, *3*(03), 446-458

variety, the PC plots of FTIR data show that the components of these wines are different and are clustered in their own individual groups which are apparently differentiated by their geographical origin or process of production.

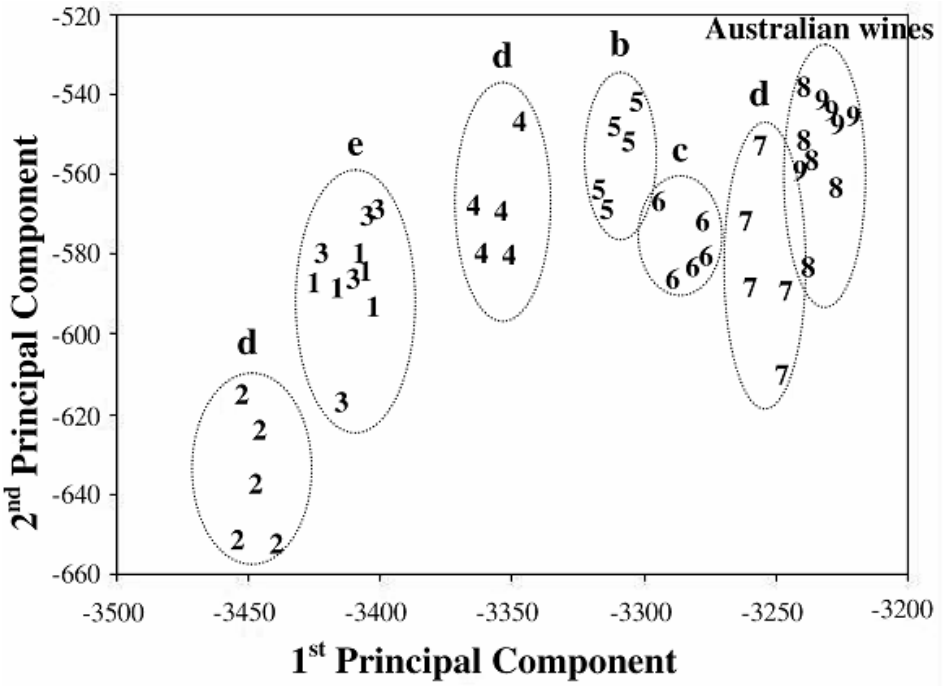

Figure 3. Scores of the wine samples on the first two principal components: 1 (white Chateau de Loei), 2 (white Chateau des Brumes), 3 (red Chateau de Loei) , 4 (red Chateau des Brumes), 5 (red Shala One), 6 (red Lumphaya), 7 (reserve red Khao Yai), 8 (red Rothbury) and 9 (red Bilyara). The letters b-d indicate the locations of wineries as defined in Figure 1

Discriminant analysis

In all, 45 PCs were used to populate the input matrix in our study. Since there are 9 discriminant functions, the charts present scatter plots showing the discriminant scores of the cases on the 9 discriminant functions with 30 PCs (eigenvalues more than 1) used in the classification. Figure 4 shows that DA resulted in better classification of Thai wines according to their brand or trademark. In the replication experiments, each wine sample was plotted at almost exactly the same point, demonstrating that the wines of different trademarks can be reproducibly separated and clearly classified. The overlap between the Rothbury and Bilyara Australian wines at the right corner indicates the close relationship of the wines which were from the same vineyard. Cross-validation was used to assess how well the discriminant function worked and whether it worked equally well for each group of the dependent variable. In this case, it correctly classified 100% of the original grouped cases and 100% of cross-validated grouped cases for Thai wines. About 80.0% of cross-validated grouped cases were correctly classified for Australia's Rothbury due to the overlapping with the Bilyara. Similar results were derived for DA and PCA, but neither of them could classify the wines clearly in terms of their geographical origin.

To investigate the potential of chemical components for wine classification, a table of equality of group means (Table 3) was generated by selected Univariate ANOVAs. This indicates

Maejo Int. J. Sci. Technol. **2009**, *3*(03), 446-458

whether there is a statistically significant difference among the dependent variable means (group) for each independent variable. The Wilks' Lambda was used as a statistical criteria to add or remove variables from the analysis. In the ANOVA, the smaller the Wilks' Lambda is, the more important the independent variable to the discriminant function becomes. In our case, Wilks' Lambda was significant by the F test with significant values for PC1, PC3, PC8, PC10 and PC16 (Table 3), which correctly classified about 88.9% of the cross-validated group cases. They were the main discriminate parameters among all wines. The important variables indicated by the higher component values in these PCs were related to the absorbance regions in the FTIR spectrum. As a result, we found that the O-H stretching and the C=C stretching vibrations of water, alcohols, higher alcohols, acids, sugars and volatile acids mainly made the wine different and separable into different areas of the scatter plot in Figure 4.

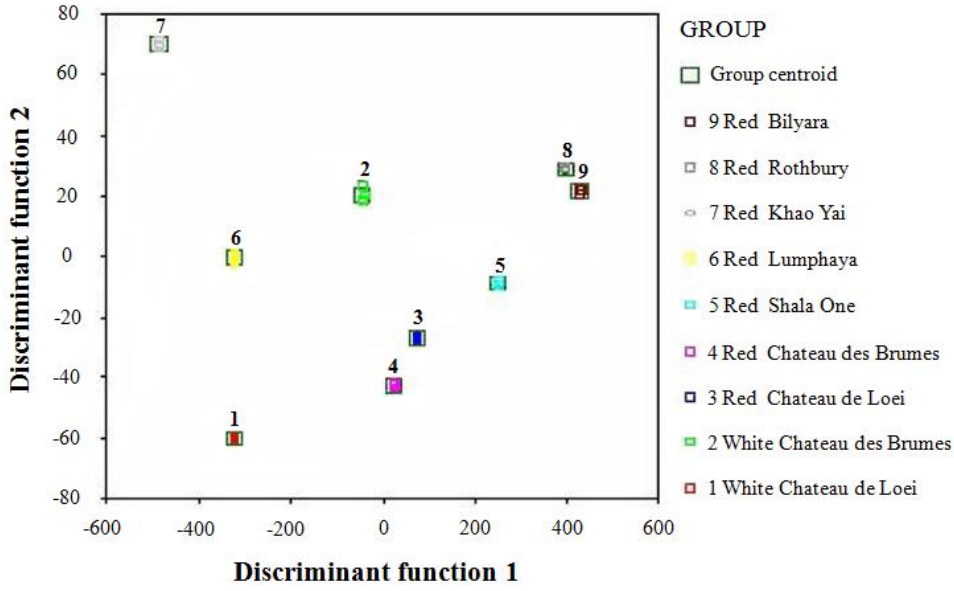

Figure 4. Group centroid and scatter plot of 9 groups of known wines

Hierarchical cluster analysis

Results from the HCA for 7 Thai wines and 2 Australian wines were reported in the form of a dendrogram using complete linkage and Euclidean squared distance (Figure 5). As a criterion for similarity on the basis of the connecting distances between parameters and their positions on the dendrogram, four distinctive clusters of wines were defined as follows:

Cluster 1, comprising a group of red wines: Australian wines, Shala One and some red wine samples of Chateau des Brumes;

Cluster 2, comprising the red wine of Chateau de Loei, white wine of Chateau des Brumes and some red wine samples of Chateau des Brumes;

Cluster 3, comprising the red wine of Lumphaya and white wine of Chateau de Loei;

Cluster 4, consisting of the red wine of Khao Yai only.

Maejo Int. J. Sci. Technol. **2009**, *3*(03), 446-458

Table 3. Tests of equality of group means

PCs	Wilks' Lambda	F test	Significant value
PC1	.006	690.109	.000
PC2	.902	.491	.854
PC3	.282	11.469	.000
PC4	.731	1.657	.143
PC5	.770	1.342	.255
PC6	.811	1.046	.421
PC7	.764	1.386	.236
PC8	.357	8.089	.000
PC9	.804	1.098	.387
PC10	.359	8.021	.000
PC11	.804	1.096	.388
PC12	.735	1.623	.153
PC13	.708	1.853	.099
PC14	.852	.782	.621
PC15	.834	.895	.531
PC16	.573	3.359	.006
PC17	.698	1.950	.082
PC18	.891	.552	.809
PC19	.791	1.192	.331
PC20	.863	.715	.677
PC21	.908	.454	.880
PC22	.924	.372	.929
PC23	.898	.510	.841
PC24	.839	.866	.554
PC25	.860	.734	.661
PC26	.939	.293	.964
PC27	.891	.550	.811
PC28	.757	1.446	.212
PC29	.952	.228	.983
PC30	.968	.150	.996
PC31	.869	.677	.708
PC32	.992	.037	1.000
PC33	.926	.360	.934
PC34	.966	.159	.995
PC35	.992	.038	1.000

Maejo Int. J. Sci. Technol. **2009**, *3*(03), 446-458

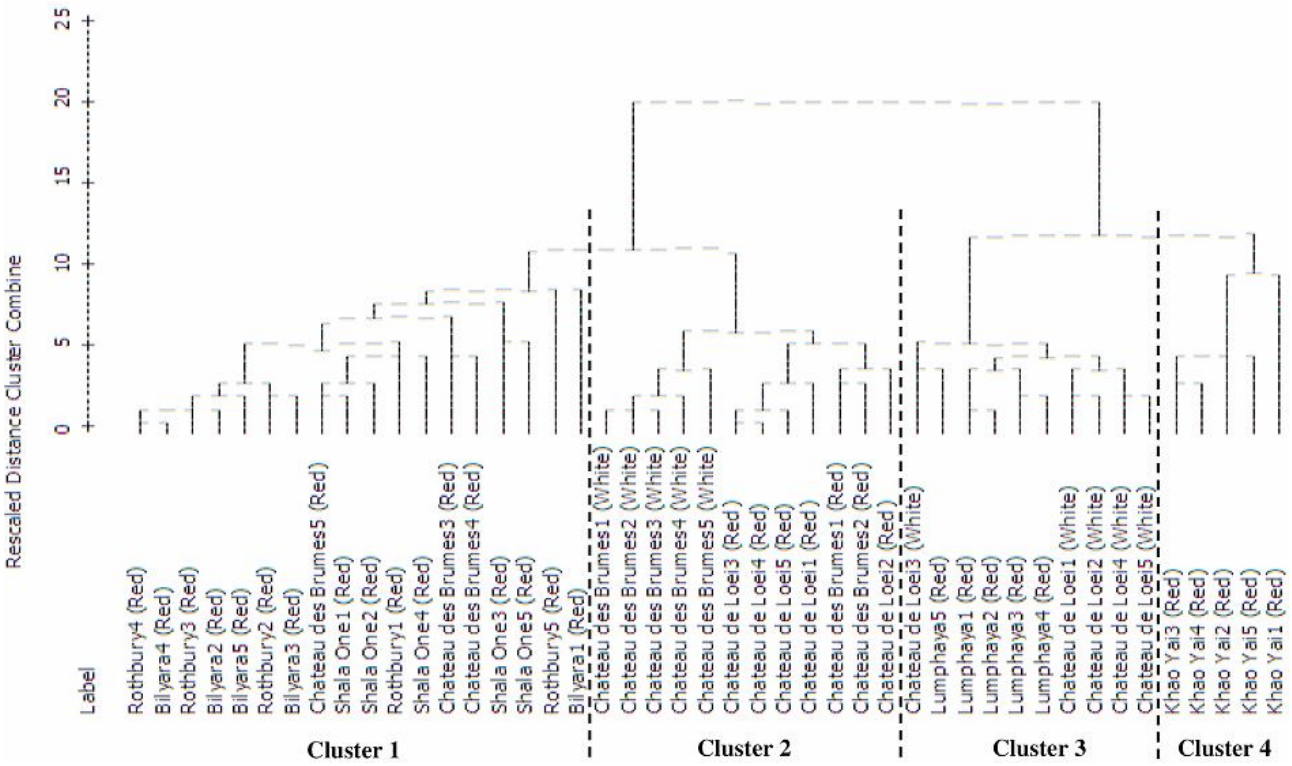

Figure 5. Dendrogram built with all variables using complete linkage and Euclidean squared distance

In comparison with the PC1/PC2 plot in Figure 3, such clusters can be visualised and similar conclusions derived although HCA gives a broader and less definitive classification than PCA, since the clustering and interpretation based on the dendrogram are largely subjective. The red wine of Chateau des Brumes is separated into the two groups in clusters 1 and 2. Red and white wines of Chateau des Brumes are located in different groups in clusters 1 and 2, while red and white wines of Chateau de Loei are located in clusters 2 and 3. Thus, this method cannot clearly classify the wines by their geographical origin.

Conclusions

A rapid and simple FTIR procedure has been developed, which can be directly applied for wine analysis. Chemometric techniques were used to distinguish between very similar chemical components of multivariate FT-IR data of red and white Thai wine samples. The PC1/PC2 plot could be used to separate Thai wines into their own individual trademarks. However, the trademark pattern could be differentiated better by DA, which was one of the supervised methods of distinguishing the group from the selected parameters. From these results, the difference in the wines studied mostly stemmed from the differences in the amount of water, alcohols, higher alcohols, acids, sugars and volatile acids. The application of the unsupervised HCA method gave a broader and less definitive classification of the wines in four main clusters which highly correlated

with the PC plot. All of the above multivariate analyses demonstrate that the wine varieties have not been differentiated by their geographical origin, although the wines were effectively distinguished by their trademarks.

Acknowledgements

The authors would like to acknowledge Naresuan University for support in experimental aspects. This research was also partly funded by the Centre for Innovation in Chemistry: Postgraduate and Research Program in Chemistry (PERCH-CIC).

References

1. E. K. Kemsley, R. H. Wilson and R. Briandet, "Approaches to adulteration detection in instant coffees using infrared spectroscopy and chemometrics", *J. Sci. Food Agr.*, **1996**, *71*, 359-366.
2. G. Downey, "Food and food ingredient authentication by mid-infrared spectroscopy and chemometrics", *TrAC Trends Anal. Chem.*, **1998**, *17*, 418-424.
3. F. Buiarelli, G. Cartoni, F. Coccioli and Z. Levetsovitou, "Determination of phenolic acids in wine by high-performance liquid chromatography with a microbore column", *J. Chromatogr. A*, **1995,** *695*, 229-235.
4. J. Villen, F. J. Senorans, G. Reglero and M. Herraiz, "Analysis of wine aroma by direct injection in gas chromatography without previous extraction", *J. Agr. Food Chem.*, **1995**, *43*, 717-722.
5. D. Chassange, J. Crouzet, R. L. Baumes, J. P. Lepoutre and C. L. Bayonove, "Determination of trifluoroacetylated glycosides by gas chromatography coupled to methane negative chemical ionization mass spectrometry", *J. Chromatogr. A.*, **1995**, *694*, 441-451.
6. K. Jurkica and J. K. Iztok, "Modern Magnetic Resonance", Springer, Dordrecht, **2008**.
7. M. Palma and C. G. Barroso, "Application of FT-IR spectroscopy to the characterisation and classification of wines, brandies and other distilled drinks", *Talanta*, **2002**, *58*, 265-271.
8. J. Sperkova and M. Suchanek, "Multivariate classification of wines from different Bohemian regions (Czech Republic)", *Food Chem.*, **2005**, *93*, 659-663.
9. K. Danzer and M. Wagner, "Multisignal calibration in optical emission spectroscopy", *Fresen J. Anal. Chem.*, **1993**, *346*, 520-524.
10. K. Danzer and K. Venth, "Multisignal calibration in spark- and ICP-OES", *Fresen J. Anal. Chem.*, **1994**, *350*, 339-343.
11. L. Munck, L. Nørgaard, S. B. Engelsen, R. Bro and C. A. Andersson, "Chemometrics in food science--a demonstration of the feasibility of a highly exploratory, inductive evaluation strategy of fundamental scientific significance", *Chemometr. Intell. Lab Syst.*, **1998**, *44*, 31-60.
12. M. Sabo, "On-line high-performance liquid chromatography/Fourier transform infrared spectrometry with normal and reverse phases using an attenuated total reflectance flow cell", *Anal. Chem.*, **1985**, *57*, 1822-1826.

Maejo Int. J. Sci. Technol. **2009**, *3*(03), 446-458

13. E. R. Kennedy and K. Ashley, "Fourier transform infrared spectrometry/attenuated total reflectance study of the reaction of pentanal and propanal with 2-(hydroxymethyl)piperidine", *Appl. Spectrosc.*, **1992**, *46*, 266-272.
14. P. T. McKittrick, N. D. Danielson and J. E. Katon, "A comparison between a micro and an ultramicro CIRCLE® cell for on-line FT-IR detection in a reverse phase HPLC system", *J. Liq. Chrom.*, **1991**, *14*, 377-393.
15. K.W. Mardia, J. B. Kent and J. M. Bibby, "Multivariate Analysis", Academic Press, New York, **1979**.
16. W. R. Klecka, "Discriminant Analysis", Sage Publications, Beverly Hills, **1980**.
17. M. J. Adams, "Chemometrics in Analytical Spectroscopy", The Royal Society of Chemistry, Cambridge, **1995**.
18. D. L. Massart and L. Kaufman, "Interpretation of Analytical Data by Use of Cluster Analysis", Wiley, New York, **1983**.
19. T. G. Cerdán, D. T. Goñi and C. A. Azpilicueta, "Accumulation of volatile compounds during ageing of two red wines with different composition", *J. Food Eng.*, **2004**, *65*, 349-356.

Maejo Int. J. Sci. Technol. **2009**, *3*(03), 459-471

Maejo International Journal of Science and Technology

ISSN 1905-7873
Available online at www.mijst.mju.ac.th

Full Paper

Time-frequency plane behavioural studies of harmonic and chirp functions with fractional Fourier transform (FRFT)

Renu Jain[1], Rajiv Saxena[2] and Rajshree Mishra[3,*]

[1] School of Mathematics and Allied Sciences (SOMAAS), Jiwaji University, Gwalior (M.P.) India
[2] Jaypee Institute of Engineering and Technology (JIET), Guna (M.P.) India
[3] School of Mathematics and Allied Sciences (SOMAAS), Jiwaji University, Gwalior (M.P.) India
[*] Corresponding author, e-mail: rajshreemishraa@gmail.com

Received: 8 June 2009 / Accepted: 29 November 2009 / Published: 9 December 2009

Abstract: The behaviour of harmonic and chirp functions was studied on the time-frequency plane with the help of fractional Fourier transform (FRFT). Studies were also carried out through simulation with different numbers of samples of the functions. Variations were observed in the maximum side-lobe level (MSLL), half main-lobe width (HMLW) and side-lobe fall-off rate (SLFOR) of the functions. The parameters of these functions were compared with a similar set of parameters of some of the popular window functions. It can thus be concluded that in the time-frequency plane, the chirp function provides better spectral parameters than those of Boxcar window function with some particular values of rotational angle. A similar type of inference can also be drawn for the harmonic function in the time-frequency plane. Of course the rotational angle might vary in this case and a comparative analysis was carried out with Fejer window and the cosine-tip window functions. This study may prove to be helpful in replacing these existing window functions in a variety of applications where a particular parameter or group of parameters of the harmonic and chirp functions are found superior.

Keywords: harmonic function, chirp function, fractional Fourier transform (FRFT), window function, spectral parameters, time-frequency plane

Introduction

The Fourier transform (FT) is the most frequently and extensively used tool in signal processing and analysis [1]. Fractional Fourier transform, generally known as FRFT, is a generalisation of FT with an order parameter `*a'*. Mathematically, the a^{th} order FRFT F^a is the a^{th} power of ordinary FT operation *F*. The first order *(a=1)* FRFT is the ordinary FT and the zeroth order FRFT is the identity transformation.

Maejo Int. J. Sci. Technol. **2009**, *3*(03), 459-471

FRFT has now become the most frequently and extensively used tool in the area of signal processing, analysis and optics. It also finds many applications in differential equations, optical beam propagation, quantum mechanics, statistical optics and optical signal processing [2-4]. In fact, in every area in which FT and frequency domain concepts are utilised, there exists a provision for the generalisation and improvisation by applying FRFT.

Fractionalisation of the transform started in 1929 by Wiener [5] by solving of the differential equations. Condon in 1937 [6] and Bargmann in 1961 [7] followed his work. Namias in 1980 and Mcbride and Kerr in 1987 did remarkable work in developing the transform, its algebra and calculus [8-9].

The definition of continuous-time FRFT given by Namias is validated to date. In 1993 Almeidia came out with the time-frequency representation of FRFT [10]. Almeidia, Zayed and Mustard contributed in developing the properties of FRFT [11-13]. On the other hand, Ozaktas and his team and many other researchers worked on computation of FRFT and on discrete version of FRFT [14-15]. Due to diversified applications of FRFT many researchers are continuously contributing in developing the transform, its discrete version and applications [3, 4, 16]. During the last 15 years an enormous amount of research publications have been noticed in this area and FRFT is now established as a very powerful tool for almost all scientific and engineering applications.

In spectral analysis of a function, three parameters are of prime importance, i.e. the maximum side-lobe level (MSLL), the half main-lobe width (HMLW) and the side-lobe fall-off rate (SLFOR). An improvement in these parameters can improve the spectral performance of the function. Figure 1 provides a graphical representation of these parameters.

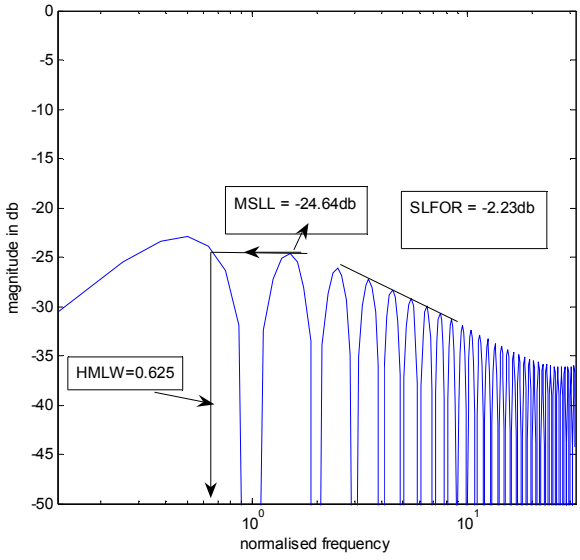

Figure 1. Parameters of harmonic function

The main objective of this paper is to study and analyse the behavioural changes of harmonic and chirp functions in the fractional Fourier domain. The harmonic function is defined by $exp\ (2\pi\ ix)$ and the chirp function is defined by $exp\ (-i\pi/4)\ exp\ (i\pi x^2)$ where the domain of the functions is a set of real numbers. We observed changes in the above three parameters of both functions in the FRFT domain, i.e. in time-frequency plane.

Maejo Int. J. Sci. Technol. **2009**, *3*(03), 459-471

Defining the Fractional Fourier Transform (FRFT)

The FRFT F^a of order $a \in R$ is a linear integral operator that maps a given function $f(x)$, $x \in R$ on to $f_a(\xi)$.

$\xi \in R$ by

$$f_a(\xi) = F^a(\xi) = \int_{-\infty}^{\infty} K_a(\xi, x)\, f(x)\, dx \quad \text{..... (1)}$$

where $K_a(\xi, x)$ is kernel of transform and defined as follows:

$$K_a(\xi, x) = C_\alpha \exp\{-i\pi(\frac{2x\xi}{\sin\alpha} - (x^2 + \xi^2)\cot\alpha)\} \quad \text{..... (2)}$$

with

$$C_\alpha = \sqrt{1 - i\cot\alpha} = \frac{\exp(-i(\pi\, sgn(\sin\alpha)/4 - \alpha/2))}{\sqrt{\sin\alpha}} \quad \text{..... (3)}$$

where $\alpha = a\frac{\pi}{2}$.

Equation (2) is defined only for a $\neq 2$ m, i.e. α is not a multiple of π.

$$K_a(\xi, x) = \delta(x - \xi) \text{ for } a = 4m \text{ or } \alpha = 2m\pi \quad \text{..... (4)}$$

and $$K_a(\xi, x) = \delta(x + \xi) \text{ for } a = 4m \pm 2 \text{ or } \alpha = (m \pm 1)\pi \quad \text{..... (5)}$$

where m is an integer.

Since $\alpha = a\frac{\pi}{2}$ appears in equations only in the argument of trigonometric functions then the definition is periodic in a (or α). Thus we will often limit our attention to the interval $a \in (-2,2]$ or $\alpha \in (-\pi, \pi]$ and sometimes $a \in [0,4)$ or $\alpha \in [0, 2\pi)$. When a is outside the interval $0 \leq |a| \leq 2$ we need simply replace a by it's modulo 4 equivalent.

Different cases can be tabulated, as given in Table 1.

Table 1. Some important cases of FRFT [16]

Operation on signal	**Value of parameter *a***	**Value of** $\alpha = a\pi/2$	**Kernel**	**Fractional operator**
FT operator	$4m + 1$	$(4m+1)\pi/2$	$\exp(-i2\pi x\xi)$	$F^1 = F$
Parity operator	$4m + 2$	$(2m+1)\pi$	$\delta(\xi + x)$	$F^2 = P$
Identity operator	$4m$	$2m\pi$	$\delta(\xi - x)$	$F^{4m} = I$
Inverse Fourier Transform (IFT) operator	$4m + 3$	$(4m+3)\pi/2$	$\exp(+i2\pi x\xi)$	$F^3 = F^{-1}$

Maejo Int. J. Sci. Technol. **2009**, *3*(03), 459-471

The discrete version of FRFT is known as discrete fractional Fourier transform (DFRFT) and evaluation of FRFT is done by using DFRFT computational techniques [15]. The DFRFT of a signal f(x) can be computed by following four steps:

(i) Multiply the function by a chirp (a function whose frequency linearly increases with time),

(ii) Take its Fourier transform with its argument scaled by cosec α,

(iii) Again multiply with a chirp, and

(iv) Multiply with a complex constant.

FRFT is now a widely studied transform and it is observed that FRFT of a signal exists under the same conditions as those for FT. The analytical expressions for FRFT of some common signals have been calculated as presented in Table 2.

Table 2. FRFT of standard functions [4]

Function	**FRFT**
1	$\frac{e^{i\alpha/2}}{\sqrt{\cos\alpha}}\ exp(-i\pi u^2 tan\alpha)$
$\delta(u-\xi)$	$\frac{e^{i(\alpha/2-\pi/4)}}{\sqrt{\sin\alpha}}\ e^{i\pi(\cot\alpha(u^2+\xi^2)-2u\xi cosec\alpha)}$
$\delta(u)$	$\frac{e^{-i(\alpha/2-\pi/4)}}{\sqrt{\sin\alpha}}\ e^{i\pi u^2\cot\alpha}$
$exp(i2\pi\xi u)$	$\frac{e^{i\alpha/2}}{\sqrt{\cos\alpha}}\ e^{-i\pi(\tan\alpha(\xi^2+u^2)-2u\xi sec\alpha)}$
$exp(-\pi u^2)$	$exp(-\pi u^2)$
$exp(i\pi\chi u^2)$	$\frac{\sqrt{1+i\tan\alpha}}{\sqrt{1+\chi\cot\alpha}}\ e^{i\pi u^2[(\chi-\tan\alpha)/(1+\chi\tan\alpha)]}$

FRFT Analysis of Harmonic Function

Spectral parameters of the harmonic function were observed in fractional Fourier domain through simulation. In one of the studies, the fractional angle α was varied from 0 to $\pi/2$ keeping the length of the harmonic function constant. These simulation studies were made by using DFRFT computation techniques.

Maejo Int. J. Sci. Technol. **2009**, *3*(03), 459-471

Figure 2 shows harmonic function in time domain and Figure 3 shows how the harmonic function evolves into its Fourier domain as angle α increases from 0 to $\pi/2$. Figure 4 represents the simulation results of harmonic function in time-frequency plane, obtained by varying either the length of function (N) or by changing the value of fractional angle (α). Some of the simulation results are given in Table 3.

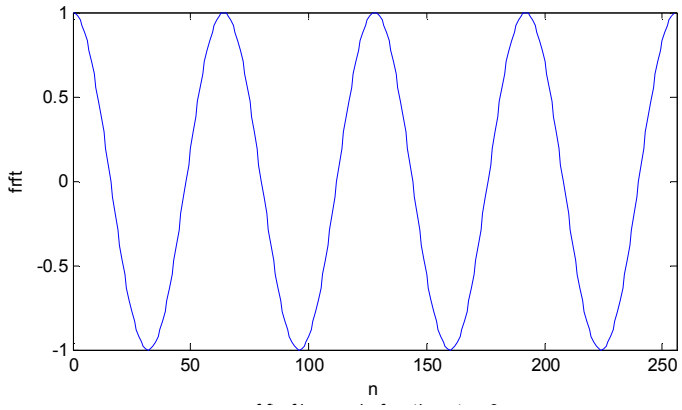

Figure 2. FRFT of harmonic function at a=0

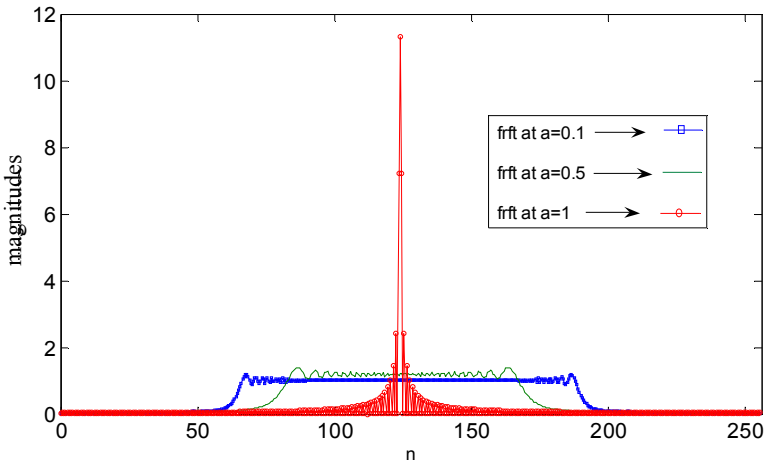

Figure 3. Magnitudes of FRFT of harmonic function by varying 'a'

It was observed that for small sizes of signal (16, 32, 64), as fractional angle α increases in the time-frequency plane, MSLL of the function decreases in a regular manner, while a slight increment is noted in SLFOR. The HMLW of the function is also regular in nature except at a few particular points, and shows increments in the time-frequency plane (Figure 5-7). For large numbers of samples, the harmonic function shows irregular behaviour in general in the time-frequency plane. In this case, it shows regularity in its behaviour only in a smaller part of α domain.

During the studies of all the above cases of harmonic function in the time-frequency plane, some specific values of fractional angle α have been noted, whereat parameters of the harmonic function in FRFT domain are better than those of Fejer window function [17] in the sense of spectral performance.

Maejo Int. J. Sci. Technol. **2009**, *3*(03), 459-471

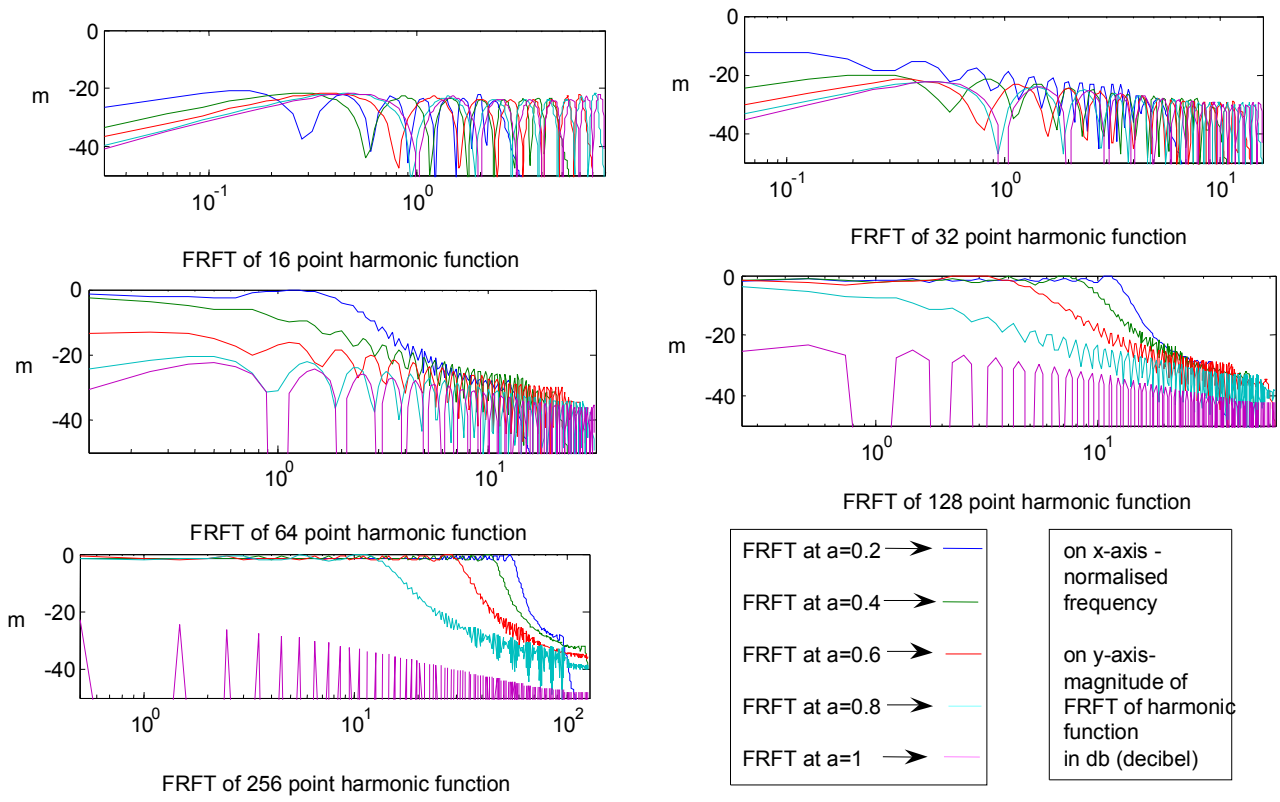

Figure 4. FRFT of harmonic function for different sizes of samples

Table 3. Parameters of FRFT of harmonic function

Fractional angle 'α'	Sample under consideration	MSLL in db*	HMLW	SLFOR in db*
3π/20	16	-22.68	0.1	-0.30
23π/50	16	-22.98	0.6563	-0.33
π/4	32	-23.16	0.45	-2.04
18π/50	32	-24	0.5625	-1.81
13π/50	64	-12	0.5	-3.42
7π/20	64	-19.2	0.625	-2.58
81π/200	128	-11.7	1.3	-4.5
9π/20	128	-17.32	0.75	-3.03
22π/50	256	-16.5	0.9	-4.2

* = decibel

Maejo Int. J. Sci. Technol. **2009**, *3*(03), 459-471

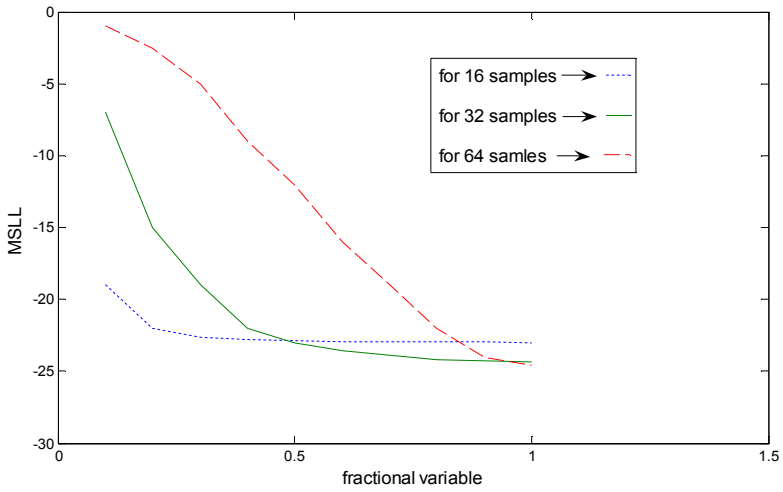

Figure 5. MSLL of FRFT of harmonic function for different sizes of samples

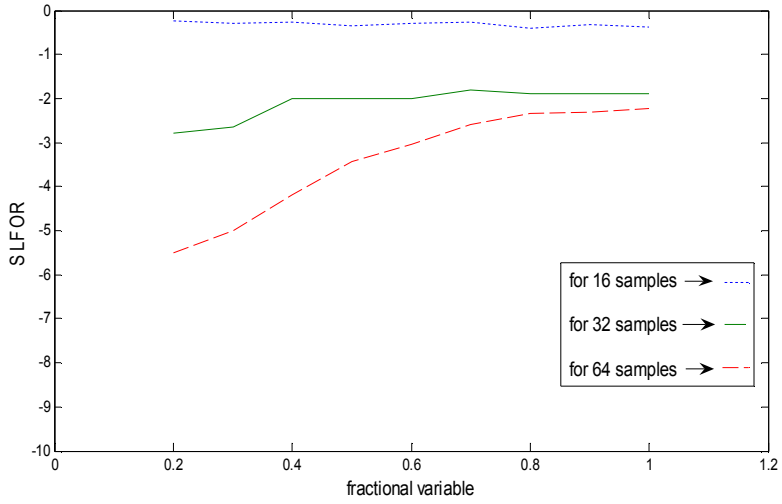

Figure 6. SLFOR of FRFT of harmonic function for different sizes of samples

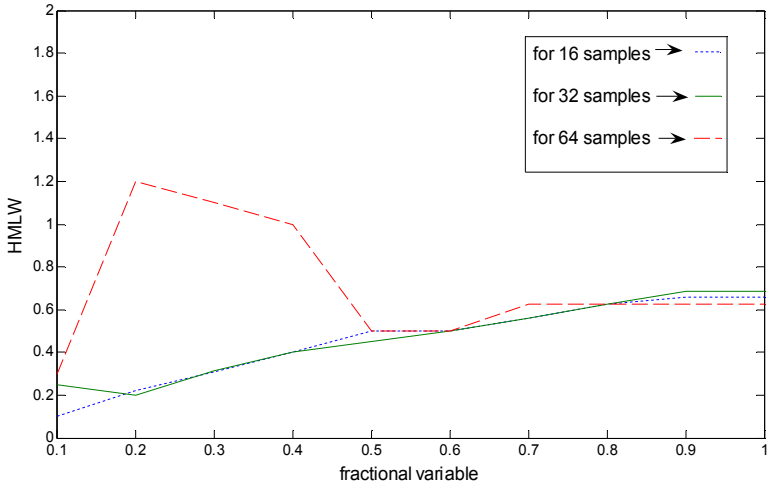

Figure 7. HMLW of FRFT of harmonic function for different sizes of samples

Maejo Int. J. Sci. Technol. **2009**, *3*(03), 459-471

FRFT Analysis of Chirp Function

FRFT of the chirp function was obtained and studied through simulation. Figure 8 shows chirp function in time domain while Figure 9 shows how the function transforms from time domain to frequency domain. Figure 10 shows the simulation results. Table 4 represents some of the simulation results for FRFT of a chirp function.

It was observed that in general the chirp function behaves in an irregular manner in time-frequency plane. Figure 10 indicates its nature in α domain for different sizes of samples and Figure 11 shows changes in MSLL of the function in fractional domain. Variation in MSLL increases in α domain when the number of samples is increased. In this case regular increments were noted only in a little part of α domain close to the angle $\alpha = \pi/2$.

HMLW of the function in general increases regularly with slight irregular variation for small samples, as shown in Figure12, while SLFOR of the same function also shows variation in an irregular manner but varies between -3 to -6 db. Large numbers of samples produced two specific results as discussed later.

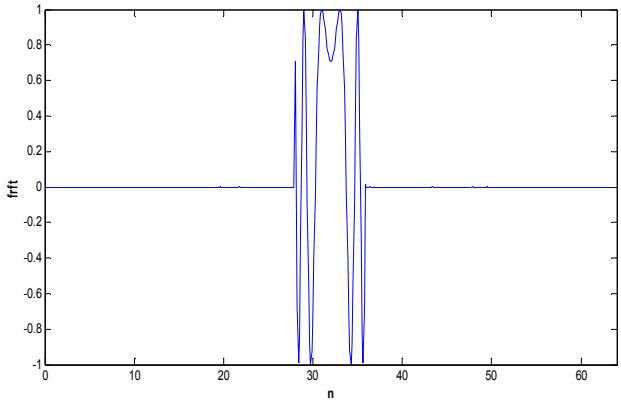

Figure 8. FRFT of chirp function at a=0

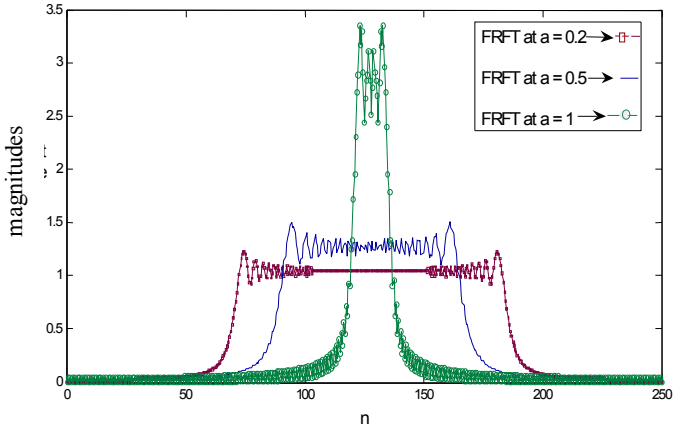

Figure 9. Magnitudes of FRFT of chirp function by varying 'a'

Maejo Int. J. Sci. Technol. **2009**, *3*(03), 459-471

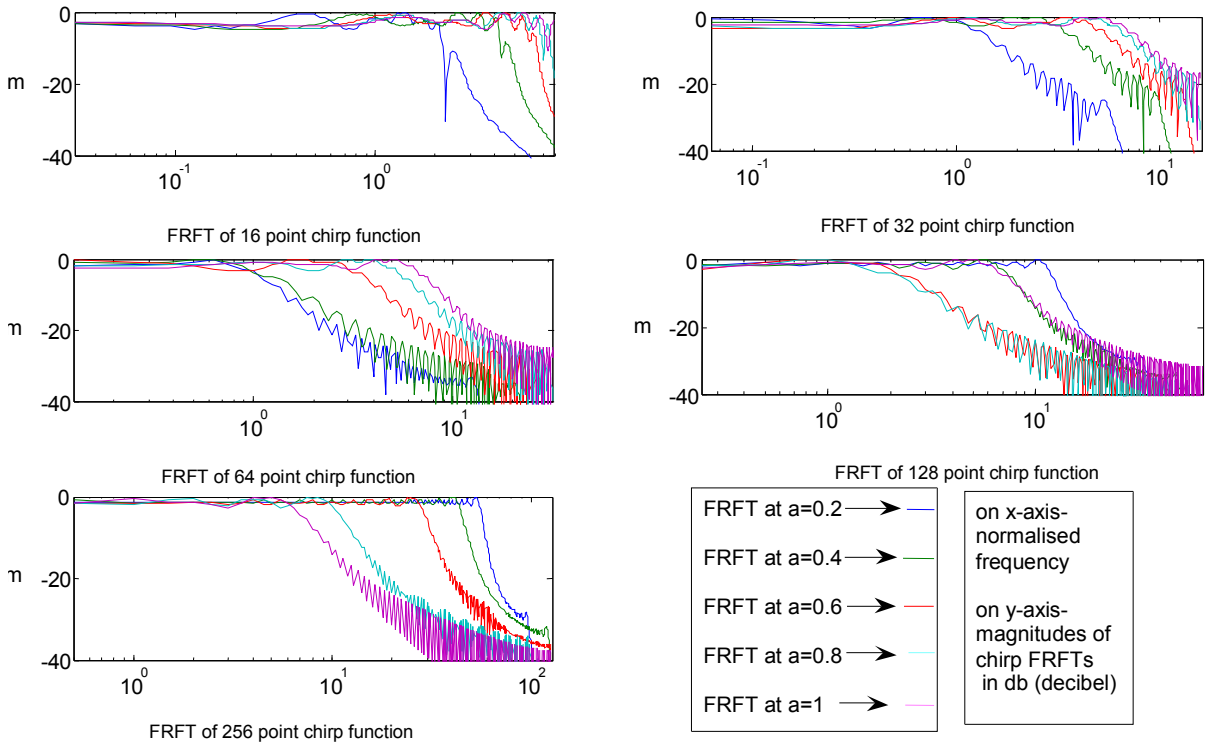

Figure 10. FRFT of chirp function for different sizes of samples

Table 4. Parameters of FRFT of chirp function

Fractional angle 'α'	Samples under consideration	MSLL (in db*)	HMLW	SLFOR (in db*)
π/20	16	-9.63	0.8	-
π/4	16	-7.2	5.1	-
3π/20	32	-4.6	2.3	-5
7π/20	32	-3.4	5.3	-5.5
13π/50	64	-3.408	2.1	-6.8
3π/8	64	-5.3	4.50	-5.2
13π/50	128	-10	5.5	-4
23π/50	128	-13.09	6.75	-5.7

* = decibel

Maejo Int. J. Sci. Technol. **2009**, *3*(03), 459-471

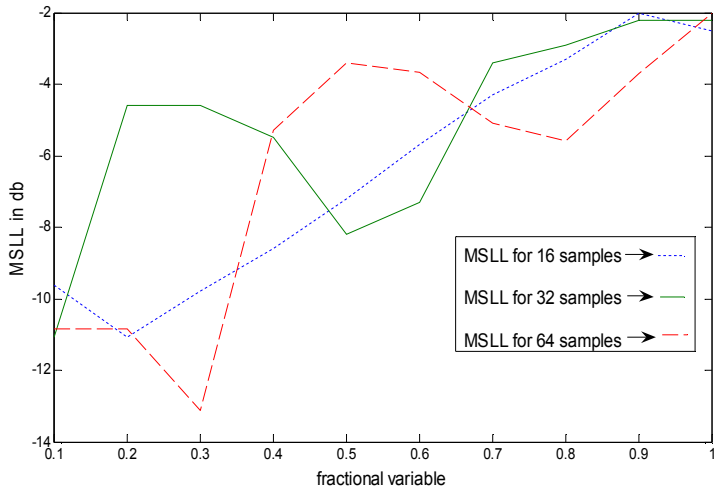

Figure 11. MSLL of FRFTs of chirp function for different sizes of samples

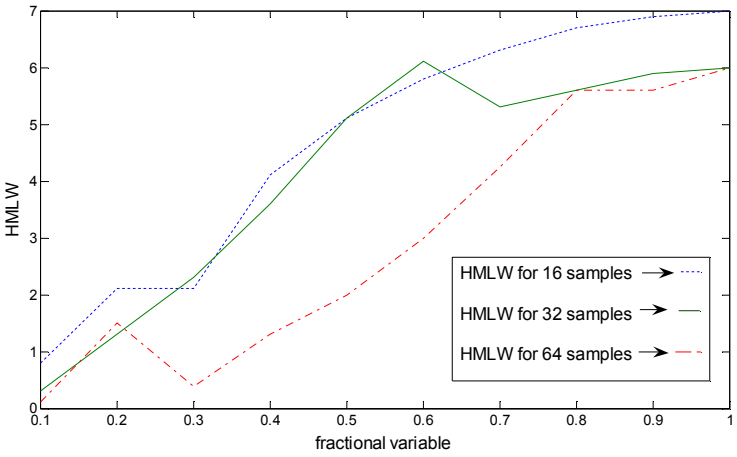

Figure 12. HMLW of FRFTs of chirp function for different sizes of samples

Discussion

It can be concluded that in the case of harmonic function, changes in HMLW, SLFOR and MSLL are in general regular in nature for small samples, but irregularity is observed when the size of samples is increased in the FRFT domain.

Two specific results for harmonic function for $\alpha = 41\pi/100$ and $9\pi/20$ were obtained during simulation studies and analysis, as shown in Figures 13-14. Parameters of these results were compared with those of cosine tip window function and Fejer window function. Superiority in results can be observed from Table 5. Frequency domain representation of harmonic function is included with its shifted version for comparison. These specific results can replace the window functions to generate a variety of applications and can also be applied according to the requirement of the spectral parameters.

Maejo Int. J. Sci. Technol. **2009**, *3*(03), 459-471

The behaviour of chirp function changes with the variation of fractional angle α with respect to the number of samples in time-frequency plane. This simulation studies have generated two important results with $\alpha = 3\pi/20$ and $\alpha = 71\pi/200$ for chirp function in fractional Fourier domain. Like the harmonic function, chirp function is not a window function but parameters of these two results are far better than the frequency domain parameters of Boxcar window function. Figure 15 shows db (decibel) plot of chirp function at $\alpha = 3\pi/20$ in time-frequency plane. Figure 16 shows db plot of the same function at $\alpha = 71\pi/200$. Comparative parameters are shown in Table 5. These two plots prove to be a better replacement for Boxcar window function and can be used as a tool for specific applications.

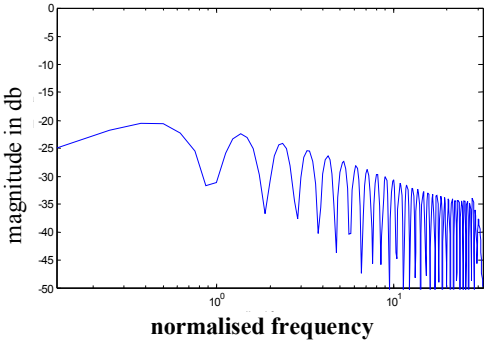

Figure 13. Magnitude of FRFT of harmonic function at a =0.82

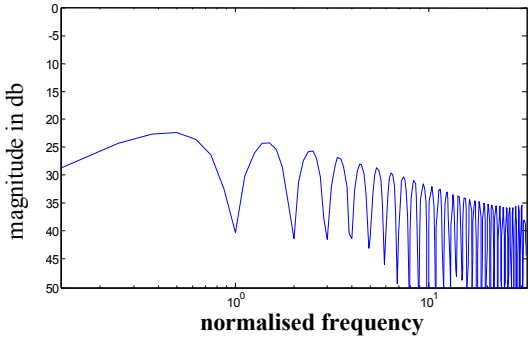

Figure 14. Magnitude of FRFT of harmonic function at a =0.9

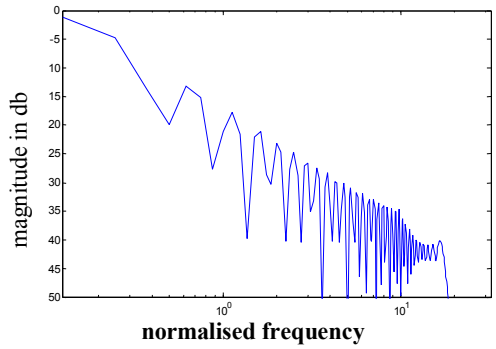

Figure 15. Magnitude of FRFT of chirp function at a =0.3

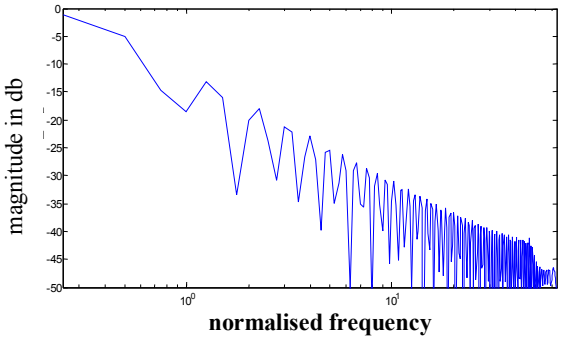

Figure 16. Magnitude of FRFT of chirp function at a =0.71

Maejo Int. J. Sci. Technol. **2009**, *3*(03), 459-471

Table 5. Comparative parameters

Function	Fractional angle α	MSLL (in db)	HMLW	SLFOR (in db)
Harmonic	41 π/100	-23	0.625	-2.3
Cosine tip window	π/2	-23	1.35	-12
Harmonic	9 π/20	-24	0.625	-2.5
Fejer window	π/2	-26	1.63	-12
Chirp	3 π/20	-13.14	0.375	-5.23
Boxcar window	π/2	-13	0.81	-6
Chirp	71 π/200	-13.16	0.8	-5

Conclusions

The FRFT domain analysis of harmonic and chirp functions has been carried out and a few cases of these functions are observed to show better spectral performances in comparison to the existing weight functions. This clearly indicates that harmonic and chirp functions with some specific values of FRFT with order `*a*′ provide a better candidate in applications wherever these weight functions are used.

References

1. R. N. Bracewell, "The Fourier Transform and Its Applications", 2nd Edn., McGraw Hill, New York, **1986**.
2. A. W. Lohmann, "Image rotation, Wigner rotation and the fractional order Fourier transform", *J. Opt. Soc. Am. A***, 1993,** *10*, 2181-2186.
3. D. Mendlovic and H. M. Ozaktas, "Fractional Fourier transform and their optical implementation: I", *J. Opt. Soc. Am., A*, **1993**, *10*, 1875-1881.
4. H. M. Ozaktas, M. A. Kutay and Z. Zalevsky, "The Fractional Fourier Transform with Applications in Optics and Signal Processing", John Wiley and Sons, New York, **2001**.
5. N. Wiener, "Hermitian polynomial and Fourier analysis", *J. Math. Phys. MIT*, **1929,** *8*, 70-73.
6. E. U. Condon "Immersion of the Fourier transform in a continuous group of functional transformations", *Proc. Nat. Acad. Sci. USA*, **1937,** *23*, 158-164.
7. V. Bargmann, "On a Hilbert space of analytic function and an associated integral transform, Part I", *Commun. Pure Appl. Math.*, **1961**, *14*, 187-214.

Maejo Int. J. Sci. Technol. **2009**, *3*(03), 459-471

8. V. Namias, "The fractional order Fourier transform and its application in quantum mechanics", *J. Inst. Math. Applic.*, **1980**, *25*, 241-245.
9. A. C. McBride and F. H. Kerr "On Namias's fractional Fourier transform", *IMA J. Appl. Math.*, **1987,** *239*, 159-175.
10. L. B. Almeida, "The fractional Fourier transform and time frequency representation", *IEEE Trans. Signal Process.*, **1994**, *42*, 3084-3093.
11. L. B. Almeida, "Product and convolution theorem for the fractional Fourier transform", *IEEE Signal Process. Lett.*, **1997**, *4*, 15-17.
12. A. I. Zayed, "A convolution and product theorem for the fractional Fourier transform", *IEEE Signal Process. Lett.*, **1998**, *5*, 101-103.
13. D. Mustard, "Fractional convolution", *J. Aust. Math. Soc. Ser. B*, **1998,** *40*, 257-265.
14. H. M. Ozaktas, O. Arikan, M. A. Kutay and G. Bozdagi, "Digital computation of the fractional Fourier transform", *IEEE Trans. Signal Process.*, **1996,** *44*, 2141-2150.
15. C. Candan, M. A. Kutay and H. M. Ozaktas, "The discrete fractional Fourier transform", *IEEE Trans. Signal Process.*, **2000,** *48*, 1329-1337.
16. R. Saxena and K. Singh, "Fractional Fourier transform, a novel tool for signal processing", *J. Indian Inst. Sci.*, **2005**, *85*, 11-26.
17. J. K. Gautam, A. Kumar and R. Saxena "Windows: A tool in signal processing" *IETE Tech. Rev.*, **1995,** *12*, 217-226.

Maejo Int. J. Sci. Technol. **2009**, *3*(03), 472-485

Maejo International Journal of Science and Technology

ISSN 1905-7873

Available online at www.mijst.mju.ac.th

Full Paper

Upregulation of glucose uptake in L8 myotubes by the extract from *Lagerstroemia speciosa*: a possible mechanism of action

Niwat Keawpradub[1] and Juntipa Purintrapiban [2, *]

[1] Department of Pharmacognosy and Pharmaceutical Botany, Faculty of Pharmaceutical Sciences, Prince of Songkla University, Hat-Yai, Songkhla, 90112, Thailand

[2] Department of Biomedical Sciences, Faculty of Medicine, Prince of Songkla University, Hat-Yai, Songkhla, 90112, Thailand

* Corresponding author, e-mail: pjuntipa@medicine.psu.ac.th

Received: 18 May 2009 / Accepted: 14 December 2009 / Published: 18 December 2009

Abstract: The leaf of *Lagerstroemia speciosa* L. is used as an anti-diabetic herbal remedy in many countries. In an attempt to discover mechanisms of action of the *L. speciosa* extract that stimulate glucose uptake, a cell-based radioactive assay of glucose uptake was performed using L8 muscle cells. In this study, the methanol fraction of *L. speciosa* leaves (LSE) contained a high level of phenolic compounds and showed strong capability to stimulate glucose uptake in a dose-dependent manner. The LSE stimulation was slightly inhibited (8.8%) by SB203580. The inhibitory effect (23.6%) of wortmannin on LSE-stimulated glucose uptake was demonstrated, suggesting LSE action on glucose transporter translocation. LSE-induced glucose uptake was completely reversed by cycloheximide. In addition, an increased amount of total glucose-transporter-1 protein was observed indicating that new protein synthesis is necessary for elevated glucose transport. LSE also enhanced insulin-stimulated glucose transport. These results suggest that LSE action may be mediated primarily via the synthesis of new transporters and involve both insulin-dependent and independent pathways.

Keywords: *Lagerstroemia speciosa*, glucose uptake, GLUT1, polyphenols, L8 myotubes

Introduction

Diabetes Type II has become a predominant public health problem with increasing rate of affecting people worldwide [1]. About one third of Type II diabetic patients need insulin to reduce their blood glucose levels, and some 40% require oral agents for satisfactory blood glucose control. Currently, due

Maejo Int. J. Sci. Technol. **2009**, *3*(03), 472-485

to lack of access to essential medicines developed through pharmaceutical research and as a part of local culture, a majority of the world's population still depends on traditional medicine for primary health care need. In addition, use of complementary and alternative medicine in the treatment of diabetes has increased steadily among the general public. In the U.S. alone, a 380% increase in the use of herbal supplements from 1990 to 1997 has been reported [2]. Thus, a provision of safe and effective traditional medical therapies could become a vital tool for increasing access to health care.

Lagerstroemia speciosa (L.) Pers. (Lythraceae) is a popular medicinal plant in South-East Asia, especially the Philippines. A decoction of *L. speciosa* leaves has been used for treatment of diabetes [3]. The extract of *L. speciosa* significantly lowered blood sugar in Type II diabetic mice and alloxan-induced diabetic rats [4-6], and stimulated glucose transport in adipocytes and Ehrlich ascites tumour cells [7-8]. Studies have shown an anti-obesity activity of extracts from this plant on KK-Ay mice and in 3T3-L1 cells [7, 9]. The hypoglycemic effect of the active component (corosolic acid) resulted from increased GLUT4 translocation in muscle of diabetic mice [10]. Recently, more active tannins, gallotannins and triterpenes were reported to enhance glucose uptake in 3T3-L1 cells [11-14]. It was also noted that the magnitude of the effect of *L. speciosa* extract was much larger than the effect of the individual active compound.

According to previous reports, glucose transport enhancement activity of the aqueous extract of *L. speciosa* leaves in 3T3-L1 adipocytes involved a rapid response (15-min) [7, 13]. However, no reports of the long-term effects or the mechanisms of action of the extract at cellular and molecular levels have been published despite the fact that the extract is commercially available [15]. This present study is designed to investigate the effects of the methanol fraction of the aqueous extract of *L. speciosa* leaves on the glucose transport in muscle cells, a physiological target cells of insulin, by employing L8 myotubes as cell model to assay for glucose uptake activities. The mechanisms by which the extract mediates the glucose transport activity in the presence of specific inhibitors are also investigated.

Materials and Methods

Materials

Rat L8 myoblasts were purchased from American Type Culture Collection (Rockville, MD). Cell culture media and supplements were acquired from Life Technologies, Inc. (Gaithersburg, MD). Bovine insulin, cytochalasin B (CB), wortmannin (WM), SB203580 (SB), cycloheximide (CHX), protease inhibitor cocktail, phloretin, α-actin antibody, enzyme-linked antibodies and standard chemicals were purchased from Sigma Chemicals (St. Louis, MO). 2-Deoxy-D-[^{3}H] glucose (2-dGlc) was obtained from Amersham Biosciences (Piscataway, NJ). A polyclonal antibody against glucose transporter 1 (GLUT1) was purchased from Santa Cruz Biotechnology, Inc. (Santa Cruz, CA). A monoclonal antibody against glucose transporter 4 (GLUT4) was purchased from R&D systems, Inc. (Minneapolis, MN). Electrophoresis and protein assay reagents were purchased from Bio-Rad (Hercules, CA). The CytoTox 96 non-radioactive cytotoxicity assay kit was purchased from Promega (Madison, WI).

Maejo Int. J. Sci. Technol. **2009**, *3*(03), 472-485

Sample preparation

Lagerstroemia speciosa leaves were collected from the medicinal plants garden of the Faculty of Pharmaceutical Sciences, Prince of Songkla University, Hat-Yai, Thailand. They were cleaned by washing with running tap water and rinsing with distilled water, and placed in a 45^{O}C oven until they were completely dried. Five grams of the powdered leaf sample were extracted with 200 ml water at 70^{O}C for 30 min. After filtering, the solution obtained was centrifuged at 5,000 *g* for 20 min and the supernatant concentrated by freeze-drying to give a crude extract. A portion of the crude extract (1.45 g) was further separated by passage through a Sephadex LH-20 column with methanol as eluent to afford 32 fractions (20 ml each). The eluted fractions were subjected to thin-layer chromatographic analysis using silica gel 60 F_{254} plates (0.20 mm thick) with ethyl acetate-chloroform-methanol (2:1:1) as developing solvent. Fractions 14-21, which showed similar chemical profiles, containing mainly 4 tailing phenolic compounds which gave greenish-blue colour upon spraying with 10% ferric chloride in absolute ethanol, were pooled and evaporated to give a dried residue of the methanol fraction (LSE: 986 mg). Upon phytochemical screening (see Table 1), besides phenolic compounds (including tannins), triterpenoids and carbohydrates were also detected in LSE. The residue (LSE) dissolved in water and sterilised with 0.45-μm filters was used for the glucose transport study.

Cell and culture conditions

L8 myoblasts were maintained and differentiated as described previously [16]. Briefly, the cells were seeded in complete Dulbecco's modified Eagle's medium (DMEM) with 10% fetal bovine serum at 35,000 cells/cm^2 in 24-well plates for glucose uptake assay and 100-mm plates for protein analysis. When cells reached ~95% confluence, differentiation was initiated by culturing them in a medium with 2% horse serum (HS). In the present experiment, ~80-85% of the myoblasts fused into myotubes. The cells were rinsed with HEPES buffered saline, pH 7.4 (HBS). Thereafter, HBS (1x final concentration) containing 2% HS, 15 mM glucose and LSE at the desired concentration (0, 20, 40, 80, 100, 120 or 140 μg/ml) or 100 nM insulin were added to the cells, which were then incubated at 37°C for 16 h. In order to investigate the effect of insulin, the medium was changed to serum-free HBS (1x) containing 25 mM glucose, and incubated at 37°C for 5 h before the assay of glucose transport. For the inhibitor studies, 2 μg/ml CHX, 100 nM WM, 10 μM SB and 40 μM CB were added individually or in combination to the LSE-treated cells at a respective time (CHX, 16 h; WM, 20 min; SB, 30 min; and CB, 30 min) prior to the end of the 16-h incubation. Phloretin (10 mM), an inhibitor of a variety of membrane transporters including facilitated glucose transport [17], was added to the incubation mixture 20 min before the uptake assay to determine the effect of non-specific uptake. Using the CytoTox 96 non-radioactive cytotoxicity assay, an aliquot from each well was taken to determine the cytotoxic effect according to the manufacturer's instructions.

2-dGlc uptake assay

The L8 myotubes were rinsed twice with 1 ml HBS. After rinsing, glucose uptake was initiated by the addition of 0.3 ml of HBS (1x) containing 2-dGlc (1 μCi/ml) without or with 100 nM insulin as the

Maejo Int. J. Sci. Technol. **2009**, *3*(03), 472-485

final concentration to the cells. After 10 min, the medium was aspirated and the plates were washed three times with ice-cold 0.9% NaCl to terminate the induced glucose uptake. The cells were lysed in 0.05 N NaOH and the radioactivity taken up by the cells was determined using a scintillation counter. Preliminary studies (data not shown) demonstrated that uptake of 2-dGlc (1 μCi/ml) was linear up to 15 min. Non-specific uptake measured in the presence of phloretin was less than 10% of the total uptake. Aliquots from each treatment were used to determine the protein concentration using the Bio-Rad protein assay.

Analysis of glucose transporter

A method described by Yu et al. [18] was used with modification. L8 myotubes grown in 100-mm plates and incubated with and without 100 μg/ml LSE were washed twice with cold phosphate-buffered saline (PBS). The cells were treated with 20 strokes in homogenising buffer (25 mM sucrose, 20 mM HEPES, pH 7.4, 2 mM EGTA, 5 mM NaN_3, protease inhibitors). Cell lysates were centrifuged at 200 *g* for 5 min. The supernatant (whole cell lysate) was collected for total GLUT1 and GLUT4 protein analysis or further centrifuged at 16,000 *g* for 15 min to pellet the plasma membrane (PM) from the supernatant or soluble (S) fraction. Protein samples (150 μg) were separated in 10% SDS-PAGE and transferred to PVDF for the Western blot analysis. Non-specific sites on the membrane were blocked with 5% non-fat dry milk. Antibodies against GLUT1 (1:700), GLUT4 (1:250) or α-actin (1:700) were added and maintained for 2 h at room temperature. Blots were then incubated with enzyme-linked second antibody followed by colourimetric or chemiluminescent detection. The immunoreactive protein was quantified using scanning densitometry.

Phytochemical screening and determination of total phenolics

Phytochemical screening of LSE was performed using the methods previously described by Farnsworth [19] and Harborne [20] with slight modification. In brief, several reagents were prepared to test for the presence of flavonoids, coumarins, anthraquinones, iridoids, cardiac glycosides, cyanogenetic glycosides, coumarins, saponins, alkaloids, tannins, carbohydrates, amino acids and peptides. The results were compared with the positive standards of each test. The amount of total phenolic compounds was determined spectrophotometrically using Folin-Ciocalteu reagent as described by Lee et al. [21] and was expressed in μg of catechin equivalent (CE) based on a calibration curve for catechin.

Statistical analyses

Three to five separate experiments were conducted in all studies and all assay conditions were performed in triplicate. All data are expressed as means ± SD. Statistical analyses were performed by a one-way analysis of variance followed by Dunnett t-tests. The level of $P<0.05$ was considered significant.

Maejo Int. J. Sci. Technol. **2009**, *3*(03), 472-485

Results

LSE-stimulated uptake of 2-dGlc by L8 myotubes in culture

Figure 1A shows the time course for the uptake of 2-dGlc in L8 myotubes induced by LSE. In contrast to previous studies in fat cells [7, 13], the response to LSE in muscle cells was found to be slow. The rate of 2-dGlc uptake increased about 1.35, 2.43 and 2.70-fold (P<0.05) of control levels at 8, 16 and 24 h respectively after exposure to 0.1 mg/ml LSE. The basal uptake activity response to prolonged (8-24 h) incubation was lower than that to short-term (0.5-2 h) exposure due to the effect of high glucose in the incubation medium [22-23]. When cells were maintained for 16 h with varying doses of LSE, a dose-dependent effect was observed (Figure 1B). The maximal uptake activity was achieved at 0.1 mg/ml LSE, and thereafter the rate decreased markedly due to the cytotoxic effect. LSE also caused a slight toxicity at dose of 0.1 mg/ml. LSE-induced uptake was blocked by cytochalasin B, which inhibits cytoskeletal reorganisation when added at 40 μM prior to the uptake assay (data not shown). This indicates that LSE actively stimulates glucose uptake in the cells and could likely activate the movement of glucose across cell membranes.

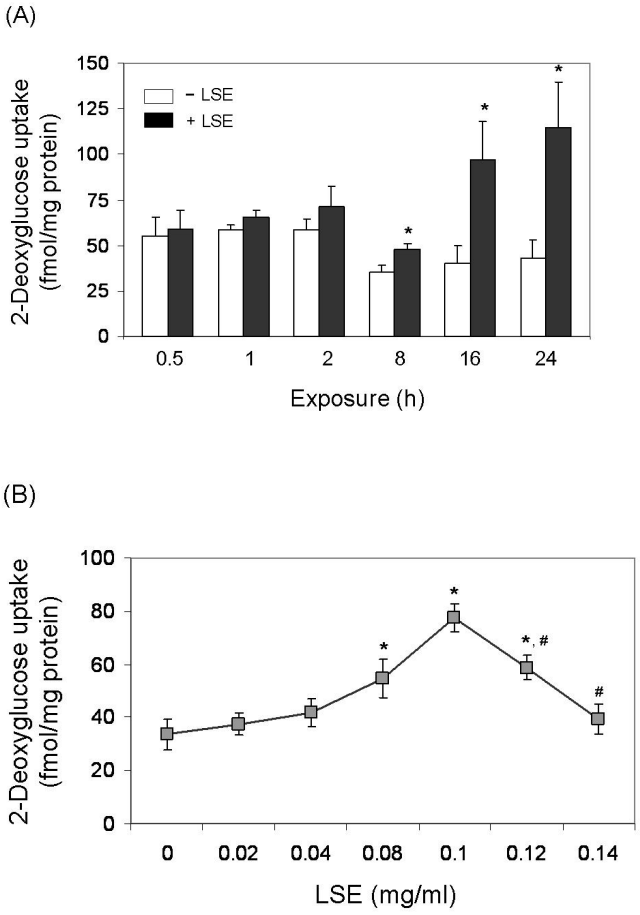

Figure 1. Time course and dose-dependent effects of LSE on 2-deoxyglucose uptake. Panel A: L8 myotubes were incubated with or without 0.1 mg/ml LSE for the time indicated; Panel B: L8 myotubes were incubated with increasing doses of LSE for 16 h prior to 10-min determination of 2-deoxyglucose uptake. Data were expressed as means ± SD of the triplicates derived from three separate experiments.

* P<0.05 vs. control cells # toxicity observed

Maejo Int. J. Sci. Technol. **2009**, *3*(03), 472-485

Figure 2 shows data from experiments in which the effects of the specific inhibitors on the uptake of 2-dGlc were examined in LSE-treated cells. CHX treatment reduced the 2-dGlc uptake rate in the control (LSE-untreated) cells by about 55%, indicating that active protein synthesis is necessary for maintaining cellular transport of glucose at the basal state. It is clear that CHX could reverse the effect of LSE. Approximately 71% reduction of LSE-stimulated 2-dGlc transport by CHX was observed. SB203580, which specifically inhibits the activity of p38 mitogen-activated protein kinase (p38 MAPK) through the interaction with its ATP-binding domain resulting in the inactivation of glucose transporter's intrinsic activity [24-25], slightly decreased the activity of LSE-induced 2-dGlc uptake (8.87 ± 3.69%, n = 5). Wortmannin, which has been shown to interact with the p110 activating subunit of phosphatidylinositol 3-kinase (PI3K) resulting in an irreversible inhibition of this kinase that leads to inhibition of GLUT4 translocation [26], only partially but significantly reduced the stimulation of LSE (23.62 ± 4.90%, n = 5). A higher degree of inhibition was observed when a combination of inhibitors was present.

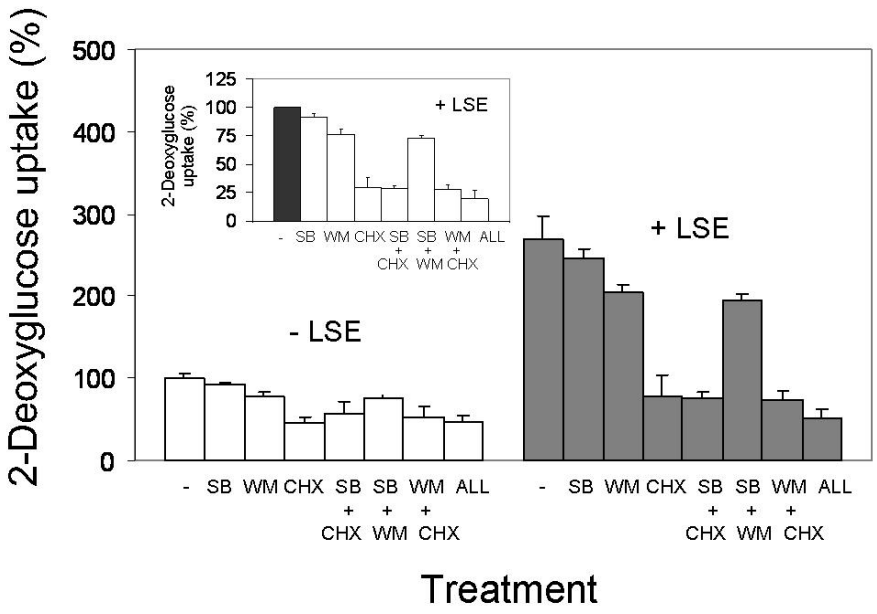

Figure 2. Inhibition of LSE-stimulated 2-deoxyglucose uptake activity by SB203580, wortmannin, and cycloheximide. L8 myotubes were pre-incubated with or without 0.1 mg/ml LSE for 16 h in the presence of SB203580 (SB), wortmannin (WM), cycloheximide (CHX) or all agents (ALL) as indicated prior to 10 min determination of 2-deoxyglucose uptake. Inset: The reduction in glucose uptake activity by inhibitors in LSE-treated cells was recalculated and expressed relative to the uptake activity of LSE alone. Data were expressed as means ± SD of the triplicates derived from five separate experiments.

* $P<0.05$ vs. values with LSE alone

Figure 3 shows the relationship between insulin and LSE effects on glucose uptake. The cells were maintained in serum-free media for 5 h to induce insulin stimulation response before the uptake assay was initiated [16, 27]. To enable the detection of additive effect, LSE at a concentration of 80 µg/ml was used. The activation of glucose transport by insulin was enhanced by 39% in the presence of

Maejo Int. J. Sci. Technol. **2009**, *3*(03), 472-485

LSE (for insulin, sugar uptake = 32.37 ± 5.92 pmol/mg protein; for LSE+insulin, sugar uptake = 45.23 ± 8.11 pmol/mg protein, n = 5). This indicates a partial additive effect of both agents.

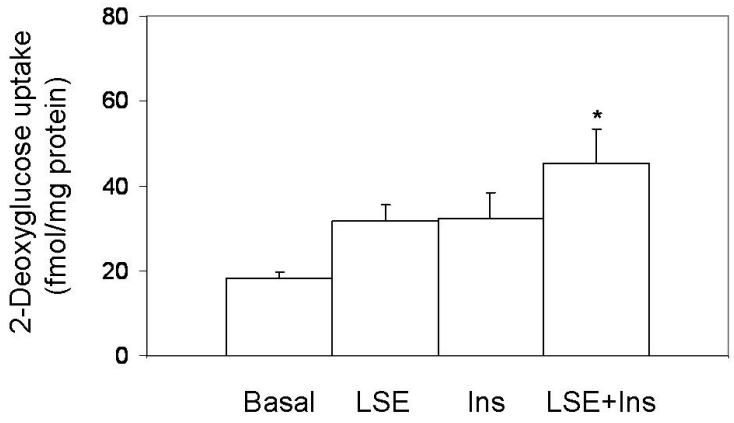

Figure 3. Additivity of insulin- and LSE-mediated uptake of 2-deoxyglucose in L8 cells. L8 myotubes were stimulated with or without 100 nM insulin and/or 0.08 mg/ml LSE for 16 h and serum-deprived for 5 h. Uptake of 2-deoxyglucose was measured over 10 min in the presence or absence of insulin. Data were expressed as means ± SD of the triplicates derived from five separate experiments.
* P <0.05 vs. values with either insulin or LSE alone

Figure 4 shows the results of a representative experiment: GLUT1 and GLUT4 content in cells exposed for 16 h or not exposed to LSE at 0.1 mg/ml. Western blot analyses of GLUT4 content from five separate experiments revealed no notable change in the amount of GLUT4 total protein in LSE cells (1.11 ± 0.27-fold) compared to that in untreated cells. In contrast, there was an increase in total GLUT1 protein content (2.15 ± 0.96-fold) in the LSE-treated cells and the level of GLUT1 protein present in the plasma membrane (PM) was much higher than that in the intracellular compartment (S). Increased GLUT1 protein content due to LSE was significantly lowered (0.74 ± 0.24-fold, n = 3) to below the basal level when CHX was present (Figure 4C). These results imply that the effect of LSE is associated with significant increase in the content of GLUT1 and the magnitude of the gain in uptake activity by LSE may be due to enhanced GLUT1 protein synthesis.

Total phenols and active constituents of LSE

The amount of total phenolics in 1 mg LSE was 409.58 ± 39.57 μg catechin equivalent (CE). Thus, polyphenols present in the maximal stimulation dose of LSE (0.1 mg/ml) was about 40.9 μg CE. This implies that increasing glucose transport in L8 muscle cells resulted mainly from the additional effect of polyphenols. Table 1 shows the results of phytochemical screening of LSE for the presence of active constituents. As evident from the Table, LSE yielded a positive result with Liebermann-Burchard test, indicating the presence of triterpenoid compounds. It was also positive with Molisch's test, suggesting the presence of free carbohydrates and/or bound sugars in the form of glycosidic compounds. Furthermore, LSE gave positive results in reactions with 1% gelatin solution and 1% ferric chloride solution, suggesting the existence of tannins.

Maejo Int. J. Sci. Technol. **2009**, *3*(03), 472-485

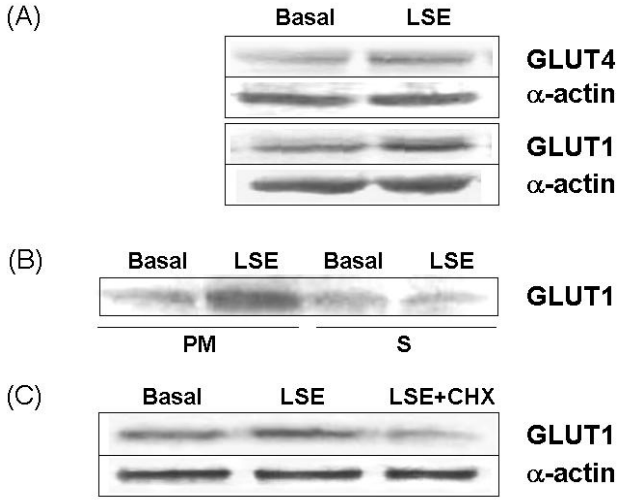

Figure 4. Determination of total GLUT4 and GLUT1 protein content (panel A), GLUT1 localisation (panel B), and the inhibitory effect of CHX on total GLUT1 level (panel C) in LSE-stimulated cells. L8 myotubes were treated with or without 0.1 mg/ml LSE and 2 μg/ml CHX for 16 h. Cells were homogenised, and total lysate, plasma membrane (PM) and intracellular fraction (S) were prepared. Samples were Western blotted and probed for GLUT1, GLUT4 and α-actin with specific antibodies. Immunoblots are representative of 3-8 samples.

Discussion

Natural remedies are viable alternatives to oral medications that may cause undesirable side effects. Indeed, many plants with a glucose-lowering effect have been used successfully for the treatment of diabetes. Particularly, one of the various botanical health care products, *L. speciosa* extract, has been made available worldwide [28-29]. However, these health care products have not been evaluated by the US FDA and have little scientific analyses to confirm the effects and mechanisms of the plant extract and the active ingredients.

It is well established that the predominant GLUT4 isoform expressed in mature muscle cells and adipocytes is primarily responsible for the increase in glucose uptake in response to insulin stimulation [30]. Increased exocytosis and decreased endocytosis in the presence of insulin, which cause a shift in the steady-state distribution of GLUT4 favouring the plasma membrane, result in increase of the amount of GLUT4 at the plasma membrane [31]. The present study has shown that the *L. speciosa* extract (LSE) is a potent activator of glucose transport in L8 muscle cells. We have demonstrated that prolonged exposure to LSE stimulates glucose transport in the absence of insulin. However, analysis of blot density displayed no effect in total GLUT4 protein content. In addition, wortmannin, an inhibitor of PI3K, which blocks the translocation of insulin-sensitive GLUT4 from its intracellular pool to the plasma membrane [32-33], partially reversed the LSE-induced 2-dGlc uptake. The present results suggest that the translocation of the GLUT4 isoform mediated via insulin-regulated, PI3K-dependent signaling is essential for LSE-induced glucose transport.

Maejo Int. J. Sci. Technol. **2009**, *3*(03), 472-485

Table 1. Phytochemical screening results of LSE

Test	LSE	Positive standard
Coumarins		Stem bark of *Alyxia reinwardtii*
(NaOH paper, UV 365 nm)	(-)	(+): blue colour under UV light
Anthraquinones		Aloe (*Aloe barbadensis*)
(Borntrager test)	(-)	(+): pink colour in the alkaline layer
Iridoids		Leaves of *Clinacanthus nutans*
(formation of pseudoindicans)	(-)	(+): green-blue solution
Cardiac glycosides		Seed kernel of *Thevetia peruviana*
Kedde's reagent test	(-)	(+): purple solution
Liebermann-Burchard test	(+): red colour (triterpenoids)	(+): green colour (steroids)
Keller-Kiliani test	(-)	(+): reddish-brown ring
Saponins		Fruit of *Sapindus rarak*
Froth test	(-)	(+): honeycomb froth (persisted for at least 30 min)
Liebermann-Burchard test	(+): red colour (triterpenoids)	(+): red colour (triterpenoids)
Flavonoids		Stem of *Derris elliptica*
(Shinoda's test)	(-)	(+): pink-red solution
Tannins		Gambir (*Uncaria gambir*)
Reaction with gelatin solution	(+): precipitate	(+): precipitate
Reaction with $FeCl_3$ solution	(+): green-blue solution	(+): green-blue solution
Alkaloids		Stem of *Arcangelisia flava*
Mayer's reagent	(-)	(+): precipitate
Dragendorff's reagent	(-)	(+): precipitate
Carbohydrates		Honey (*Apis mellifera*)
(Molisch's test)	(+): purple ring	(+): purple ring
Amino acids and peptides		Soy bean (*Glycine max*)
Biuret test	(-)	(+): violet solution
Ninhydrin test	(-)	(+): grayish-blue solution

Note : (-) = negative result
(+) = positive result

Maejo Int. J. Sci. Technol. **2009**, *3*(03), 472-485

It was reported by Liu et al [7, 13] that exposure to *L. speciosa* extract results in rapid activation of glucose uptake of serum-starved adipocytes. Employing serum deprivation that involves the depletion of GLUT1 prior to treatment of adipocyte and muscle cell cultures has been practiced in several studies, and this strategy allows the detection of strongly stimulated glucose transport in response to insulin and other stimulators which mediate GLUT4 translocation [17, 27, 34]. In addition, insulin, for example, has been shown in these studies to be capable of increasing the rate of glucose transport in adipocytes 15- to 20-fold, whereas about a 2-fold increase is achieved in muscle cells. In the present study, we have demonstrated that short-term exposure to LSE does not activate glucose transport in L8 cells. One possible reason is that the LSE effect on GLUT4 translocation is small (~23% of wortmannin-dependent inhibition), thus the increasing glucose uptake activity resulting from GLUT4 translocation is undetected under conditions in which the basal uptake is not down-regulated as previously reported by Diedrich [16] and Klip et al. [27].

GLUT1, which is plasma-membrane-localised with a relatively small amount found in intracellular membrane compartments in cells and tissues in the basal state [35], was reported to mediate a significant fraction of non-insulin-dependent transport of glucose [30]. GLUT1 gene expression is regulated by various stimuli including cell stress factors, mitochondria inhibitors, hypoglycemia tumour necrosis factor α and prolonged insulin exposure [36-41]. Studies in Clone 9 cells that express GLUT1 but not GLUT2 or GLUT4 have revealed that GLUT1 activation and translocation are not influenced by inhibitors of PI3K and p38 MAPK, which reportedly prevent GLUT4 translocation and/or activation by insulin [42], suggesting that GLUT1 expression may be mediated by a different mechanism. A lag period of more than 2 h preceding the increase in transport rate by LSE in the present study reflects the time required for the concentration of glucose transporters to increase above the threshold level whereby the stimulation of transport can be detected. Our results in L8 cells indicate that exposure to LSE increases both the number of GLUT1 at the cell surface and the GLUT1 total protein levels. Furthermore, cycloheximide blocks the activation of glucose uptake by LSE and diminishes LSE's effect on increasing GLUT1 protein level. These indicate that a component of glucose transport stimulation associated with LSE action is the number of GLUT1 up-regulated via GLUT1 protein expression. It is known that the mRNA half-life is linked to its translation and its stability also affects the rate of change of its abundance following an increase in transcription [43]. At the protein level, the half-life of GLUT1 could be increased or decreased by particular stimuli [39, 44]. Further studies on the actual mechanism by which LSE increases GLUT1 protein content that can be attributed to either altered GLUT1 gene expression or post-translation regulation of GLUT1 are necessary. Remarkably, cycloheximide interferes with LSE-induced glucose uptake, suggesting that the regulation is dependent on translation.

The p38 MAPK-dependent pathway has been implied in enhancing the intrinsic activity of GLUT1 and GLUT4 at the cell surface [24-25]. Inhibition of p38 MAPK with specific inhibitor SB203580 reduces insulin-induced glucose uptake without an effect on insulin-induced GLUT4 translocation [25]. In the present study, SB203580 has a small but significant inhibitory effect on LSE-induced glucose uptake, demonstrating that the activation of p38 MAPK is involved in LSE action. We have shown that LSE-mediated glucose uptake in L8 cells is apparently associated to the mechanisms by which insulin signals glucose transport. A further increase in insulin-stimulated glucose transport by LSE provides

Maejo Int. J. Sci. Technol. **2009**, *3*(03), 472-485

evidence that LSE may also target diverse cascades, some of which lead to increased glucose transport. It has been reported that muscle contraction and hypoxia or metabolic stress cause a normal glucose transport response involving activation of 5'-AMP-activated kinase (AMPK) in the insulin-resistant skeletal muscles, in which insulin signalling of glucose transport and GLUT4 translocation are impaired [45]. Thus, taken together, these data suggest that LSE activates glucose transport in L8 muscle cells and involves the synthesis of GLUT1 and the activation of PI3K and p38 MAPK as well as the insulin-independent signalling, which may operate in tandem with the insulin-dependent pathway.

In this present study, a significant amount of phenolic compounds in LSE has also been detected. This is in good agreement with a previous study [46] that reported a high content (10.3%) of polyphenols in the leaf extract of *L. speciosa*. In addition, studies have shown that the most active components of *L. speciosa* leaves are polyphenols. These include ellagitannins (i.e. lagerstroemin, flosin B and reginin A) and corosolic acid, which have been shown to activate glucose transport in cell culture [8, 11]. Recent reports demonstrated the lowering effect of corosolic acid on postchallenge plasma glucose levels in human subjects and established its inhibitory effect on glycogen phosphorylase *a* [46, 47]. The antidiabetic activity of the leaf extract (standardised to contain 1% corosolic acid) in human has been described [15]. The presence of tannins and triterpenoids in LSE is consistent with recent studies, which reported more tannins and triterpenes in *L. speciosa* and their capacity to enhance glucose uptake in fat cells [11-13]. Furthermore, the activation of the insulin receptor by lagerstroemin (a polyphenol) has also been demonstrated in the Chinese hamster ovary cells [48]. Thus, it is apparent that LSE contains several active polyphenols that may act synergistically or through multiple mechanisms.

Conclusions

The present study has established that the extract of *L. speciosa* exerts a direct up-regulatory effect on GLUT1 protein expression and, in part, the GLUT4 translocation, which results in the gain of glucose transporters at the plasma membrane. The mechanisms of action contributing to increased glucose transport involve both the activation of insulin-dependent and insulin-independent signalling pathways.

Acknowledgement

This work was supported in part by grants from the Faculty of Medicine, Prince of Songkla University.

References

1. J. C. Seidell, "Obesity, insulin resistance and diabetes--a worldwide epidemic", *Br. J. Nutr.,* **2000**, *83* Suppl.1, S5-S8.

Maejo Int. J. Sci. Technol. **2009**, *3*(03), 472-485

2. D.M. Eisenberg, R. B. Davis, S. L. Ettner, S. Appel, S. Wilkey, M. Van Rompay and R. C. Kessler, "Trends in alternative medicine use in the United States, 1990-1997: Results of a follow-up national survey", J. Am. Med. Assoc., **1998**, *280*, 1569-1575.
3. D. P. Carew and T. F. Chin, "Constituents of Lagerstroemia speciosa Flosreginae Retz", Nature, **1961**, *190*, 1108-1109.
4. T. Kakuda, I. Sakane, T. Takihara, Y. Ozaki, H. Takeuchi and M. Kuroyanagi, "Hypoglycemic effect of extracts from *Lagerstroemia speciosa* L. leaves in genetically diabetic KK-AY mice", *Biosci. Biotechnol. Biochem.*, **1996**, *60*, 204-208.
5. H. Hong and W. J. Maeng, "Effects of malted barley extract and banaba extract on blood glucose levels in genetically diabetic mice", *J. Med. Food*, **2004**, *7*, 487-490.
6. Y. Mishra, M. S. Y. Khan, R. Zafar and S. S. Agarwal, "Hypoglycaemic activity of leaves of Lagerstroemia speciosa (L) Pers.", *Indian J. Pharmacol.*, **1990**, *22*, 174-176.
7. F. Liu, J. Kim, Y. Li, X. Liu, J. Li and X. Chen, "An extract of *Lagerstroemia speciosa* L. has insulin-like glucose uptake-stimulatory and adipocyte differentiation-inhibitory activity in 3T3-Li cells", *J. Nutr.*, **2001**, *131*, 2242-2247.
8. C. Murakami, K. Myoga, R. Kasai, K. Ohiani, T. Kurokawa, S. Ishibashi, F. Dayrit, W. G. Padolina and K. Yamasaki, "Screening of plant constituents for effect on glucose transport activity in Ehrlich ascites tumour cells", *Chem. Pharm. Bull.*, **1993**, *41*, 2129-2131.
9. Y. Suzuki, T. Unno, M. Ushitani, K. Hayashi and T. Kakuda, "Antiobesity activity of extracts from Lagerstroemia speciosa L. leaves on female KK-Ay mice" *J. Nutr. Sci. Vitaminol.* (Tokyo), **1999**, *45*, 791-795.
10. T. Miura, Y. Itoh, T. Kaneko, N. Ueda, T. Ishida, M. Fukushima, F. Matsuyama and Y. Seino, "Corosolic acid induces GLUT4 translocation in genetically type 2 diabetic mice", *Biol. Pharm. Bull.*, **2004**, *27*, 1103-1105.
11. T. Hayashi, H. Maruyama, R. Kasai, K. Hattori, S. Takasuga, O. Hazeki, K. Yamasaki and T. Tanaka, "Ellagitannins from *Lagerstroemia speciosa* as activators of glucose transport in fat cells", *Planta. Med.*, **2002**, *68*, 173-175.
12. Y. Okada, A. Omae and T. Okuyama, "A new triterpenoid isolated from *Lagerstronemia speciosa* (L.) Pers.", *Chem. Pharm. Bull.* (Tokyo), **2003**, *51*, 452-454.
13. X. Liu, J. K. Kim, Y. Li, J. Li, F. Liu and X. Chen, "Tannic acid stimulates glucose transport and inhibits adipocyte differentiation in 3T3-L1 cells", *J. Nutr.*, **2005**, *135*, 165-171.
14. G. Klein, J. Kim, K. Himmeldirk, Y. Kao and X. Chen, "Antidiabetes and anti-obesity activity of *Lagerstroemia speciosa*", *Evid.-Based Complement. Alternat. Med.*, **2007**, *4*, 401-407.
15. W. V. Judy, S. P. Hari, W. W. Stogsdill, J. S. Judy, Y. M. A. Naguib, and R. Passwater, "Antidiabetic activity of a standardized extract (Glucosol) from *Lagerstroemia speciosa* leaves in Type II diabetics. A dose-dependence study", *J. Ethnopharmacol.*, **2003**, *87*, 115-117.
16. D. F. Diedrich, "Photoaffinity-labeling analogs of phlorizin and phloretin: synthesis and effects on cell membranes", *Methods Enzymol.*, **1990**, *191*, 755-781.
17. J. Purintrapiban and S. Ratanachaiyavong, "The effects of insulin and metformin on glucose uptake in L8 myotubes", *ScienceAsia*, **2003**, *29*, 341-346.

18. B. Yu, L. A. Poirier and L. E. Nagy, "Mobilization of GLUT-4 from intracellular vesicles by insulin and K(+) depolarization in cultured H9c2 myotubes", *Am. J. Physiol.*, **1999**, *277*, E259-E267.
19. N. R. Farnsworth, "Biological and phytochemical screening of plants", *J. Pharm. Sci.*, **1966**, *55*, 225-276.
20. J. B. Harborne, "Phytochemical Methods", Chapman and Hall, London, **1973**.
21. K. Y. Lee, S. T. Weintraub and B. P. Yu, "Isolation and identification of a phenolic antioxidant from *Aloe barbadensis*", *Free Rad. Biol. Med.*, **2000**, *28*, 261-265.
22. S. Sasson and E. Cerasi, "Substrate regulation of the glucose transport system in rat skeletal muscle", *J. Biol. Chem.*, **1986**, *261*, 16827-16833.
23. S. Sasson, N. Kaiser, M. Dan-Goor, R. Oron, S. Koren, E. Wertheimer, K. Unluhizarci and E. Serasi, "Substrate autoregulation of glucose transport: Hexose 6-phosphate mediates the cellular distribution of glucose transports", *Diabetologia*, **1997**, *40*, 30-39.
24. L. F. Barros, M. Young, J. Saklatvala and S. A. Baldwin, "Evidence of two mechanisms for the activation of the glucose transporter GLUT1 by anisomycin: p38 (MAP kinase) activation and protein synthesis inhibition in mammalian cells", *J. Physiol.*, **1997**, *504*, 517-525.
25. G. Sweeney, R. Somwar, T. Ramlal, A. Volchuk, A. Ueyama and A. Klip, "An inhibitor of p38 mitogen-activated protein kinase prevents insulin-stimulated glucose transport but not glucose transporter translocation in 3T3-L1 adipocytes and L6 myotubes", *J. Biol. Chem.*, **1999**, *274*, 10071-10078.
26. H. Yano, S. Nakanishi, K. Kimura, N. Hanai, Y. Saitoh, Y. Fukui, Y. Nonomura and Y. Matsuda, "Inhibition of histamine secretion by wortmannin through the blockade of phosphatidylinositol 3-kinase in RBL-2H3 cells", *J. Biol. Chem.*, **1993**, *268*, 25846-25856.
27. A. Klip, G. Li and W. J. Logan, "Induction of sugar uptake response to insulin by serum deprivation in fusing L6 myoblasts", *Am. J. Physiol.*, **1984**, *247* [Endocrinol Metab 10], E291-E296.
28. R. Sahelian, "Banaba leaf extract", http://www.raysahelian.com/ banaba.html (Retrieved: July 28, 2008).
29. "GlucoTrim-48™ for balancing blood sugar", http://www.naturalways.com/ glucosol.htm (Retrieved: July 28, 2008).
30. J. E. Pessin and G. I. Bell, "Mammalian facilitative glucose transporter family: structure and molecular regulation", *Annu. Rev. Physiol.*, **1992**, *54*, 911-930.
31. A. Rudich and A. Klip, "Push/pull mechanisms of GLUT4 traffic in muscle cells", *Acta. Physiol. Scand.*, **2003**, *178*, 297-308.
32. T. Okada, Y. Kawano, T. Sakakibara, O. Hazeki and M. Ui, "Essential role of phosphatidylinositol 3-kinase in insulin-induced glucose transport and antilipolysis in rat adipocytes. Studies with a selective inhibitor wortmannin", *J. Biol. Chem.*, **1994**, *269*, 3568-3573.
33. Y. Kaburagi, S. Satoh, H. Tamamoto, R. Yamamoto-Honda, K. Tobe, K. Veki. T. Yamauchi, E. Kono-Sugita, H. Sekihara, S. Aizawa, S. W. Cushman, Y. Akanuma, Y. Yazaki and T. Kadowaki, "Role of insulin receptor substrate-1 and pp60 in the regulation of insulin-induced glucose transport and GLUT4 translocation in primary adipocytes", *J. Biol. Chem.*, **1997**, *272*, 25839-25844.
34. S. C. Frost and M. D. Lane, "Evidence for the involvement of vicinal sulfhydryl groups in insulin-activated hexose transport by 3T3-L1 adipocytes", *J. Biol. Chem.*, **1985**, *260*, 2646-2652.

Maejo Int. J. Sci. Technol. **2009**, *3*(03), 472-485

35. A. W. Hudson, M. Ruiz and M. J. Birnbaum, "Isoform-specific subcellular targeting of glucose transporters in mouse fibroblasts", *J. Cell Biol.*, **1992**, *116*, 785-797.
36. D. Y. Hwang and B. F. Ismail, "Stimulation of GLUT-1 glucose transporter expression in response to hyperosmolarity", *Am. J. Physiol. Cell Physiol.*, **2001**, *281*, C1365-C1372.
37. J. Z. Zhang, A. Behrooz and B. F. Ismail, "Regulation of glucose transporter by hypoxia", *Am. J. Kidney Dis.*, **1999**, *34*, 189-202.
38. N. Bashan, E. Burdett, A. Guma, R. Sargeant, L. Tumiati, Z. Liu and A. Klip, "Mechanisms of adaptation of glucose transporters to changes in the oxidative chain of muscle and fat cells", *Am. J. Physiol.*, **1993**, *64*, C430-C440.
39. R. J. McMahon and S. C. Frost, "Nutrient control of GLUT1 processing and turnover in 3T3-L1 adipocytes", *J. Biol. Chem.*, **1995**, *270*, 12094-12099.
40. D. Szalkowski, S. White-Carrington, J. Berger and B. Zhang, "Antidiabetic thiazolidinediones block the inhibitory effect of tumor necrosis factor-alpha on differentiation, insulin-stimulated glucose uptake, and gene expression in 3T3-L1 cells", *Endocrinology*, **1995**, *136*, 1474-1481.
41. K. M. Tordjman, K. A. Leingang, D. E. James and M. M. Mueckler, "Differential regulation of two distinct glucose transporter species expressed in 3T3-L1 adipocytes: effect of chronic insulin and tolbutamide treatment", *Proc. Natl. Acad. Sci. U.S.A.*, **1989**, *86*, 7761-7765.
42. L. F. Barros, K. Barnes, J. C. Ingram, J. Castro, O. H. Porras and S. A. Baldwin, "Hyperosmotic shock induces both activation and translocation of glucose transporters in mammalian cells", *Pflügers Archiv.*, **2001**, *442*, 614-621.
43. J. Ross, "mRNA stability in mammalian cells", *Microbiol. Rev.*, **1995**, *59*, 423-450.
44. R. J. Sargeant and M. R. Paquet, "Effect of insulin on the rates of synthesis and degradation of GLUT1 and GLUT4 glucose transporters in 3T3-L1 adipocytes", *Biochem. J.*, **1993**, *290*, 913-919.
45. A. Krook, H. Wallberg-Henriksson and J. R. Zierath, "Sending the signal: Molecular mechanisms regulating glucose uptake", *Med. Sci. Sports Exercise*, **2004**, *36*, 1212-1217.
46. M. Fukushima, F. Matsuyama, N. Ueda, K. Egawa, J. Takemoto, Y. Kajimoto, N. Yonaha, T. Miura, T. Kaneko, Y. Nishi, R. Mitsui, Y. Fujita, Y. Yamada and Y. Seino, "Effect of corosolic acid on postchallenge plasma glucose levels", *Diabetes Res. Clin. Pract.*, **2006**, *73*, 174-177.
47. X. Wen, J. Xia, K. Cheng, L. Zhang, P. Zhang, J. Liu, L. Zhang, P. Ni and H. Sun, "Pentacyclic triterpenes. Part 5: Synthesis and SAR study of corosolic acid derivatives as inhibitors of glycogen phosphorylases", *Bioorg. Med. Chem. Lett.*, **2007**, *17*, 5777-5782.
48. K. Hattori, N. Sukenobu, T. Sasaki, S. Takasuga, T. Hayashi, R. Kasai, K. Yamasaki and O. Hazeki, "Activation of insulin receptors by lagerstroemin", *J. Pharmacol. Sci.*, **2003**, *93*, 69-73.

Maejo Int. J. Sci. Technol. **2009**, *3*(03), 486-497

Maejo International Journal of Science and Technology

ISSN 1905-7873
Available online at www.mijst.mju.ac.th

Full Paper

Moisture sorption of Thai red curry powder

Sudathip Inchuen [1,*], Woatthichai Narkrugsa [1] and Pimpen Pornchaloempong [2]

[1] Faculty of Agro Industry, King Mongkut's Institute of Technology Ladkrabang, Bangkok, 10520 Thailand
[2] Department of Food Engineering, Faculty of Engineering, King Mongkut's Institute of Technology Ladkrabang, Bangkok, 10520 Thailand
* Corresponding author, Tel. +66812944469; Fax +6623264091; E-mail: sudathip4@hotmail.com

Received: 1 June 2009 / Accepted: 25 December 2009 / Published: 28 December 2009

Abstract: Moisture sorption study was conducted on Thai red curry powder prepared by two different drying methods, viz. microwave and hot-air drying. Moisture sorption isotherms of the red curry powder at 30 °C and water activity in the range of 0.113-0.970 were determined by a static gravimetric method. The isotherms exhibited Type III behaviour. The moisture sorption data were fitted to several sorption models and a non-linear regression analysis method was used to evaluate the constants of the sorption equations. The fit was evaluated using the coefficient of determination (R^2), the reduced chi-square (χ^2) and the root mean square error (RMSE). The GAB model followed by the Lewiski-3 model gave the best fit to the experimental data. The monolayer moisture content, taken as the safe minimum moisture level in the red curry powder, was determined using the BET equation and was found to range between 0.080 - 0.085 gram water per gram dry matter.

Keywords: moisture sorption isotherm, monolayer moisture content, Thai red curry powder

Introduction

Thai red curry paste is a well-known curry paste used to enhance several spicy Thai dishes. The paste is prepared from dried red chili, garlic, shallot, lemon grass, galangal, spices and additives such as salt and sugar, homogeneously blended to obtain an orange-red paste. It provides the colourful, spicy and authentic fragrance of certain dishes. Moreover, it has been reported that the major ingredients of this product such as chili [1-2], garlic [3], shallot [4], lemon grass and galangal root [5-6] are good sources of phenolic compounds. These compounds in herbs and spices have been found to be major contributors to human health with multiple positive biological effects

Maejo Int. J. Sci. Technol. **2009**, *3*(03), 486-497

such as antioxidant activity, antimutagenic and/or anticarcinogenic activity, and anti-inflammatory action [7-8]. In general, the red curry paste has a high moisture content and therefore is very perishable, having a limited shelf life. The growing popularity of Thai food around the world creates the need to preserve this product. Drying is one of the preservation methods that can extend the shelf life of the red curry paste. The dried paste is milled to a powder to be used mainly as a culinary supplement and has long storage life at room temperature.

During the processing and storage of agricultural products, physical, chemical and microbiological changes occur. The changes are influenced particularly by the moisture content and water activity of food material. Equilibrium moisture content of a food material is defined as its moisture content attained when the vapour pressure of water present in the food material has reached an equilibrium with its surroundings. It is a thermodynamic property and has practical significance in both drying and storage of foods. It is affected by the relative humidity and temperature. Water activity on the other hand is defined as the ratio of vapour pressure of water over the foodstuff to that of pure water at the same temperature. The relationship between moisture content and water activity in food at constant temperature and pressure is often expressed as a moisture sorption isotherm. It can give information on the sorption mechanism and the interaction of food with water. The typical shape of the sorption isotherm may change depending on the type of product and reflects the way in which water binds to the system [9]. The drying method can also significantly affect the sorption properties of some dry products such as model fruit powders (dried pectin-sugar gels) [10] and dried locust bean gum-pectin-starch composite gels [11].

Several equations have been used to describe the sorption isotherms of many food materials [12-16]. Some of these models are based on theories on the sorption mechanism; others are purely empirical or semi-empirical. However, none of these equations describes accurately the sorption isotherm over the whole range of water activity or for different types of food materials. According to Labuza, cited by Al-Muhtaseb et al. [12], no sorption isotherm model could fit data over the entire range of relative humidity because water is associated with the food matrix by different mechanisms in different water activity regions.

The information on the moisture sorption behaviour of food is essential for determining the interaction of water with food substances. It is also useful for food processing operations such as drying, mixing, packing and storage, since it can be used to calculate drying time and predict the behaviour of ingredients upon mixing. It can also help make packaging selection, model moisture changes that occur during storage, and estimate shelf life stability [16-17]. Furthermore, the monolayer moisture content or the minimum moisture level is of importance to the physical and chemical stability of dehydrated materials with regard to lipid oxidation, enzyme activity, non-enzymatic browning and structural characteristics [9].

The moisture sorption data for red curry powder are very rare in the literature. Therefore, in this paper, the investigation of the equilibrated moisture content of red curry powder at various relative humidity values and prepared by different drying methods is carried out. The suitability of various mathematical models for fitting the isotherm and the safe storage moisture content limits of red curry powder are also evaluated.

Maejo Int. J. Sci. Technol. **2009**, *3*(03), 486-497

Materials and Methods

Raw materials

Fresh Thai red curry paste was obtained from Namprick Maesri Partnership, Ltd. (245 Petkasem Road, Nakornpathom,Thailand) and stored at -60 ºC until use. The ingredients of this product consisted of dried red chili (35%), garlic (23%), shallot (20%), salt (7%), lemon grass (6%), spices (5%), sugar (3%) and galangal (1%). The moisture, crude fibre, ash, crude fat and protein (N x 6.25) of the product were determined by the methods of AOAC [18] and it was found to contain 70 % water, 9 % fibre, 8 % ash, 4 % fat and 3 % protein.

Sample preparation

The red curry paste samples were taken out of storage and thawed at room temperature to 20^{o}C. Fitty-five (±1) grams of the paste material were uniformly spread on a 180x180 mm translucent polyethylene sheet of 1-mm thickness and dried in a microwave oven (Hitachi, MR-30A, Thailand) or a hot-air oven (Path OV663, Thailand) to a final moisture content of approximately 8% by the following conditions:

Microwave drying: The samples were dried at three different levels of microwave output power (180, 360 and 540 W) with drying time of 23, 12 and 8 min respectively.

Hot-air drying: The samples were dried at three different drying temperatures (60, 70 and 80^{o} C) with constant air velocity of 9.02 m/s and drying time of 240, 180 and 130 min respectively.

Dried products were broken into small pieces, milled with an analytical mill (Retsch, ZM1000, Germany) and passed through a 0.25-mm sieve. The resulting powders were then sealed in aluminum foil bags to prevent moisture absorption and stored at -4 ºC for further studies.

Moisture sorption isotherms

Sorption isotherms were determined by a static-gravimetric method using air-tight glass jars, each containing a saturated salt solution. The salts used were $LiCl_2$, CH_3COOK, $MgCl_2$, K_2CO_3, KI, NaCl, KCl and K_2SO_4, which gave the water activity (a_w) values at 30°C of 0.113, 0.216, 0.324, 0.432, 0.679, 0.751, 0.836 and 0.970 respectively [9]. To determine the sorption, about 0.5 (± 0.001) gram of a sample of red curry powder was accurately weighed into a previously weighed aluminum pan. The pan was then placed on a plastic receptacle inside the jar over a saturated salt solution. The jar was then tightly closed and placed in an electric oven at 30°C. At high water activity ($a_w \geq 0.751$) a small quantity of toluene was placed in a capillary tube fixed in the jar to prevent microbial spoilage of the sample [19]. All samples were weighed every week until a difference of less than 0.001 gram in two consecutive weighings was achieved, when the moisture in the sample was assumed to be at equilibrium. After the equilibrium was reached, the moisture content was determined using the oven method by heating at 105ºC to constant weight [18]. All determinations were performed in triplicate.

The experimental data of all samples were fitted to ten sorption equations (seven two-parameter models, two three-parameter models and one four-parameter model) shown in Table 1. The parameters of the sorption models were estimated from experimental results using a non-linear regression analysis (Statistica for Windows 5.0 software, StatSoft, Inc. 1984-1995).

Maejo Int. J. Sci. Technol. **2009**, *3*(03), 486-497

Table 1. Sorption models used for fitting experimental data [9, 12-16]

Model name	Model equation
(Two parameters)	
Oswin	$W_e=A(a_w/1-a_w)^B$
Caurie	$W_e=\exp(A+Ka_w)$
Smith	$W_e=A+(B\ln(1-a_w))$
Lewicki-2	$W_e=A((1/a_w)-1)^{B-1}$
BET*	$W_e= X_mCa_w/[(1-a_w)(1-a_w+Ca_w)]$
Haslay	$a_w=\exp(-A/W_e^B)$
Henderson	$(1-a_w)=\exp(-AW_e^B)$
(Three parameters)	
GAB	$W_e=X_mCKa_w/[(1-Ka_w)(1- Ka_w +CKa_w)]$
Lewicki-3	$W_e=A[(1/(1-a_w)^B)-(1/(1+a_w^C))]$
(Four parameters)	
Peleg	$W_e=A(a_w)^C+ B(a_w)^D$

Notes: a_w = water activity; W_e = moisture content at equilibrium (grams water per gram dry matter); X_m = monolayer moisture content (grams water per gram dry matter); A, B, C, D and K = moisture sorption constants

*Sorption data fitted for water activity ≤ 0.432

Statistical analysis

The goodness of fit of tested mathematical models to the experimental data was evaluated with the coefficient of determination (R^2), reduced chi-square (χ^2) and root mean square error (RMSE) [14-15]. The higher the R^2 value and the lower the χ^2 and RMSE values, the better is the fit. The χ^2 and RMSE can be calculated as follows:

$$\chi^2 = \frac{\sum_{i=1}^{N} (W_{e,exp,i} - W_{e,pre,i})^2}{N - z}$$

$$RMSE = \sqrt{\frac{1}{N}\sum_{i=1}^{N}(W_{e,exp,i} - W_{e,pre,i})^2}$$

where $W_{e,exp,i}$ is the i^{th} experimental moisture content at equilibrium, $W_{e,pre,i}$ is the i^{th} predicted moisture content at equilibrium, N is the number of observations and z is the number of constants in the sorption model.

Results and Discussion

Sorption isotherms

The initial moisture content of microwave-dried and hot-air-dried red curry powders were found in the range of 0.082-0.086 gram water per gram dry matter. Moisture sorption isotherms of these samples are shown in Figure 1. As the initial moisture content of the red curry powder was

Maejo Int. J. Sci. Technol. **2009**, *3*(03), 486-497

low, adsorption was dominant. The equilibrated moisture content (W_e) of the red curry powder increased with water activity (a_w). This might be due to the fact that the vapour pressure of water present in samples increased with that of the surroundings. The moisture content increased very slowly with increase in water activity up to 0.432. From this point on there was a gradual increase in moisture content with increase in water activity up to 0.851, beyond which there was a steep rise in moisture in all samples.

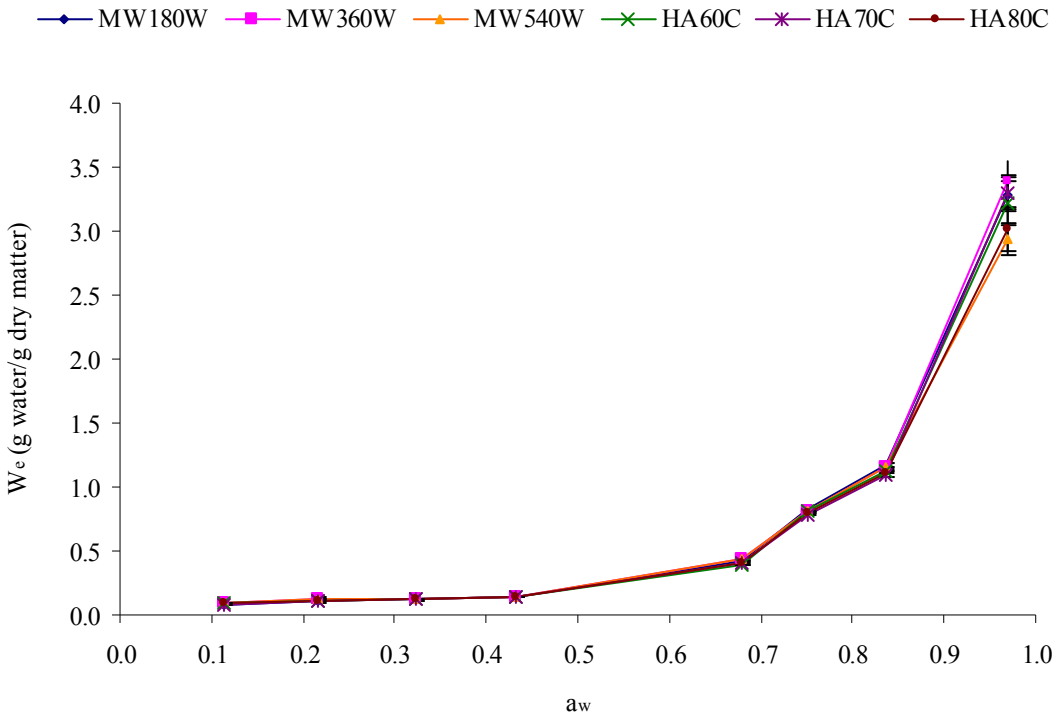

Figure1. Moisture sorption isotherms of Thai red curry powders prepared by microwave drying (MW) and hot-air drying (HA)

According to the classification of Brunauer et al. [12], all sorption isotherms obtained exhibited Type III behaviour, in which a small amount of water is adsorbed at low water activity and a larger amount is adsorbed at higher water activity, and once the bulk moisture point has been reached, the powder rapidly adsorbs large amounts of water vapour, causing it to deliquesce and leading to a steep rise in the third part of the curve, corresponding to the formation of hydrate [11]. The linear shape at the first part of the isotherms is caused by water adsorption on to the biopolymers and the sharp increase in water content at high water activity is due to the gradual dissolution of solutes such as salts and sugars [10]. These results suggest that the red curry powder is characterised by high hygroscopicity as a result of high solute content (salt and sugar) mostly in the amorphous state, which promotes undesirable effects (e.g. caking).

Al-Muhtaseb et al. [12] reported that foods rich in soluble components show isotherms with Type III behaviour owing to the solubility of the components in water. Similar isotherm behaviour has been found in crushed chilies [14], pistachio nut paste [19], model fruit powder [10,20],

Maejo Int. J. Sci. Technol. **2009**, *3*(03), 486-497

pineapple pulp powder [21], fruits rich in sugar such as grape, apricot and apple [22] and salted alligator meat [23].

It is known that the shape and position of an isotherm for food is influenced by sample composition, physical structure (crystalline or amorphous), pretreatment and method of processing [21]. According to Figure 1, however, the effect of drying method on the shape and position of the red curry powder isotherm is not evident. This means that the states of adsorbed water of the red curry powder during sorption process were not much affected by the method of drying. Moreover, all red curry powder samples had slight difference in the amount of equilibrated moisture content over the entire water activity levels, which indicated that the drying methods did not significantly affect the adsorption capacity of the samples either. Similar results were obtained by Debnath et al. [17] on freeze-dried, vacuum-shelf-dried and through-flow-dried onions. In contrast, Tsami et al. [10] found that freeze-dried pectin-sugar gels had a higher adsorption capacity than microwave-dried, vacuum-dried and convective air-dried samples in that order. Lee and Lee [24] and Giri and Prasad [25] also found that freeze-dried mushrooms had a higher adsorption capacity than microwave-dried and air-died ones in that order. Sundaram and Durance [11] found that the convective air-dried locust bean gum-pectin-starch composite gels had a higher adsorption capacity than freeze-dried and microwave vacuum-dried samples in that order up to 0.8 a_w level. These researchers suggested that moisture sorption capacity of the dry products was in accordance with structural properties such as shrinkage and porosity (total pore area and pore size distribution), which mainly depend on the drying method. Moreover, the effect of drying method on the sorption capacity of different materials may not be the same.

Fitting of sorption models to equilibrium moisture data

The experimental equilibrated moisture content data at any water activity of red curry powder from microwave and hot-air drying methods were fitted against the water activity on ten different sorption models listed in Table 1. The statistical test methods, the coefficient of determination (R^2), the reduced chi-square (χ^2) and the root mean square error (RMSE) were used to select the best fitting equation. The estimated parameters and statistical analysis of the ten models are presented in Table 2. The results show that the highest probability of fitting the experimental data with the highest values for R^2 and lowest values for χ^2 and RMSE are obtained with the GAB model for all the red curry powder samples. Mathematical comparison of the experimental and predicted results gives R^2 values ranging between 0.99639-0.99753 (average 0.99696), χ^2 values ranging between 0.00451-0.00580 (average 0.00504) and RMSE values ranging between 0.05308-0.06022 (average 0.05608). The fitted sorption isotherms for the model with the experimental data are illustrated in Figure 2.

Normally, parameters in the GAB equation have physical meaning: X_m is the monolayer content, C is the total heat of sorption of the first layer, and K is a factor correcting the properties of multilayer molecules with respect to the bulk liquid [19]. However, there are some other limit values for parameters C and K suggested by Lewicki [26] based on the mathematical analysis of the model. In order to guarantee a relatively good description of the isotherm and to fulfill the

Maejo Int. J. Sci. Technol. **2009**, *3*(03), 486-497

Table 2. Statistical results and estimated values of several model parameters for different drying conditions

Model	Parameter	Microwave drying			Hot-air drying		
		180 W	360 W	540 W	60 °C	70 °C	80 °C
Two parameters							
Oswin							
	A	0.33648	0.32630	0.34232	0.35039	0.34215	0.35615
	B	0.65178	0.66792	0.62815	0.64678	0.66175	0.61036
	R^2	0.98892	0.99200	0.98801	0.98878	0.99145	0.98526
	χ^2	0.01565	0.01184	0.01480	0.01662	0.01334	0.01746
	RMSE	0.10835	0.09425	0.10537	0.11164	0.10004	0.11443
Caurie							
	A	-5.58930	-5.82891	-5.32475	-5.48757	-5.70087	-5.06514
	B	6.95845	7.23285	6.61666	6.87698	7.12712	6.32436
	R^2	0.99335	0.99274	0.99290	0.99413	0.99344	0.99440
	χ^2	0.00939	0.01075	0.00877	0.00869	0.01025	0.00662
	RMSE	0.08392	0.08978	0.08108	0.08074	0.08766	0.07049
Smith							
	A	-0.30889	-0.32477	-0.26495	-0.31367	-0.33029	-0.24857
	B	-0.92524	-0.94499	-0.86580	-0.94819	-0.97144	-0.85031
	R^2	0.94904	0.94273	0.95534	0.95187	0.94578	0.96288
	$\chi 2$	0.06775	0.07996	0.05165	0.06701	0.07975	0.04109
	RMSE	0.22542	0.24488	0.19681	0.22418	0.24456	0.17555
Lewicki-2							
	A	0.33648	0.32630	0.34232	0.35039	0.34215	0.35615
	B	0.34822	0.33208	0.37185	0.35322	0.33825	0.38964
	R^2	0.98823	0.99152	0.98720	0.98806	0.99093	0.98422
	χ^2	0.01565	0.01184	0.01480	0.01662	0.01334	0.01746
	RMSE	0.10835	0.09425	0.10537	0.11164	0.10004	0.11443
BET							
	X_m	0.08017	0.08339	0.08464	0.08356	0.08321	0.08287
	C	429.62592	145.333057	1333229.36	107.06766	1326.3384	618734.8
	R^2	0.96880	0.91936	0.89922	0.95998	0.87758	0.84921
	χ^2	0.00002	0.00006	0.00006	0.00003	0.00009	0.00010
	RMSE	0.00328	0.00566	0.00570	0.00418	0.00666	0.00723
Haslay							
	A	0.17562	0.17495	0.17492	0.18406	0.18449	0.18302
	B	0.91551	0.92786	0.94602	0.90163	0.91205	0.91593
	R^2	0.96782	0.97037	0.96476	0.97085	0.96589	0.96384
	χ^2	2.12845	1.79900	1.86518	2.76614	2.43855	2.87668
	RMSE	1.26346	1.16157	1.18274	1.44035	1.35237	1.46885
Henderson							
	A	1.86038	1.89811	1.87708	1.80529	1.82196	1.82029

Maejo Int. J. Sci. Technol. **2009**, *3*(03), 486-497

Table 2. (Continued)

Model	Parameter	Microwave drying			Hot-air drying		
		180 W	360 W	540 W	60 °C	70 °C	80 °C
	B	0.78050	0.80097	0.81029	0.77582	0.79150	0.79160
	R^2	0.93792	0.94151	0.93691	0.94296	0.94013	0.94008
	χ^2	0.16648	0.23175	0.13049	0.15781	0.21300	0.08008
	RMSE	0.35335	0.41691	0.31283	0.34403	0.39968	0.24507
Three parameters							
GAB							
	X_m	0.51270	0.36958	0.45741	0.58185	0.42026	0.70660
	C	0.36373	0.55482	0.45222	0.32846	0.48915	0.28460
	K	0.91039	0.93380	0.90986	0.90335	0.92692	0.87733
	R^2	0.99658	0.99726	0.99639	0.99714	0.99753	0.99683
	χ^2	0.00580	0.00487	0.00535	0.00509	0.00463	0.00451
	RMSE	0.06022	0.05517	0.05781	0.05638	0.05379	0.05308
Lewicki-3							
	A	0.70377	0.62745	0.80473	0.75473	0.67691	0.96289
	B	0.46590	0.50227	0.41554	0.45390	0.48925	0.36552
	C	6.71382	6.71161	6.89649	6.75285	6.68133	7.03462
	R^2	0.99552	0.99672	0.99571	0.99595	0.99682	0.99576
	χ^2	0.00759	0.00582	0.00635	0.00720	0.00596	0.00603
	RMSE	0.06887	0.06033	0.06302	0.06706	0.06102	0.06140
Four parameters							
Peleg							
	A	1.91516	1.98273	1.77474	1.95455	2.02753	1.71775
	B	1.91516	1.98273	1.77474	1.95455	2.02753	1.71775
	C	6.06913	6.32743	5.76744	5.99412	6.22799	5.49316
	D	6.06913	6.32743	5.76744	5.99412	6.22799	5.49316
	R^2	0.98904	0.98822	0.98782	0.98978	0.98893	0.98933
	χ^2	0.02322	0.02617	0.02256	0.02269	0.02594	0.01896
	RMSE	0.10776	0.11440	0.10621	0.10651	0.11388	0.09737

Maejo Int. J. Sci. Technol. **2009**, *3*(03), 486-497

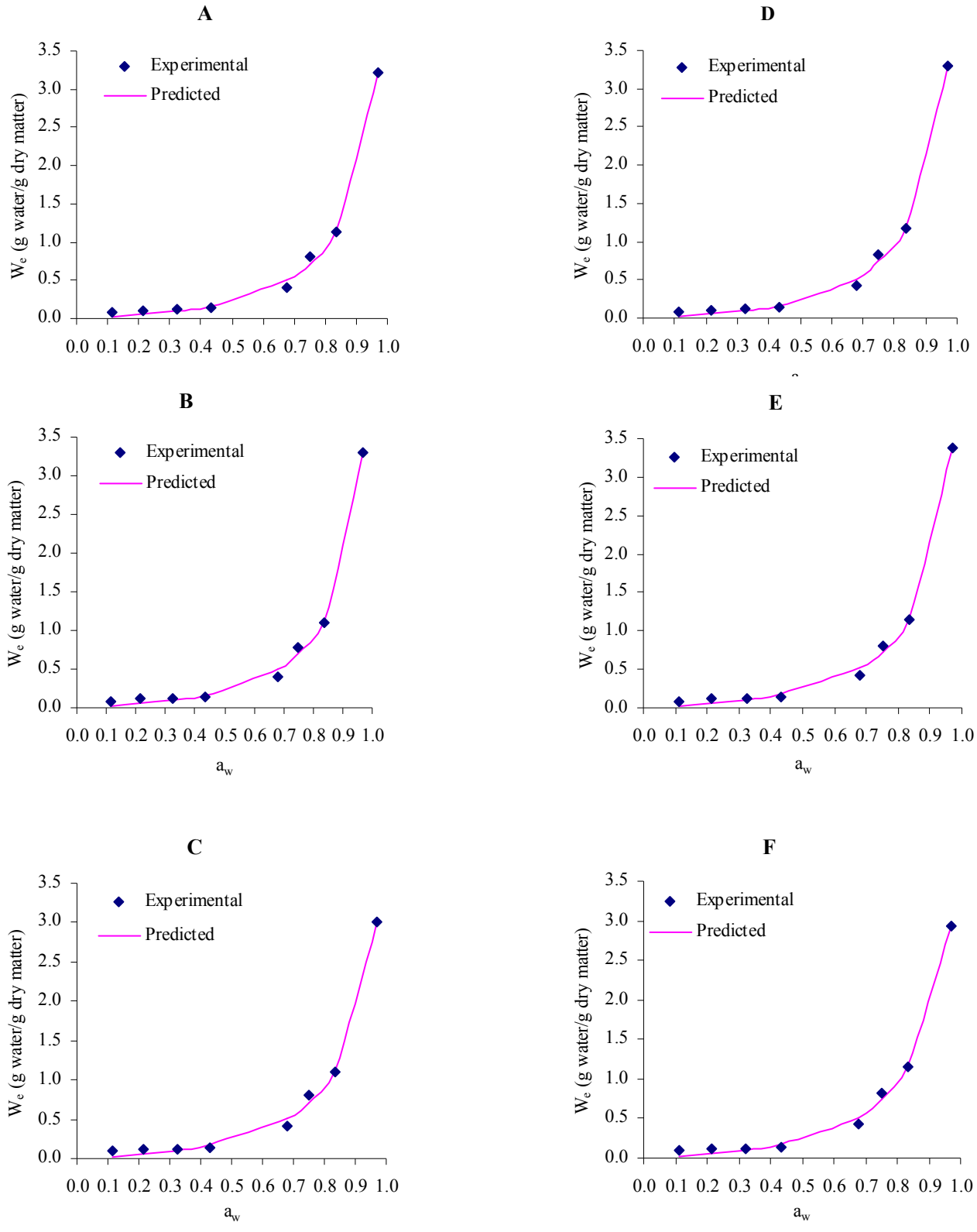

Figure 2. Comparison of experimental and predicted (GAB model) sorption isotherms of Thai red curry powder prepared by microwave drying at 180 W (**A**), 360 W (**B**), 540 W (**C**) and hot-air drying at 60 °C (**D**), 70 °C (**E**) and 80 °C (**F**)

Maejo Int. J. Sci. Technol. **2009**, *3*(03), 486-497

requirements of the BET model as well as to assure that the estimated X_m values differ by not more than ± 15% from the true monolayer capacity, the above author stated that the parameters should assume values in the ranges $5.67 \leq C \leq \infty$ and $0.24 \leq K \leq 1$. In the present study, the estimated C results are not in accordance with the limit values and are therefore considered as not fulfilling the theoretical requirements. So the values of the GAB parameters obtained in this work lack any physical meaning. Similar results were found by Lewicki [26] for apple cellular fibre, carrot, coffee, mushroom, wheat bran flour and yeast isotherms. The physically impossible values of the GAB parameters have been reported by several researchers. The high value of X_m has been reported by Arslan and Toğrul [14] on the study of crushed chilies. Furthermore, the negative value of C and the value higher than unity of K have been found by Maskan and Göğus [19] on the study of pistachio nut paste.

The second best model that fits the experimental data of all the red curry powders is the Lewicki-3 model. Statistical data for the Lewicki-3 correlation are: R^2 ranging between 0.99552-0.99682 (average 0.99608), χ^2 ranging between 0.00582-0.00759 (average 0.00649) and RMSE ranging between 0.06033-0.06362 (average 0.06362). Lewicki [24] theorised that the Lewicki-3 model consists of two functions subtracted from each other assuming the two processes occur in parallel. The first process prevails at high water activity while the second plays a major role at low water activity. The model was found to give a higher probability of good fit for the experimental data compared to the GAB and Peleg equations. Nevertheless, no physical significance could be assigned to the parameters of the equation. On the other hand, the Henderson, Haslay and Smith equations provide the worst representations of the data.

Monolayer moisture content

The value of the monolayer moisture content (X_m) is of particular interest, since it indicates the amount of water that is strongly adsorbed to specific sites at the food surface. It is considered as the optimum value to assure food stability. For most dry foods, the rate of quality loss due to chemical reactions is negligible at the monolayer value. Therefore, this value is important for the storage of red curry powder, since at this moisture level water does not act as a solvent, being biologically inert.

The X_m value in this study was determined by using the BET equation and was found to range between 0.080-0.085 gram water per gram dry matter, the values at which the red curry powder keeps very well on storage for a long period of time. Tsami et al. [10] following adsorption at 25°C found for model fruit powder the X_m values between 0.060-0.097, which is the same in the order of magnitude as X_m estimated in the present work. The X_m values for lemon juice and pineapple powder, however, were between 0.146-0.166 gram water per gram dry matter following adsorption at 20-50°C [16,21]. Kaymak-Ertekin and Gedik [22] found for grapes, apricots and apples X_m values between 0.095-0.220 gram water per gram dry matter, and those for potato between 0.067-0.073 gram water per gram dry matter following adsorption and desorption at 30-60°C. The value of X_m for red curry powder thus seems to be lower than those for high-sugar fruits and fruit powder but higher than those for starchy foods.

Maejo Int. J. Sci. Technol. **2009**, *3*(03), 486-497

Conclusions

This study presents data on moisture sorption of Thai red curry powder prepared by two different drying methods, i.e. microwave drying at 180, 360 and 540 W, and hot-air drying at 60, 70 and 80˚C, over a range of water activity (0.113-0.970) at 30°C. It was found that the red curry powder exhibited Type III sorption isotherms which were not affected by the drying methods. The GAB model followed by the Lewicki-3 model was found to be most suitable for fitting the moisture sorption data. The monolayer moisture content derived from the BET model ranged between 0.080-0.085 gram water per gram dry matter. The moisture sorption data obtained could give useful information to guide the processing, packaging and storage of Thai red curry powder at ordinary temperature.

Acknowledgement

The authors would like to thank Namprick Maesri Limited Partnership for supplying the red curry paste used in this study.

References

1. N. Deepa, C. Kaur, B. George, B. Singh and H. C. Kapoor, "Antioxidant constituents in some sweet pepper (*Capsicum annuum* L.) genotypes during maturity", *LWT - Food Sci. Technol.*, **2007,** *40*, 121-129.
2. M. Materska and I. Perucka, "Antioxidant activities of the main phenolic compounds isolated from hot pepper fruit (*Capsicum annuum* L.)", *J. Agric. Food Chem.*, **2005**, *53*, 1750-1756.
3. N. Leelarungrayub, V. Rattanapanone, N. Chanarat and J. M. Gebicki, "Quantitative evaluation of the antioxidant properties of garlic and shallot preparation", *Nutr.*, **2006**, *22*, 266-274.
4. E. Fattorusso, M. Iorizzi, V. Lanzotti and O. Taglialatela-Scafati, "Chemical composition of shallot (*Allium ascalonicum* Hort.)", *J. Agric. Food Chem.*, **2002**, *50*, 5686-5690.
5. T. Juntachote, E. Berghofer, F. Bauer and S. Siebenhandl, "The application of response surface methodology to the production of phenolic extracts of lemongrass, galangal, holy basil and rosemary", *Int. J. Food Sci. Technol.*, **2006**, *41*, 121-133.
6. T. N. Ly, M. Shimoyamada, K. Kato and R. Yamauchi, "Isolation and characterization of some antioxidative compounds from the rhizomes of smaller galangal (*Alpinia officinarum* Hance)", *J. Agric. Food Chem.*, **2003**, *51*, 4924-4929.
7. Y. J. Surh, "Anti-tumor promoting potential of selected spices ingredients with antioxidative and anti-inflammatory activities", *Food Chem. Toxicol.*, **2002**, *40*, 1091-1097.
8. S. Karakaya, "Bioavailability of phenolic compounds", *Crit. Reviews Food Sci. Nutr.*, **2004**, *44*, 453-464.
9. L. N. Bell and T. P. Labuza, "A Textbook of Moisture Sorption", 2nd Edn., American Association of Cereal Chemists, Inc., St. Paul, **2000**.

Maejo Int. J. Sci. Technol. **2009**, *3*(03), 486-497

10. E. Tsami, M. K. Krokida and A. E. Drouzas, "Effect of method drying on sorption characteristics of model fruit powders", *J. Food Eng.*, **1999**, *38*, 381-392.
11. J. Sundaram and T. D. Durance, "Water sorption and physical properties of locust bean gum-pectin-starch composite gel dried using different drying methods", *Food Hydrocolloid,* **2008** *22*, 1352-1361.
12. A. H. Al-Muhtaseb, W. A. M. McMinn and T. R. A. Magee, "Moisture sorption isotherm characteristics of food products: A review", *Trans. Inst. Chem. Eng.*, **2002**, *80*, 118-128.
13. U. S. Shivhare, S. Arora, J. Ahmed and G. S. V. Raghavan, "Moisture adsorption isotherms for mushroom", *LWT - Food Sci. Technol.*, **2004**, *37*, 133-137.
14. N. Arslan and H. Toğrul, "Moisture sorption isotherms of crushed chillies", *Biosyst. Eng.*, **2005**, *90*, 47-61.
15. V. R. Sinija and H. N. Mishra, "Moisture sorption isotherms and heat of sorption of instant (soluble) green tea powder and green tea granules". *J. Food Eng.*, **2008**, *86*, 494-500.
16. L. Martinelli, A. L. Gobas and J. Telis-Romero, "Thermodynamic and quality properties of lemon juice powder as affected by maltodextrin and Arabic gum", *Drying Technol.*, **2007**, *25*, 2035-2045.
17. S. Debnath, J. Hemavathy and K. K. Bhat, "Moisture sorption studies on onion powder", *Food Chem.*, **2002**, *78*, 479-482.
18. K. Helrick (Ed.), "Approved Official Methods of Analysis", 15th Edn., Association of Official Analytical Chemists (AOAC), Washington, DC, **1990**.
19. M. Maskan and F. Göğüş, "The fitting of various models to water sorption isotherms of pistachio nut paste", *J. Food Eng.*, **1997**, *33*, 227-237.
20. A. E. Drouzas, E. Tsami and G. D. Saravacos, "Microwave/vacuum drying of model fruit gels", *J. Food Eng.*, **1999**, *39*, 117-122.
21. A. L. Gabas, V. R. N. Telis, P. J. A. Sobral and J. Telis-Romero, "Effect of maltodextrin and Arabic gum in water vapor sorption thermodynamic properties of vacuum dried pineapple pulp powder", *J. Food Eng.*, **2007**, *82*, 246-252.
22. F. Kaymak-Ertekin and A. Gedik, "Sorption isotherms and isosteric heat of sorption for grapes, apricots, apples and potatoes", *LWT - Food Sci. Technol.*, **2004**, *37*, 429-438.
23. J. F. L. Filho, P. F. Romanelli, S. H. R. Barboza, A. L. Gabas and J. Telis-Romero, "Sorption isotherms of alligator's meat (*Caiman crocodiles yacare*)", *J. Food Eng.*, **2002**, *52*, 201-206.
24. P. P. Lewicki, "A three parameter equation for food moisture sorption isotherms", *J. Food Process Eng.*, **1998**, *21*, 127-144.
25. P. P. Lewicki, "The application of the GAB model to food water sorption isotherms", *Int. J. Food Sci. Technol.*, **1997**, *32*, 553-557.